Akkretionsscheibenmodelle mit äußerer Einstrahlung

Diplomarbeit

von

Nicolay J. Hammer

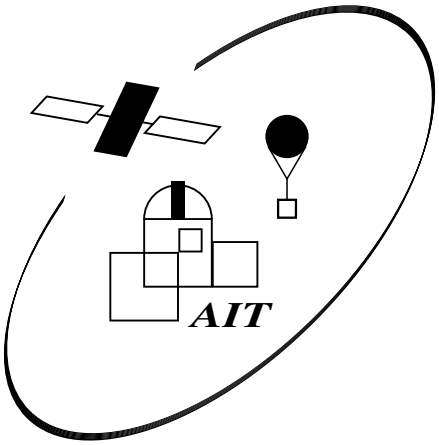

Eberhard-Karls-Universität Tübingen

Fakultät für Mathematik und Physik

Institut für Astronomie und Astrophysik
Abteilung Astronomie

Juli 2004

Irradiated Accretion Disc Models

Diploma Thesis

by

Nicolay J. Hammer

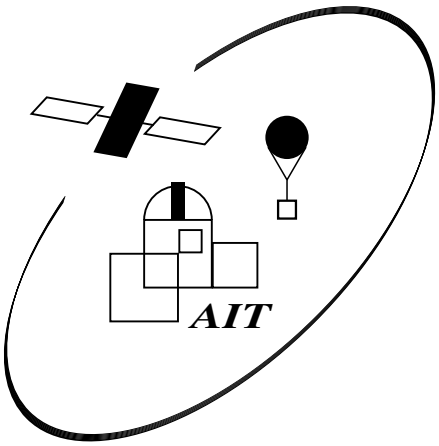

Eberhard-Karls-University Tübingen

Department for Mathematics und Physics

Institut for Astronomy und Astrophysics
Section Astronomy

July 2004

FLUCTUAT NEC MERGITUR

for my parents

Elvira and Joachim

Contents

List of Tables

List of Figures

Kurzfassung

Die meisten bekannten Akkretionsscheiben in Doppelsternsystemen haben eine wasserstoffreiche Zusammensetzung und in nur wenigen System findet man heliumreiche Scheiben. Momentan sind elf dieser nach ihrem Prototyp AM CVn benannten Kataklysmischen Veränderlichen bekannt, in denen der Donorstern ein entarteter Heliumstern ist.

Vor einigen Jahren wurde die Existenz einer anderen Art von Doppelsternsystemen voraus gesagt, in denen die Scheibe H und He frei sein sollte. Inzwischen hat man sechs dieser Systeme gefunden, deren Scheibe hauptsächlich aus Metallen wie O, Ne und Mg (Juett, Psaltis & Chakrabarty 2001; Schulz et al. 2001) besteht, was darauf schließen läßt, daß der Donorstern der Kern eines C/O Weißen Zwerges ist. Dabei ist die Überhäufigkeit von Ne auf Diffusionsprozesse (Yungelson, Nelemans & van den Heuvel 2002) zurückzuführen, die vor Beginn des Massenübertrags durch Roche Lobe Overflow im Weißen Zwerg stattfanden. Aufgrund der Tatsache, daß die Komponenten des Systems sehr kompakte Objekte sind, was wiederum dazu führt, daß das ganze System äußerst kompakt ist, bezeichnet man solche Systeme als ultra-kompakte Doppelsternsysteme.

Die Bestimmung der Häufigkeiten von chemischen Elementen durch quantitative Spektroskopie und den Vergleich mit synthetischen Spektren aus Modellrechnungen ist sehr wichtig, um die Entwicklung solcher Binärsysteme und den inneren Aufbau von Weißen Zwergen zu verstehen.

Der prominenteste dieser ultra-kompakten Doppelsternsysteme ist der LMXB (low mass X-ray binary) 4U 1626-67. Das System besteht aus einem 7.66 s Röntgenpulsar mit einem Weißen Zwerg von ca. $0.02\,M_\odot$ (Chakrabarty 1998) als Begleiter. Der Neutronenstern besitzt ein starkes Magnetfeld, welches von Orlandini et al. (1998) anhand von Zyklotronresonanzlinien zu $\sim 3\times10^{12}$ G bestimmt wurde. Das System hat eine kurze Bahnperiode von nur ca. 42 min (Middleditch et al. 1981), was ein starkes Indiz dafür ist, daß der Begleiter extrem wasserstoffarm sein muss (Paczynski & Sienkiewicz 1981).

Chakrabarty (1998) ermittelte eine Röntgenleuchtkraft von ungefähr $7\times10^{36} \lesssim L_x \lesssim 5\times10^{37}$erg s^{-1}, womit man eine Akkretionsrate von ca. $2\times10^{-10}\,M_\odot\,\mathrm{yr}^{-1}$ erhält. Das Doppelsternsystem hat bei einem Bahnabstand von nur 300 0000 km (Schulz et al. 2001)und eine ziemlich große Akkretionsscheibe, die vom Gezeitenradius bei 200 000 km bis hinein zum Korotationsradius bei 6 500 km reicht, wo die Scheibe durch das Magnetfeld des Neutronensterns zerstört wird.

In solch kompakten Doppelsternsystemen kann man die äußere Bestrahlung der Akkretionsscheibe durch die Röntgenstrahlung, welche durch die Akkretion auf die Polkappen des Neutronensterns entsteht, nicht mehr vernachlässigen. Weite Teile des Scheibenspektrums sind durch Effekte, welche die Bestrahlung verursacht, dominiert. Als Beispiel kann man hier zuerst Emissionslinien von hochionisierten Elementen, wie O V oder C IV nennen.

Eines der größten numerischen Probleme, welches bei der Berechnung von bestrahlten Akkretionsscheibenmodellen auftritt, ist die ungewöhnliche Temperaturschichtung und Struktur der

Scheibe, welche starke Probleme mit den Besetzungszahlen der atomaren Energieniveaus in unterschiedlichen Tiefen mit sich bringt. Durch die Implementierung eines so genannten tiefenabhängigen Modellatoms sollen diese Probleme in meiner Diplomarbeit gelöst werden.

In der Dissertation von Nagel (2003) wurde das Programm-Paket ACDC entwickelt, mit dem man die Vertikalstruktur und das synthetische Spektrum einer Akkretionsscheibe berechnen kann.

Dazu wird eine radiale Scheibenstruktur entsprechend dem α-Scheiben-Ansatz von Shakura & Sunyaev (1973) angenommen und die Scheibe anschließend in eine Zahl konzentrischer Ringe zelegt. Für diese werden dann, unter der Annahme von plan-paralleler Symmetrie, die Gleichungen des hydrostatischen- und des radiativen-Gleichgewichts zusammen mit den non-LTE Ratengleichungen und dem Strahlungstransport gelöst. Dabei wird die beschleunigte Lambda Iteration (ALI) (Werner & Dreizler 1999) verwendet. Die kinematische Viskosität wird durch die Reynoldszahl parametrisiert, wobei für den vertikalen Verlauf die Beschreibung von Hubeny & Hubeny (1998) verwendet wird.

Während der Diplomarbeit wurde ein tiefenabhängiges Modellatom (DEPTOM) entwickelt und als Programm-Modul in den ACDC-Code implementiert. DEPTOM vergleicht die Besetzungszahlen der einzelnen Ionisationsstufen während der ALI-Iteration mit einem unteren Limit. Liegt der Wert einer Besetzungszahl mehrmals unter diesem von außen vorgegebenen Limit, so wird die Ionisationsstufe im Ratengleichungssystem ausgeschaltet. Dies kann nicht durch auf Null setzen der entsprechenden Gleichung erfolgen. Es ist notwendig die Ionisationsstufe komplett aus der Ratenmatrix zu entfernen, da sich diese sonst nicht mehr invertieren läßt. Das Entfernen eines Teils der Ratenmatrix ist aber mit erheblichem Aufwand verbunden, da sicher gestellt werden muss, daß die Zuordnung von Übergangen und Atomniveaus im weiteren Iterationsprozess stimmt.

DEPTOM ist in der Lage, Ionisationsstufen, die numerische Probleme erzeugen, zu erkennen und aus der Berechnung zu nehmen. Dadurch ist ACDC stabiler und etwas leistungsfähiger geworden.

Es ist nun erstmals möglich ein Modell einer bestrahlten Akkretionsscheibe, die von 6 500 km bis 100 000 km reicht, mit ein und demselben Modellatom zu rechnen. Dies entspricht einem Temperaturbereich von 14 000 K bis 500 000 K. Die Struktur und Temperaturschichtung der Scheibe hat nun ein glatten Verlauf und zeigt keine Schwankungen mehr, die auf numerische Instabilitäten hindeuten.

Abstract

Most of the known accretion discs in binary systems are composed of hydrogen rich material. Only a very small number of systems is known, in which a helium rich accretion disc is found. Today eleven of this cataclysmic variables, named after the prototype AM CVn, are known.

A few years ago, a new type of binary system was predicted, in which the disc is supposed to be free of hydrogen and helium. Nowadays six systems are known, with an accretion disc principally composed of C, O, Ne and Mg (Juett, Psaltis & Chakrabarty 2001; Schulz et al. 2001). This fact leads to the assumption, that the donor star is a white dwarf with a C / O core. The over abundance of Ne, found in these systems, is due to diffusion processes in the history of the white dwarf.

To determine the abundances of the chemical species, using quantitative spectral analysis is very useful to learn more about the evolution of binary systems and the constitution of white dwarfs.

The most prominent representative of these ultra compact binary systems is the LMXB (low mass X-ray binary) 4U 1626-67. The system is consisting of a 7.66 s X-ray pulsar as primary component and a $0.02\,M_\odot$ as secondary (Chakrabarty 1998). The fairly high magnetic field strength of the neutron star ($\sim 3 \times 10^{12}$ G) was measured by Orlandini et al. (1998) using cyclotron resonance lines. The rather short binary period of about 42 min suggests that the companion must be very hydrogen poor (Paczynski & Sienkiewicz 1981).

Chakrabarty (1998) calculated a X-ray luminosity of $7 \times 10^{36} \lesssim L_x \lesssim 5 \times 10^{37}$ erg s^{-1}. Therewith one gets an accretion rate of about $2 \times 10^{-10}\,M_\odot\,yr^{-1}$. Having a binary separation of only 300 0000 km (Schulz et al. 2001), the system has a quite huge accretion disc. The disc is extended from the co-rotation radius at 6 500 km, where the strong magnetic field of the X-ray pulsar destroys the disc, to the tidal radius at 200 000 km.

In such compact binary systems one can not neglect the external irradiation of the accretion disc by the neutron star. The external irradiation dominates the disc spectrum over a wide range. One may find emission lines of highly ionised elements, like O V or C IV.

One of the biggest numerical problems, occurring during the calculation of an irradiated accretion disc model, is the non-common temperature stratification and structure. This causes severe problems with the occupation numbers of some atomic levels. These problems should be solved by implementing the depth dependent model atom, during my thesis work.

During his PhD thesis, Nagel (2003) has developed the numeric code package ACDC. Therewith one can calculate the vertical structure and the emergent synthetic spectrum of an accretion disc.

By assuming a radial disc structure corresponding to the α-disc approach of Shakura & Sunyaev (1973), the disc is separated in a set of concentric disc rings. Afterwards, assuming plane-parallel geometry, the equation of hydrostatic and radiative equilibrium are solved consistently together with non-LTE rate equations and the radiation transfer equation. Therefore the ALI method (accelerated

lambda iteration, Werner & Dreizler (1999)) is used. The kinematic viscosity is parameterised by the Reynolds number. The vertical run of the viscosity is taken from Hubeny & Hubeny (1998).

During the work presented here the depth dependent model atom (DEPTOM) was developed and implemented in ACDC as a code module. DEPTOM is comparing the occupation numbers of every ionisation stage, during the ALI iteration, to a lower limit. Ionisation stages which are several times below the limit, are deactivated. This could not be done by setting the corresponding rate equation to zero, because then the rate matrix could not be inverted any more. The associated parts of the rate matrix system have to be cut out, which is difficult. One has to assure that the corelation between the atomic levels and the transitions is still true.

DEPTOM identifies the trouble making ionisation stages and deactivates them. Thus the calculation is numerical more stable and ACDC is more powerful.

Now, it is possible to calculate a disc model from 6 500 km to 100 000 km, using the same model atom. Thereby a temperature range from 14 000 K up to 500 000 K is covered by the disc model. The structure and the temperature stratification of the disc model shows no longer features, which are connected to numerical instabilities.

Part I

Introduction

Chapter 1

Motivation

1.1 The Dawn of Astronomy

Sapere aude (Kant 1781)! Ever since the dawn of mankind, human beings were fascinated by the myriads of white and coloured lights at the black velvety night sky above them. They inspired them to ask questions, like *where do we come from and where do we go*. Hence mankind started to study the positions of objects at the night sky and the objects themselves. Astronomy was born as the oldest natural science and one of the oldest cultural possessions of humanity.

Millennia later some of the stars were found to vary their brightness, which caused fear, because the sky was the only thing believed not to change. But this made variable stars very interesting for the astronomers, of that time. They are still interesting today, especially those which are a binary star system with a compact object like an white dwarf, a neutron star or a black hole.

These systems are often so close, that they undergo roche lobe overflow (see section 2.2) and therefore have an accretion disc. Due to the fact that accretion is the most effective physical way to release energy, the disc generates tremendous luminosity, sometimes a hundred thousand times the solar value.

1.2 The Designation of this Thesis

The first part of my thesis work was to develop the code for a so called depth dependent model atom to avoid numerical problems and implement this code into the non-LTE accretion disc model code ACDC (Nagel 2003). If the accretion disc is irradiated, one will get an unusual temperature structure in the disc. Namely one will get very hot outer layers of the disc. Inside one will find an temperature structure like in the non-irradiated case with a transition layer lying in between. Now in the hot parts of the disc, the low ionisation stages of the model atom will be occupied very weakly, as in the cooler parts of the disc the high ionisation stages will be occupied very weakly. These very weakly occupied ions cause grave numerical problems solving the rate equation matrix. The depth dependent model atom identifies the trouble making ions in dependence of the depth grid and deactivates them, to prevent problems with the inverting of matrix.

The second part of this thesis work was to compare the modified code with the standard version of ACDC, when calculating models for irradiated discs in ultra compact binary systems, like the soft X-ray source 4U 1626-67. Recently, a couple of these ultra compact binaries were discovered, in which the disc is mainly composed of metals like carbon, oxygen and neon. The donor stars seem to be white dwarfs with C/O-cores, whereas the accreting objects are neutron stars. They all

have orbital periods well below the orbital period minimum of cataclysmic variables (e.g. 4U 1626-67 ~ 42 min, see Middleditch et al. (1981)). To study the evolutionary history of the binary system and the internal structure of the white dwarf progenitor it is necessary to determine the metal abundances by quantitative spectral analysis of the disc spectra.

In the chapters of part I of my thesis I will first give a very short introduction on accretion discs in binary systems and low mass X-ray binaries (LMXBs). Then I will give a short but complete overview over non-LTE accretion disc modelling.

In the part II the theory of non-LTE rate equation systems will be described in an accurate way and it will be shown that the Newton-Raphson-Iteration is an adequate method to solve the non-LTE rate equation system. I will also discuss the special implementation used in the codes at the IAAT.

Afterwards in part III the depth dependent model atom (DEPTOM) will be introduced. There I will discuss the basic ideas of the DEPTOM and some of the problems implementing it. I will also describe all new developed code subroutines as well as the things that I have changed in existing ACDC subroutines.

At last in part IV of the thesis I like to show accretion disc models and synthetic spectra for the ultra compact LMXB 4U 1626-67 and 4U 0614+091, that I have calculated with the modified ACDC code. The advantages and potentialities of the new ACDC code and the DEPTOM will be discussed in this part, too.

Chapter 2

Accretion Discs in Binary Systems

2.1 Binary Star Systems

There is an innumerable number of stars in the universe, our home galaxy has already billions, and most of them are not alone. They have one (binary star systems) or more companions (multiple star systems). If the system contains more than half a dozen stars, you won't call it a multiple system, but a star cluster. No sharp defined borderline is dividing the two concepts.

For my thesis close binary systems are the important ones. If there is a close pair of stars in a multiple system, you can neglect the remote components of the system and handle the pair as a close binary system.

Close binary systems can exist in four basic configurations: detached systems, semi detached systems, contact binary systems and systems with a common envelope. Figure 2.1 elucidates the four different cases.

If the system is semi detached and one component is a compact star like a white dwarf, a neutron star or a black hole, roche lobe overflow will occur and usually an accretion disc is formed. This is explained in the next section.

2.2 Roche Lobe Overflow and Accretion

The roche lobe is defined as the first common equipotential line of two massive bodies in the Co-rotating coordinate system. Studying the stabilities of planet moons Edouard Roche, a French mathematician and astronomer of the nineteenth century, originally found the roche potential associated with the roche lobe. The roche potential can be written in the following expression

$$\Phi_R(\vec{r}) = -\frac{GM_1}{\|\vec{r}-\vec{r}_1\|} - \frac{GM_2}{\|\vec{r}-\vec{r}_2\|} + \frac{1}{2}(\omega\Lambda\vec{r})^2 \qquad . \tag{2.1}$$

The ω denotes the keplerian orbital frequency

$$\omega = \left[\frac{G(M_1+M_2)}{a^3}\right]^{\frac{1}{2}} \cdot \vec{e} \qquad . \tag{2.2}$$

Note that G denotes the gravitational constant, M_x the masses of the two stars and a the distance of the major axis of the binary system's orbit. The roche potential is plotted in Figure 2.2 and Figure 2.3.

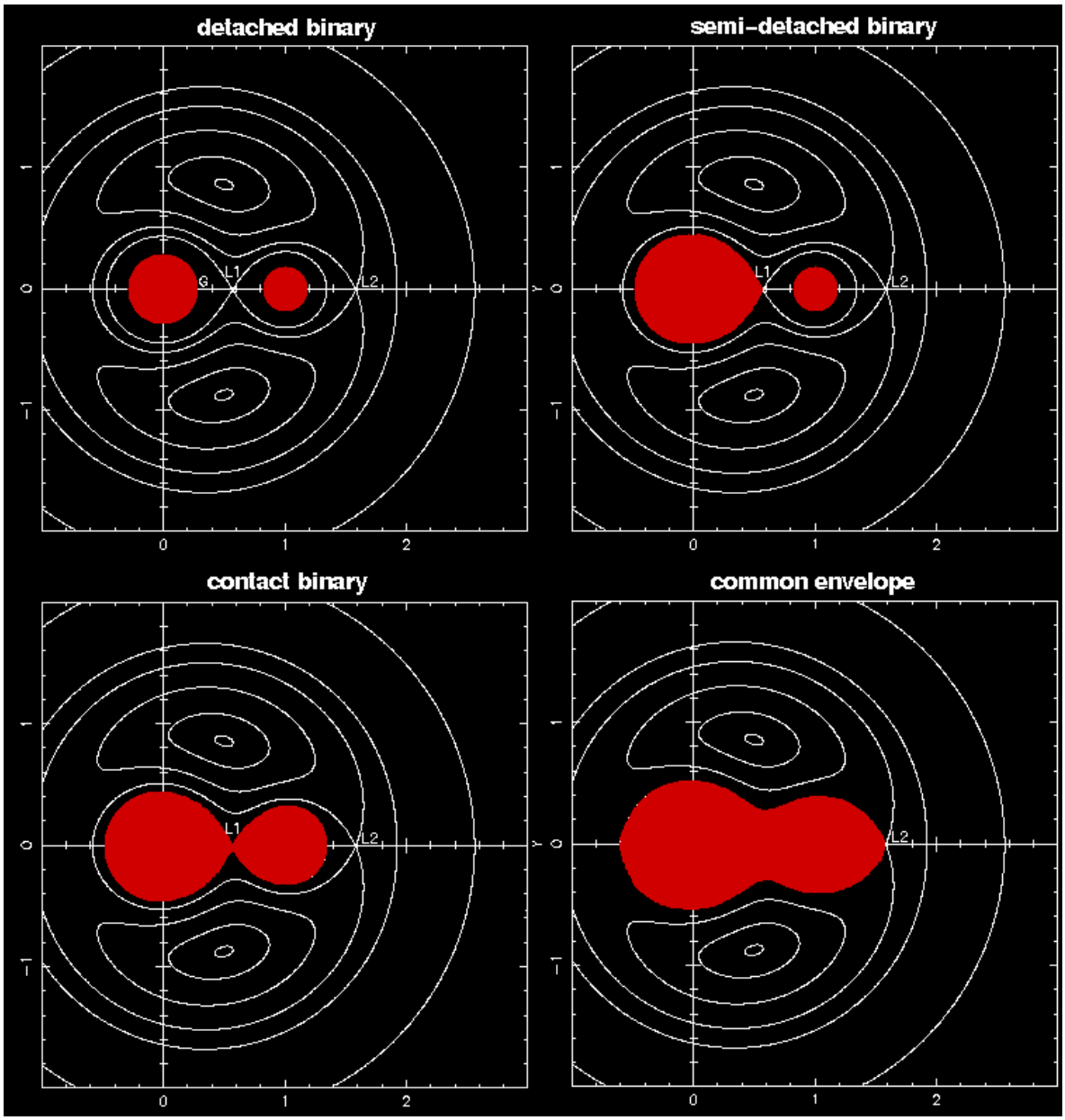

Figure 2.1: Types of binary star systems

(Dhillon 2001)

If one of the two companions fills its roche lobe, due to evolution as a red giant or due to orbit shrinking, material can flow to the other component. Because of conservation of angular momentum the material can not fall straight onto the primary, but orbits it. An accretion ring is formed, which will elapse to a thin accretion disc, due to inner friction. One calls an accretion disc thin if its diameter is much bigger than its vertical dimension.

The inner friction is responsible for transport of angular momentum to the outer parts of the disc and for conversion of potential energy into heat. The thermal energy is transported to the surface of the disc and then radiated away. This mechanism allows the compact member of the binary system

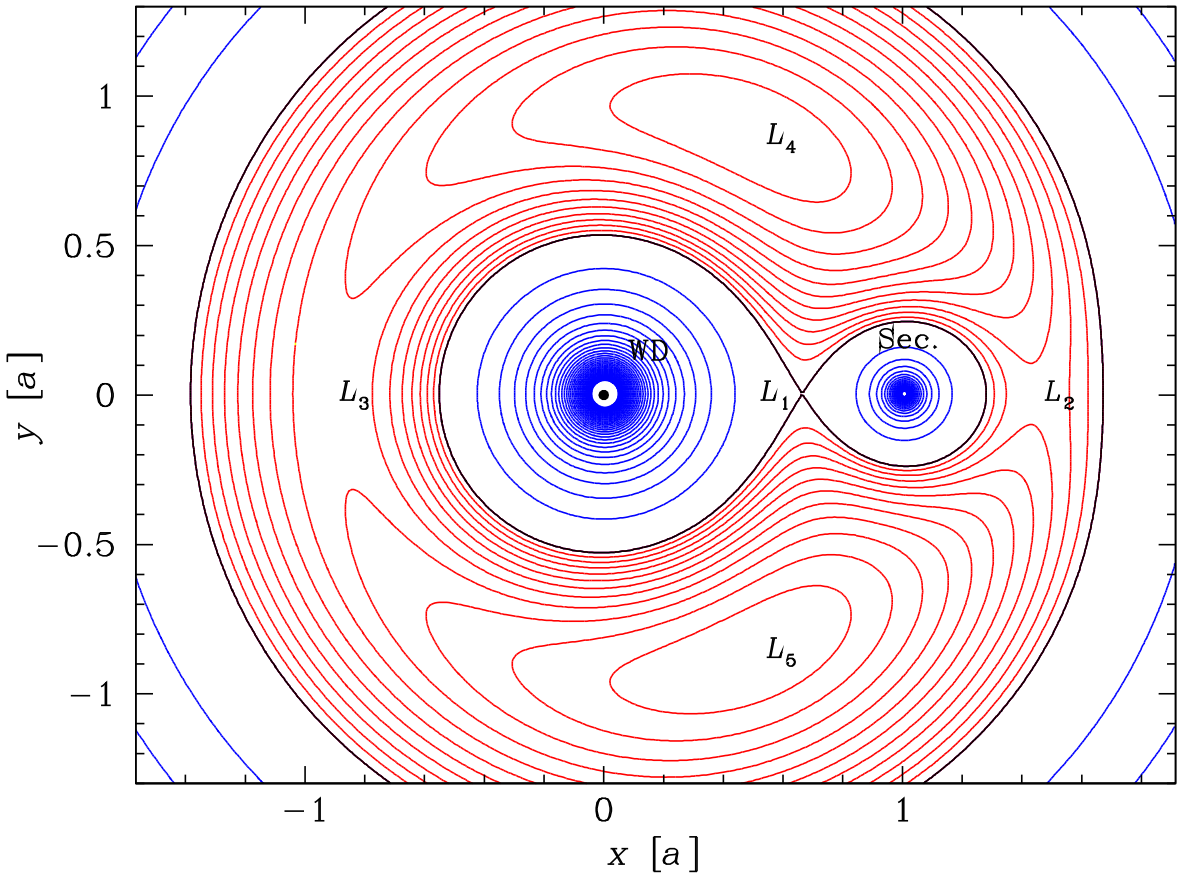

Figure 2.2: Equipotential lines of a binary system with a mass ratio of 5.0 (Kube 2002)

to accrete material. As mentioned at the beginning (section 1.1), accretion is the most effective way to produce energy. One can convert into energy up to 15% of the rest mass, which is more than twenty times the value you can get by the fusion of hydrogen to helium. Accretion is one of the most important astrophysical processes known. It drives almost all of the high power processes in the universe, e.g. Active Galactic Nuclei (AGN) and it is responsible for lot of other phenomena. In nearly every accretion phenomenom, one will find an accretion disc. It can clearly be said that accretion discs are one of the most frequently things in the universe. A very good review over accretion phenomena is given by Frank, King & Raine (2002).

One class of objects with accretion discs are the cataclysmic variable stars. In all cases a white dwarf accretes material from a companion, typically a regular star. This is usually done with an accretion disc, except in one subclass called polars. There the strong magnetic field lines of the white dwarf lead the material directly to the magnetic poles. Thus no accretion disc is formed. Cataclysmic variable stars and all their exciting phenomena are best described in Hellier (2001). The next three mentioned phenomena are cataclysmic variables.

One of the phenomena, where accretion discs are directly responsible for, are dwarf novae. There the white dwarf accretes material from its companion with an accretion rate, where instabilities in the disc structure occur. During these instabilities the inner friction of the disc changes nearly instantaneously. Due to that the accretion rate and the energy release in the disc jumps up, and a dwarf nova

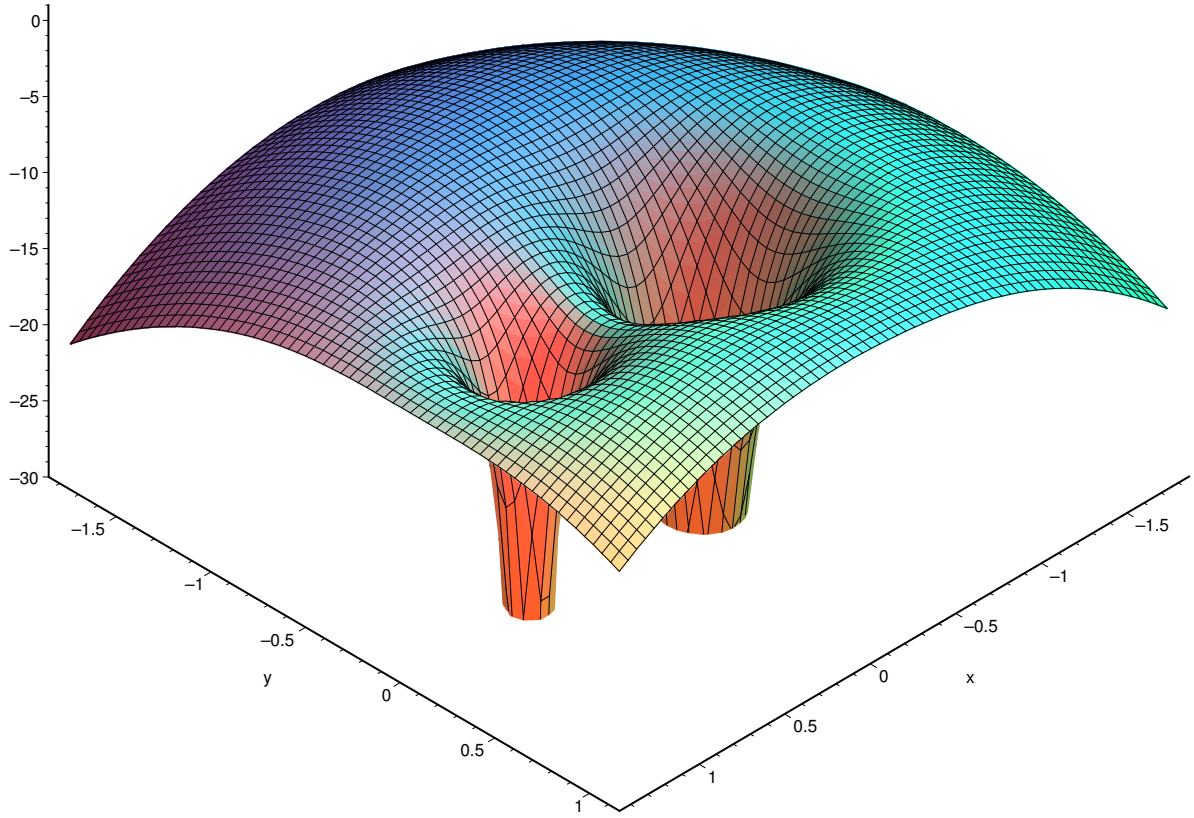

Figure 2.3: 2D Plot of the equipotential surface of a binary star system with a mass ratio of 2.5

outburst can be seen.

Another thing related to cataclysmic variables are novae. The white dwarf accretes material upon a low rate. Thus the material, generally hydrogen, degenerates during its accumulation on the white dwarf's surface. From time to time the bottom of the degenerated hydrogen layer initiates explosive nuclear burning and the following explosion leads to a nova eruption.

If the accretion rate is higher, the material will not degenerate on the surface, but will be constantly burned thermonuclear to helium. Whensoever the mass of the white dwarf is near Chandrasekhar's limit at $1.44\,M_\odot$ [1], this enables itself to grow over it. The following collapse will trigger thermonuclear runaway burning processes in the degenerated carbon core of the white dwarf. It will explode as a type Ia supernova.

Another class of objects related to accretion disc, are X-ray binaries. Everything one has to known about them can be found in Lewin, van Paradijs & van den Heuvel (1995). X-ray binaries are divided in two subclasses, low mass X-ray binaries (LMXBs) and high mass X-ray binaries (HMXBs). In the first case the companion is a star with approximately one solar mass. Is the companion an early type star with several solar masses, one would call the system a high mass X-ray binary.

Another way to classify X-ray binaries is to have a closer look at the accreting compact object. First there are objects with a mass below $\sim 2.5\,M_\odot$, which is the so called Oppenheimer-Volkoff limit. These objects are often found to pulsate in X-rays and turn out to be accreting neutron stars, surrounded by an accretion disc. Examples are the famous source Her-X1 or the object I am interested in, 4U1626-67. For these objects one can measure the strength of the magnetic field by analysing

[1] $M_\odot$, i.e. one solar mass, is equivalent to 1.989×10^{33} g (Zimmermann & Weigert 1999)

cyclotron resonance lines of electrons in the magnetic field, as first done by Trümper et al. (1978).

The other ones having a mass above the Oppenheimer-Volkoff limit and are accreting black holes surrounded by an accretion disc. They often have strange behaviours, most of them are highly time variable, e.g. Cyg-X1. Some of them, e.g. SS 433 (Hjellming & Johnston 1988), seem even to have sorts of jets, gaseous outflows along the rotation axis of the accretion disc. They show the same behaviour as small AGN, thus they are called micro quasars.

The last class of objects with an accretion disc on completely different scales, are active galactic nuclei. They suppose to be super massive black holes with up to billions of solar masses in the centre of galaxies. The black holes are surrounded by huge accretions discs, which generates tremendous amounts of thermal energy resulting in upto 10^{15} solar luminosities.

Chapter 3

Accretion Disc Modelling

The first steps in stellar spectroscopy by Wollaston and Fraunhofer (1823) marked the beginning of the work on stellar atmospheres. Herschel first realized that the black lines in the spectrum seen by Wollaston and Fraunhofer, today they are called Fraunhofer lines, were the finger prints of the chemical species in the stars. It took decades until Kirchhoff and Bunsen developed the theory of spectral analysis. After that, beginning with the work of Father Secchi, stars where classified after their spectral shape by Cannon & Pickering (1918). Hertzsprung (1911) and Russell (1913) completed the development by plotting the spectral type against the absolute magnitude in a diagram [2].

Shortly after the creation of quantum mechanics and the development of the first electronic computers Albrecht Unsöld started working on the theory of stellar atmospheres (e.g., Unsöld 1930, 1934). He was also a pioneer of stellar atmosphere modelling with numerical methods.

Five years after the discovery of Sco-X1, the first extra solar X-ray source, Shklovsky (1967) suggested that those X-ray sources are powered by accretion. This concept was originally suggested by Salpeter (1964) as power source for quasars. Finally, Shakura & Sunyaev (1973) founded the standard theory of accretion discs.

Since the non-LTE accretion disc modelling is a relatively new astrophysical domain (Hubeny & Hubeny 1997; Nagel 2003), the general overview in this chapter is mainly based on the lectures *Physik der Sternatmosphären I + II*. The lectures were given by Prof. Dr. K. Werner during the semesters in winter and summer 2000 / 2001 at the University Tübingen. One may find more informations in the literature of stellar atmosphere modelling, e.g. the lecture script R.J. Rutten (2000).

Solving the radiative transfer equation in full three dimension is extremely computing intensive. Therfore the disc in ACDC (Nagel 2003) is assumed to be rotational symmetric and then divided in several concentric disc rings. For those disc rings the equation of hydrostatic and radiative equilibrium are solved consistently together with non-LTE rate equations, under assumption of plane-parallel symmetry. Therefore the ALI method (accelerated lambda iteration, Werner & Dreizler (1999)) is used. The kinematic viscosity is parameterised by the Reynolds number and the vertical characteristic is taken from Hubeny & Hubeny (1998).

[2] Note that the Hertzsprung-Russell-Diagram (HRD) is plotted today the other way round.

3.1 The Radiation Field

By defining the specific intensity field.

$$I_\nu(\nu,\vec{n},\vec{r},t) := \frac{\Delta E}{\Delta\nu\,\Delta t\,\Delta\omega\,\Delta\sigma} \quad , \tag{3.1}$$

one can describe the macroscopic radiation. Hereby E_ν is the energy of the radiation field

- in frequency interval $[\nu,\nu+\Delta\nu]$
- in the time interval $[t,t+\Delta t]$
- at the solid angle $\Delta\omega = sin\,\theta\,\Delta\theta\,\Delta\phi$ around $\vec{n}$
- through the surface element $\Delta\sigma = \Delta A\ cos\,\theta$ (at the position $\vec{z}\perp\vec{n}$)

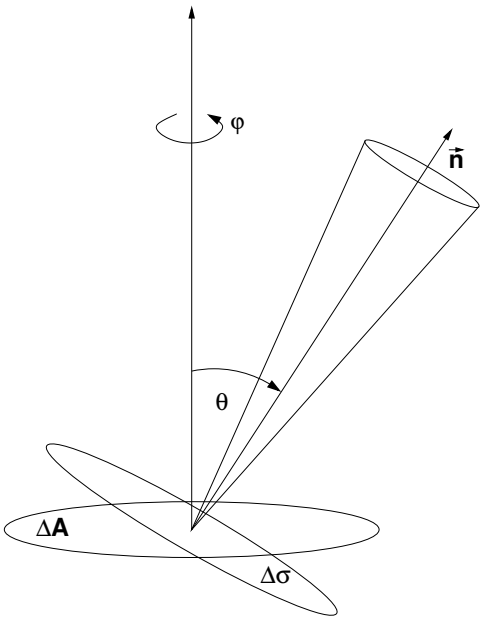

Figure 3.1: Sketch of the parameters defining the radiation field

The geometrical definition of the surface element is shown in Figure 3.1. Note that polarisation is not considered. This would be necessary in presence of strong magnetic fields, like on neutron stars (e.g. Deetjen 2002).

Usually two geometries are used in stellar atmospheres. If the atmosphere is thin compared to the radius of the star (e.g. solar type stars), plane-parallel geometry

$$I_\nu = I_\nu(\nu,\mu,z) \tag{3.2}$$

is used, if not (e.g. Red Giants) one will use spherical symmetry

$$I_\nu = I_\nu(\nu,\mu,r) \quad . \tag{3.3}$$

In both cases μ is defined as

$$\mu := cos\,\theta \qquad . \tag{3.4}$$

In the accretion disc modelling code ACDC, only the plane-parallel geometry (shown in Figure 3.2) is adopted. The next step is to define the angular integrals or moments of intensity.

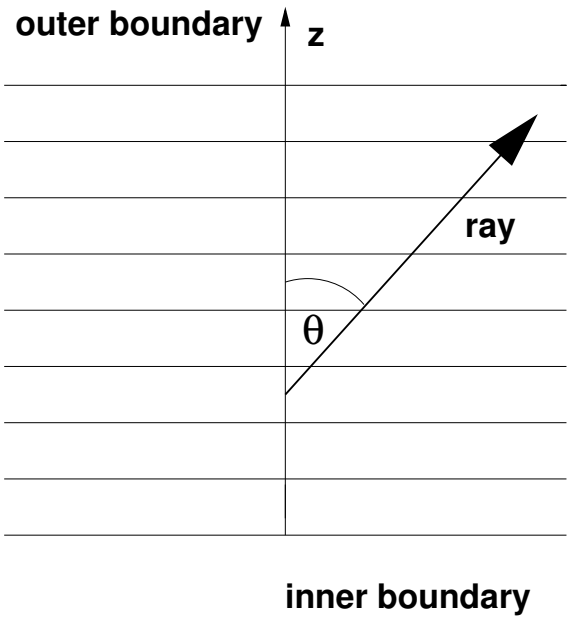

Figure 3.2: The plane-parallel geometry

1. I_ν, incident intensity, zeroth moment of intensity.
2. J_ν, mean intensity, first moment of intensity.
3. H_ν, Eddington flux, second moment of intensity.
4. K_ν, K integral, third moment of intensity.

$$J_\nu(z) = \frac{1}{2}\int_{-1}^{+1} I_\nu d\mu \tag{3.5}$$

$$H_\nu(z) = \frac{1}{2}\int_{-1}^{+1} \mu I_\nu d\mu \tag{3.6}$$

$$K_\nu(z) = \frac{1}{2}\int_{-1}^{+1} \mu^2 I_\nu d\mu \tag{3.7}$$

Using the moments of intensity the energy density can be defined as

$$\begin{aligned} u_\nu &= \frac{4\pi}{c} J_\nu \\ u &= \int_{\nu=0}^{\infty} u_\nu d\nu \\ &= \int_{\nu=0}^{\infty} \frac{4\pi}{c} J_\nu d\nu \quad . \end{aligned} \tag{3.8}$$

For the special case of an isotropic radiation field, one can express the radiation pressure by the energy density

$$P_r(\nu) = \frac{1}{3} u_\nu \quad . \tag{3.9}$$

The flux of radiation

$$\vec{\mathcal{F}}_\nu = \oint_{4\pi} I_\nu(\vec{n}) \vec{n} d\omega \tag{3.10}$$

is connected to the first moment of intensity.

Assuming plane-parallel geometry in a one dimensional accretion disc ring, one will find

$$\begin{aligned} \mathcal{F}_{\nu,x} &= \mathcal{F}_{\nu,y} = 0 \\ \mathcal{F}_{\nu,z} &= \int\int I_\nu \, n_z \, d\omega \\ n_z &= cos\,\theta, \quad d\omega = sin\,\theta \, d\theta \, d\phi \\ \mathcal{F}_{\nu,z} &= \int\int I_\nu \, cos\,\theta \, sin\,\theta \, d\theta \, d\phi \quad . \end{aligned} \tag{3.11}$$

Using Equation 3.11 together with Equation 3.4, we get

$$\begin{aligned} \mathcal{F}_\nu &:= \mathcal{F}_{\nu,z} = 2\pi \int_{-1}^{+1} I_\nu \mu \, d\mu = J_\nu \\ \mathcal{F}_\nu &:= \pi \cdot F_\nu \\ \mathcal{F}_\nu &:= 4\pi \cdot H_\nu \quad . \end{aligned} \tag{3.12}$$

Thereby, F_ν is the astrophysical flux and H_ν the so called Eddington flux. Note, the astrophysical flux is introduced, because it is equivalent to the accretion disc flux. Due to the fact, that no accretion disc was resolved until today, one can only observe the disc averaged flux. Only the sun and a few other stars (e.g. Betelgeuse in the Orion) can be observed as a resolved objects.

Now, one has to define the luminosity, which is the sum of the radiation over the complete spectral range of a star. Therefore one has to integrate over all frequencies

$$\mathcal{F} = \int_0^{\infty} \mathcal{F}_\nu \, d\nu \quad . \tag{3.13}$$

Afterwards one can write down the definition of the luminosity. Note that *in* and *out* denotes the inner and outer radii of the disc.

$$\begin{aligned} L &:= 2\pi \left(R_{\text{out}}^2 - R_{\text{in}}^2 \right) \mathcal{F} \\ &:= 2\pi^2 \left(R_{\text{out}}^2 - R_{\text{in}}^2 \right) F \\ &:= 16\pi^2 \left(R_{\text{out}}^2 - R_{\text{in}}^2 \right) H \end{aligned} \tag{3.14}$$

Luminosities of cosmic objects can vary over a wide range, from $10^{-5}\,L_\odot$[3] for the faintest stars over $10^5\,L_\odot$ for X-ray binaries up to tremendous $10^{15}\,L_\odot$ for the most powerful AGN.

Radiation of a source in thermal equilibrium is something special. In that case the source is called a black body. The radiation field is isotropic, homogenous, time independent and nonpolarised

$$I_\nu = I_\nu(\nu, \vec{n}, \vec{r}, t) = B_\nu(\nu, T) \tag{3.15}$$

and the intensity is described by the Kirchhoff-Planck function

$$B_\nu(\nu, T) = \frac{2h\nu^3}{c^2}\left[e^{\frac{h\nu}{kT}} - 1\right]^{-1} \quad , \tag{3.16}$$

shown in Figure 3.3.

The Kirchhoff-Planck function contains the following natural constants:

c is the speed of light[4]

h is the Planck constant[5]

k is the Boltzmann constant[6]

The Planck function can be characterised by two other important physical laws. First by the Wien's law, which gives the position of the emission maximum

$$\nu_{\max} = 2.8214\frac{kT}{h} \quad , \tag{3.17}$$

secondly by the Stefan-Boltzmann radiation law, which describes total (frequency integrated) emission

$$B_{\max}(T) = \frac{\sigma}{\pi}T^4 \quad . \tag{3.18}$$

σ[7]$= \frac{2\pi^5 k^4}{15c^2h^3}$ denotes the Stefan-Boltzmann constant.

The last important astrophysical variable one has to define, is the so called effective temperature T_{eff} of an object.

$$T_{\text{eff}} := \left(\frac{L}{4\pi\sigma}\right)^{\frac{1}{4}} \cdot R^{-\frac{1}{2}} \tag{3.19}$$

T_{eff} is the temperature of a black body having the same astrophysical flux as the object.

[3] $L_\odot$, i.e. one solar luminosity, is equivalent to $3.847 \times 10^{33}\,\text{erg}\,\text{s}^{-2}$ (Zimmermann & Weigert 1999)

[4] c is equivalent to $2.997925 \times 10^{10}\,\text{cm}\,\text{s}^{-2}$ (Bronstein et al. 1999)

[5] h is equivalent to $6.626076 \times 10^{-27}\,\text{erg}\,\text{s}$ (Bronstein et al. 1999)

[6] k is equivalent to $1.380658 \times 10^{-16}\,\text{erg}\,\text{K}^{-2}$ (Bronstein et al. 1999)

[7] σ is equivalent to $5.67051 \times 10^{-5}\,\text{erg}\,\text{cm}^{-2}\,\text{s}^{-2}\,\text{K}^{-4}$ (Bronstein et al. 1999)

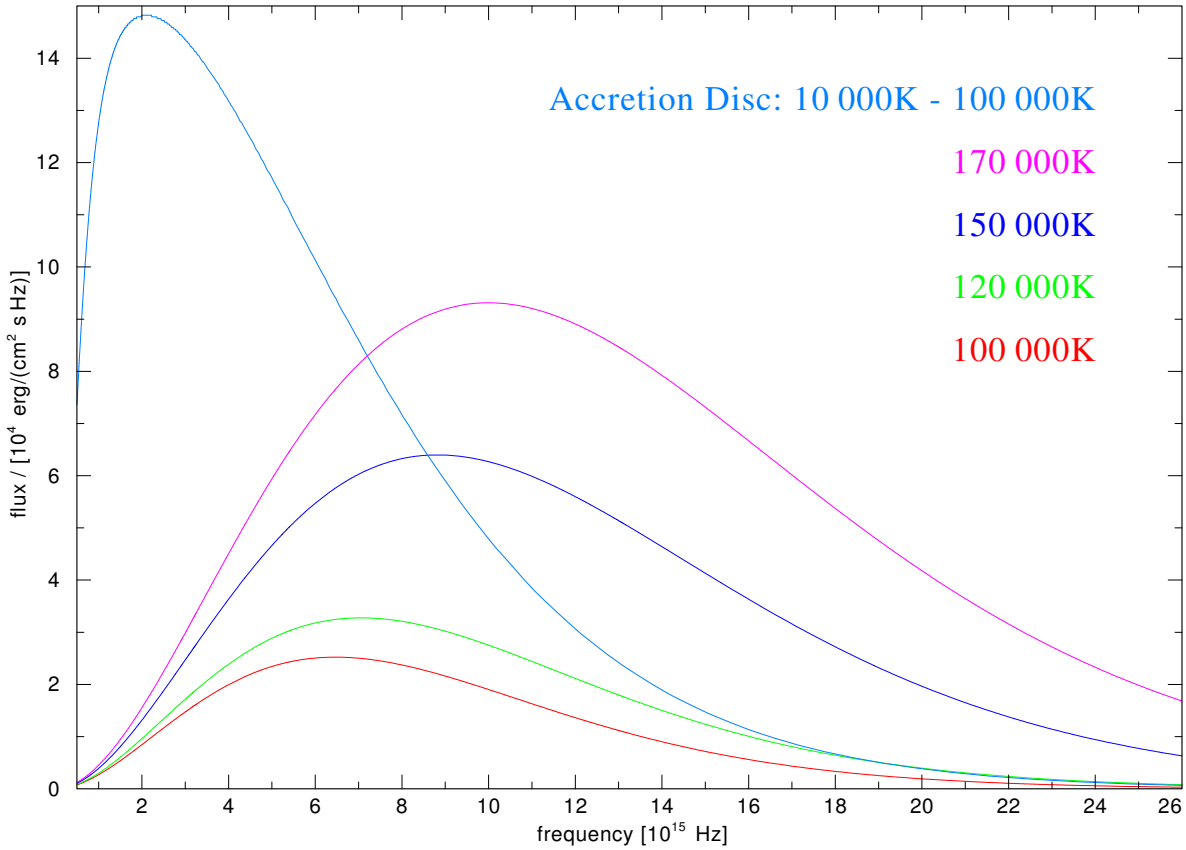

Figure 3.3: The Planck function for different temperatures

3.2 The Radiation Transport

In this section the transport of radiation through a medium, in the case of an accretion disc through plasma, will be described. If radiation passes through material, energy can be detracted from or added to the radiation field.

This procedure can be divided into several different physical processes:

1. real absorption $\longrightarrow$ photon annihilation, the energy goes into the plasma
   (a) photo-ionisation ('bound-free-absorption')
   (b) photo-excitation ('bound-bound-absorption')
2. real emission $\longrightarrow$ photon production, the energy is deprived from the plasma
   (a) photo-recombination ('bound-free-emission')
   (b) photo-emission ('bound-bound-emission')

3. scattering $\longrightarrow$ the photon interacts with a scattering centre, changes its direction, but hardly its energy (frequency) and therefore only a small energy transfer with the plasma

   (a) elastically scattering at free electrons

   $\longrightarrow$ Thomson scattering, scattering without energy exchange

   $\longrightarrow$ Compton scattering, scattering with energy exchange

Note that there is one process missing, the fluorescence, which is in fact a mixture of processes mentioned before.

Now the radiation transfer equation (RTE) can be prepared. On the right hand side of the RTE, one finds the specific intensity, which can be expressed in different geometries. For the Intensity in plane-parallel geometry one finds

$$I_\nu = I_\nu(\ell,\mu) \quad , \tag{3.20}$$

whereas ℓ denotes the geometrical depth. The geometrical depth is connected to the path s of an optical ray by

$$d\ell = \mu ds \quad . \tag{3.21}$$

Inserting Equation 3.21 in Equation 3.20 leads to

$$\frac{dI_\nu}{ds} = \frac{dI_\nu}{d\ell}\mu \quad . \tag{3.22}$$

Thereafter the left hand side of the RTE has to be treated. On that side one has to consider a few special cases. Firstly the case without any absorption

$$\frac{dI_\nu}{ds} = 0 \quad \longrightarrow \quad T_\nu = \text{const.} \tag{3.23}$$

and secondly the case with absorption only. Then the loss of intensity is proportional to the overall intensity. That can be expressed as

$$dI_\nu = -\kappa I_\nu\, ds \quad . \tag{3.24}$$

In that case, κ[8] denotes the opacity or absorption coefficient. In the common case the opacity

$$\kappa = \kappa(\nu,\vec{r},\vec{n},t) \tag{3.25}$$

is a complex function of several variables of state. Nevertheless, one may find a coordinate system, in which the opacity is isotropic and therefor time independent. Then one can write

$$\kappa = \kappa(\nu,\vec{r}) \quad . \tag{3.26}$$

For plane-parallel geometry, the opacity can be written as

$$\kappa \;=\; \kappa(\nu,z) \quad . \tag{3.27}$$

At that point it is suggestive to introduce another, more useful depth variable. One of the problems of the geometrical depth ℓ is, that it is measured from the outer boundary to the centre plane of the

[8] κ has the dimension of $length^{-1}$ and the physical unit cm^{-1}

accretion disc. However, the outer boundary is not defined clearly. This can be solved by introducing the optical depth τ. For the case of absorption only, the RTE can be expressed as

$$\begin{aligned} \frac{dI_\nu}{ds} &= -\kappa I_\nu \\ -\mu\frac{dI_\nu(\nu,\mu,\ell)}{d\ell} &= -\kappa(\nu,\ell)I_\nu(\nu,\mu,\ell) \quad . \end{aligned} \tag{3.28}$$

By transforming $\ell \longrightarrow \tau(\nu)$[9], one gets the definition

$$d\tau := \kappa d\ell \quad . \tag{3.29}$$

As the standardisation constraint one may use $\tau = 0$ for $\ell = 0$. That leads to the dimensionless variable

$$\tau(\nu,\ell) = \int_{\ell=0}^{\ell} \kappa(\nu,\ell')d\ell' \tag{3.30}$$

and finally to another form of the RTE

$$\frac{dI_\nu(\mu,\tau)}{d\tau} = \frac{1}{\mu}I_\nu(\mu,\tau) \quad . \tag{3.31}$$

τ can be interpreted as the mean penetration depth of the photons in the accretion disc. Using that one can define the mean free path length

$$s_f = \frac{\ell_f}{\mu} := \frac{1}{\kappa} \quad . \tag{3.32}$$

The common case will be involving absorption and emission in the accretion disc. Emission can be handled as absorption with a negative algebraic sign. Therefore emission is like absorption proportional to the overall intensity. Thus one can write

$$dI_\nu = \eta_\nu\, ds \quad . \tag{3.33}$$

Here η_ν[10] denotes the emission coefficient, also called emissivity. The complete radiative transfer equation can be written as

$$\begin{aligned} \frac{dI_\nu}{ds} &= \eta_\nu - \kappa \cdot I_\nu \\ &= \kappa(S_\nu - I_\nu) \quad , \end{aligned} \tag{3.34}$$

if we define the source function S_ν as

$$S_\nu := \frac{\eta_\nu}{\kappa} \quad . \tag{3.35}$$

The complete RTE can be expressed in plane-parallel geometry with the geometrical depth ℓ and the optical depth τ as

$$-\mu\frac{dI_\nu(\nu,r,\mu)}{d\ell} = \kappa(\nu,r)[S_\nu(\nu,r,\mu) - I_\nu(\nu,r,\mu)] \quad . \tag{3.36}$$

[9] Note that the optical depth $\tau = \tau(\nu)$ is frequency dependent

[10] η has the dimension of $\frac{intensity}{length}$ and the physical unit $\mathrm{erg\,cm^{-3}\,sterad^{-1}}$

The RTE is a differential equation of first order. Those can be solved by integration (e.g. shown in Bronstein et al. 1999). By using the integrating factor or Euler multiplier the solution can be found. Therewith the emergent intensity

$$I_\nu^+(\tau=0) = \int_0^\infty S_\nu(\tau') e^{\left(-\frac{\tau'}{\mu}\right)} \frac{d\tau'}{\mu} \tag{3.37}$$

can obtained as a solution of the RTE in a half infinite approximation ($\tau_{max} \to 0$). Note that τ_{max} is the inner boundary of the disc.

The Eddington-Barbier relation

$$I_\nu^+(\tau=0) \approx S_\nu(\tau=\mu) \tag{3.38}$$

can be obtained in same manner.

Assuming local thermodynamic equilibrium (LTE), one can make another approximation

$$S_\nu(\nu,z) \approx B_\nu(\nu,z) \quad . \tag{3.39}$$

It has been shown, how the moments of the radiation field are defined and how to solve the RTE in the case of non-irradiated accretion discs. If one combines Equation 3.37 and Equation 3.38, one gets the famous Schwarzschild-Milne equations

$$J_\nu(\tau) = \frac{1}{2}\int_0^\infty S_\nu(\tau') E_1(|\tau'-\tau|) d\tau' \quad := \quad \Lambda_\tau(S_\nu(\tau)) \tag{3.40}$$

$$\begin{aligned} H_\nu(\tau) &= \frac{1}{2}\int_\tau^\infty S_\nu(\tau') E_2(|\tau'-\tau|) d\tau' \\ &\quad -\frac{1}{2}\int_0^\tau S_\nu(\tau') E_2(|\tau'-\tau|) d\tau' \quad := \quad \Phi_\tau(S_\nu(\tau)) \end{aligned} \tag{3.41}$$

$$K_\nu(\tau) = \frac{1}{2}\int_0^\infty S_\nu(\tau') E_3(|\tau'-\tau|) d\tau' \quad := \quad \mathcal{X}_\tau(S_\nu(\tau)) \quad . \tag{3.42}$$

In that case

$$E_\varepsilon(\zeta) = \int_1^\infty \rho^{-\varepsilon} e^{-\zeta\rho} d\rho \tag{3.43}$$

is the integral exponential function of order ε.

Now one has established the Schwarzschild-Milne-Relations and their expressions as operators Λ_τ, Φ_τ and $\mathcal{X}_\tau$. By discretise these operators one can use them for the numerical calculation of accretion discs. This numerical method is called accelerated lambda iteration (ALI). It will be discussed in section 3.7.

Finally one may obtain, how to calculate the moments of intensity with numerical methods. One takes Equation 3.31 as first momentum and calculates the higher moments with Equation 3.6 and Equation 3.7. Therewith one will get

$$\mu\frac{dJ_\nu}{d\tau} = I_\nu - S_\nu \tag{3.44}$$

$$\frac{dH_\nu}{d\tau} = J_\nu - S_\nu \tag{3.45}$$

$$\frac{dK_\nu}{d\tau} = H_\nu - S_\nu \quad . \tag{3.46}$$

Equation 3.44, Equation 3.45 and Equation 3.46 are all differential equations of first order. They can not be solved by their own, because the equation of the n-th momentum contains the (n+1)-th momentum. One has to find a closure to the equation system. This may be done with the Eddington factor

$$K_\nu = f_\nu \cdot J_\nu \quad .$$

Integration the Eddington approximation provides

$$\begin{aligned} K_\nu &\approx \frac{1}{3} \cdot J_\nu \\ f_\nu &\approx \frac{1}{3} \quad . \end{aligned} \tag{3.47}$$

This value for f_ν can be used as a start value for an iterative method, to get a better approximation.

Finally it has been shown, how to solve the radiative transfer equation and the equations for the moments of the radiation field.

3.3 The Energy Equilibrium

Invoking radiative equilibrium, there are some requirements to the accretion disc. The overall energy should be conserved and the energy transport should be solely radiative. With these constraints total energy then can be written as

$$E_{\text{kin}} + E_{\text{rad}} + E_{\text{conv}} = 0 \quad . \tag{3.48}$$

Note that for the following approach convective energy will be neglected.

First one may have a closer look at the kinetic energy, dissipated in the accretion disc. Therefore some expressions to describe the mechanics of the disc are needed. They are listet below.

$M_\star$, mass of the central object

$R_\star$, radius of the central object

R, radius of the accretion disc

Σ, mass of the disc column

Υ, kinematic viscosity

$w(m)$, depth dependent kinematic viscosity

ω, Keplerian angular frequency

v_ϕ, Keplerian velocity

ρ, density

m, mass depth

$\aleph > 0$, damping parameter

G, gravitational constant

Re, Reynolds number

Now, one can express the dissipated energy as (Nagel 2003)

$$E_{\text{kin}} = \Upsilon\Sigma\left(R\frac{d\omega}{dR}\right)^2 = \frac{9}{4}\Upsilon\Sigma\frac{GM_\star}{R^3} \quad . \tag{3.49}$$

If the column mass m is introduced, one can write the dissipated energy as a function of the column mass

$$E_{\text{kin}} = \frac{9}{4}\frac{GM_\star}{R^3}w(m)\rho \quad , \tag{3.50}$$

using the depth dependent kinematic viscosity

$$w(m) = a\bar{w}(\aleph + 1)\left(\frac{m}{M_0}\right)^\aleph \tag{3.51}$$

and the depth averaged kinematic viscosity

$$\bar{w} = \frac{1}{M_0}\int_0^{M_0} w(m)dm \quad . \tag{3.52}$$

From this equation, the scale factor a can be derived. The kinematic viscosity can be written in terms of the Reynolds number or in terms of the parameter α. If one wants to use the α approximation from Shakura & Sunyaev (1973), the velocity of sound c_s and the height of the disc has to be known. This is usually not the case, so one would have to calculate the kinematic viscosity in a iterative process. Thus it is a more useful approach to use the Reynolds number Re.

In the standard disc model, one has

$$M_0 = \frac{1}{2}\Sigma \quad , \tag{3.53}$$

with that, one finally gets

$$M_0 = \frac{\dot{M}_\star Re}{6\pi\sqrt{GM_\star R}}\left(1-\sqrt{\frac{R_\star}{R}}\right) \quad . \tag{3.54}$$

Secondly one can write down the energy which will be radiated away

$$E_{\text{rad}} = 4\pi\int_0^\infty (S_\nu - J_\nu)d\nu \quad , \tag{3.55}$$

by using the source function. Together with the second moment of intensity, one can express Equation 3.55 as

$$\frac{dH_\nu}{dm} = \frac{\chi_\nu}{\rho}(S_\nu - J_\nu) \quad , \tag{3.56}$$

which finally leads to

$$\frac{dH_\nu}{dm} = -\frac{9}{16\pi}\frac{GM_\star}{R^3}\omega(m) \quad . \tag{3.57}$$

Now, it can be clearly seen, that in contrast to radiative stellar atmospheres, the vertical radiative flux in accretion discs is not conserved.

Using the Schwarzschild-Milne-Equations(Equation 3.40) and some more approximations, one can solve the radiative transport . Therefor one may use the accerlerated lambda iteration (ALI, see section 3.7).

A simple but very instructional problem is, to solve the radiation transport under constraint of the radiative equilibrium.This is the so called grey atmosphere, where the opacity

$$\kappa(\nu) \neq \kappa = \text{const.} = \bar{\kappa} \tag{3.58}$$

is constant.

However, this approximation is not very realistic. One may use a capable average over the opacity. Comparing the grey case to the non-grey case, one may find a $\bar{\kappa}$, which is equivalent to the frequency integral. This approximation is known as the Rosseland opacity

$$[\kappa_R]^{-1} = \left(\frac{4\sigma}{\pi}T^3\right)^{-1}\cdot\int_0^\infty \frac{1}{\kappa(\nu)}\frac{dB_\nu}{dT}d\nu \quad , \tag{3.59}$$

with the associated Rosseland optical depth

$$\tau_{\text{Ross}}(z) = \int_0^z \bar{\kappa}_{\text{Ross}}(z')dz' \quad . \tag{3.60}$$

The Rosseland opacity κ_{Ross} is important to calculate the temperature correction and the constitution of accretion discs.

3.4 The Hydrostatic Equilibrium

Assuming equilibrium of the central compact object's gravitational force and the centrifugal force of the Keplerian rotation, one gets the the equation of hydrostatic equilibrium

$$\frac{dP}{dz} = -\frac{GM_\star}{R^3} z\rho \quad . \tag{3.61}$$

Therewith P denotes the total pressure

$$P = P_{\rm rad} + P_{\rm gas} \quad , \tag{3.62}$$

which is the sum of the gaseous and the radiative pressure.

In this approach the self gravity of the disc is neglected. As a fundamental difference to plane parallel stellar atmospheres, the gravity is dependent from the geometrical depth.

As already mentioned in Equation 3.52, one introduces the column mass m. Therewith the hydrostatic equilibrium can be written as

$$\frac{dP}{dm} = -\frac{GM_\star}{R^3} z \quad . \tag{3.63}$$

It has been found that the equation of hydrostatic equilibrium can be implemented more stable as a differential equation of second order. Then one has to solve it as a two point boundary value problem. Combining Equation 3.61 and Equation 3.63, one gets

$$\frac{dz}{dm} = -\frac{1}{\rho} \quad . \tag{3.64}$$

Deriving Equation 3.61 a second time, using Equation 3.64 and the velocity of sound

$$c_s^2 = \frac{P}{\rho} \quad , \tag{3.65}$$

one will find the equation of hydrostatic equilibrium

$$\frac{d^2P}{dm^2} = -\frac{c_s^2}{P}\frac{GM_\star}{R^3} \tag{3.66}$$

as a differential equation of second order.

The inner boundary value can be found through Taylor expansion and for the outer boundary value, one may use the approximation from Hubeny (1990).

The assumption of hydrostatic equilibrium is in general a very raw approximation. Effects like convection and turbulence in the disc can not be taken into account by this approach.

3.5 Emission and Absorption

For the calculation of synthetic spectra emission and absorption processes are extremely important. They will be discussed in this Subsection.

Accretion discs are like stellar atmospheres composed of different chemical species with abundances which are characteristic for the observed objects. For accretion discs this depends on the chemical composition of the donor star. The mass fraction β_k of the chemical element k is defined as

$$\sum_k \beta_k = 1 \quad . \tag{3.67}$$

element	N_k/N_H	mass fraction β_k (%)	number fraction (%)
H	1.0	$58.76 \cdot 10^{-6}$	$1.0 \cdot 10^{-3}$
He	$1.0 \cdot 10^{3}$	$23.32 \cdot 10^{-6}$	1.0
C	$1.5 \cdot 10^{4}$	10.50	15.0
Ne	$1.5 \cdot 10^{4}$	17.65	15.0
Mg	$1.5 \cdot 10^{4}$	21.26	15.0
O	$5.4 \cdot 10^{4}$	50.36	54.0

Table 3.1: Chemical composition used for a set of accretion disc models for 4U 1626-67

In Table 3.1 the chemical composition used for a set of accretion disc models for ultra compact low mass X-ray binary system 4U 1626-67 is given as an example. To calculate synthetic spectra one will need more information, than the abundances of the chemical elements the disc is consisting of. Detailed information about the energy levels of an specific element and possible transitions between levels is needed too. All these informations are provided by the model atom for the disc calculation. The model atom usually is a long data table read by the accretion disc model code. It contains information about the types of transitions described in the following list.

RBB-transition: bound-bound-transition between two levels by emitting or absorbing a photon

CBB-transition: bound-bound-transition between two levels caused by a collision

RBF-transition: bound-free-transition between a level and the continuum by emitting or absorbing a photon

CBF-transition: bound-free-transition between a level and the continuum caused by a collision

RFF-transition: acceleration of an electron in the coulomb field of an ion by emission of bremsstrahlung

Note that these transition types are the basic ones and there are some more types which will just be mentioned briefly. For example the RLU-transitions and RLL-transitions used for calculations with iron group elements (see page 30).

There is another class of transition like processes, the scattering processes. The Thomson and the Compton scattering by free electrons and the Rayleigh scattering by atoms, ions and molecules.

In the theory of electrodynamics the line transitions can be approached by a harmonic oscillator. Because an excited levels has a non-infinite life-span, the harmonic oscillator has to be damped, so the profile function of the emission and absorption lines is a Lorentz profile

$$\varphi(\nu) = \frac{\left(\frac{\gamma}{4\pi^2}\right)}{(\nu_0 - \nu)^2 \left(\frac{\gamma}{4\pi^2}\right)^2} \quad , \tag{3.68}$$

with a characteristic value for the full width at half maximum (FWHM).

Note that γ is the classical radiation damping constant, defined as

$$\gamma = \frac{2}{3} \frac{e^2 \omega_0}{m c^2} \quad . \tag{3.69}$$

Here e[11] is the elementary charge and ω_0 the resonance frequency of a damped harmonic oscillator.

[11] e is equivalent to $1.60217733 \times 10^{-19}$ C (Bronstein et al. 1999)

Figure 3.4 shows a Lorentzian profile function. Now the absorption cross section of a specific line transition can be written in dependence of the profile function

$$\sigma(\nu) = \sigma_0 \cdot \varphi(\nu) \quad . \tag{3.70}$$

For every transition from a lower level l to a upper level u, one gets a specific cross section. Therefore it is very useful to express the cross section σ_0 by the so called oscillator strength

$$\sigma_0 = \sigma_{lu} = \frac{\pi e^2}{mc} \cdot f_{lu} \quad . \tag{3.71}$$

The oscillator strengths are specified in the model atom. In fact the line transition and all other tran-

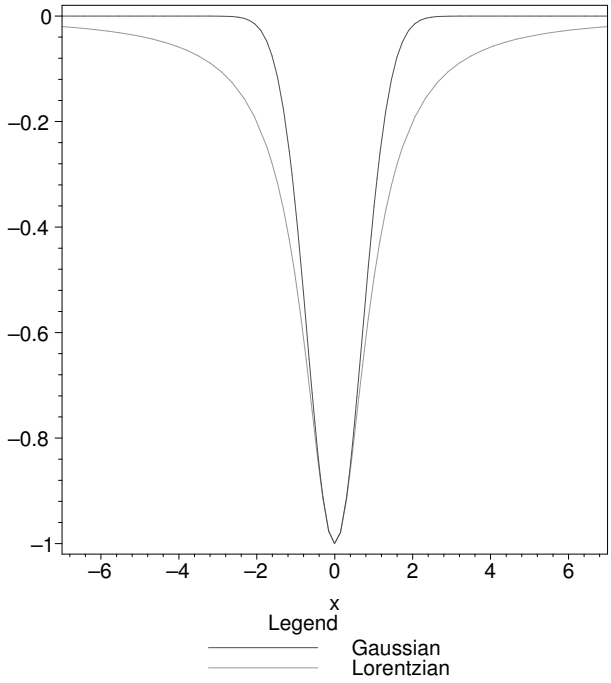

Figure 3.4: Gaussian and Lorentzian profiles

sitions are perturbed by different effects. This results in different forms of line broadening. The main effects are discussed in a short form now. Note that the not so important effects are only mentioned.

First we have the pressure broadening, which can be divided in several sub effects, namely the linear Stark effect, the self pressure broadening, the quadratic Stark effect and the van der Waals broadening. They all result in a Lorentzian profile function, with another damping constant

$$\gamma_{\text{press}} = \frac{1}{\tau_{\text{press}}} \quad , \tag{3.72}$$

where $\tau_{\text{press.}}$ is the average time between two collisions of our atom with another particle.

A very important broadening is the Doppler broadening caused by the thermal motion of the particles in the disc plasma. The velocity distribution is a Gaussian shaped function and therefore the profile function for the Doppler broadening is also a Gaussian

$$\varphi = \frac{1}{\Delta\nu_{\text{th.}}\sqrt{\pi}} e^{-\frac{(\nu-\nu_0)^2}{\Delta\nu_{\text{th.}}^2}} \quad . \tag{3.73}$$

A Gaussian profile function is shown in Figure 3.4. Another broadening effect resulting in a Gaussian profile function is the micro turbulence.

In a real accretion disc several of these effects are important. The profile function of a line transition will be a folded function. This function is called Voigt profile funtion

$$H(\rho,\zeta) = \frac{\rho}{\pi}\int_{-\infty}^{\infty}\frac{e^{-\varsigma^2}}{(\zeta-\varsigma)^2+\rho^2}d\varsigma \qquad . \tag{3.74}$$

Note that this function can not be shown analytically. One has to do that with approximation formulae or numerically.

The methods discussed now are, due to the limited computational possibilities nowadays, only useful for light metals like the C, N, O elements. If one wants to handle elements with a lot more lines, other methods are required. Therefore thousands of levels of the iron group elements are combined together to a relatively small number (typically 10 - 20) of super-levels (or energy bands). Then they can be handled by the ALI (accelerated lambda iteration) method. This statistical approach has it's analogue in the ODF (opacity distribution function) (Kurucz 1979) and the OS (opacity sampling) approaches in LTE (local thermal equilibrium) model atmosphere codes (Anderson 1985; Werner & Dreizler 1999). The line transitions between super-levels are defined in the atomic data files by the RLU-transitions. The RLL-transitions indicate the LTE line transitions inside one of these sampled super-levels.

Note that if one calculates cool disc models for cataclysmic variables etc., molecule opacities can not be neglected. In that case one has to use analogous methods to the ones used for the iron group elements. This is due to the fact that molecules have electronic transitions and transitions between their rotational and vibrational modes.

To get the cross sections for the bound-free transitions on has to use quantum mechanical calculations for all the chemical elements. This was done e.g. by the opacity project (Seaton et al. 1994; Seaton 1987).

The cross sections for the free-free transitions can be calculate, using the generalised Kramers' formula

$$\sigma_{ff}(\nu) = \frac{16\pi^2}{3\sqrt{3}}\frac{Z^2e^6}{hc\,(2\pi m)^{\frac{2}{3}}}\frac{1}{\nu^3}\frac{1}{\sqrt{T}}\bar{g}_{ff}(n,\nu,T) \qquad , \tag{3.75}$$

The $\bar{g}_{ff}$ denotes an atomic constant called Gaunt factor.

3.6 non-LTE Rate Equations

Because the non-LTE rate equation system is one of the central part of this thesis, only a short overview is given in this section. Setting up and solving the non-LTE rate equation system will be shown in detail in the theory Part II of the thesis.

If one assumes that a model disc ring (see section 8.3) is static and in a steady state, one may describe the total rate of particle transitions as

$$n_{ik}\sum_{j\neq i}P_{ij}-\sum_{j\neq i}n_{jk}P_{ji}=0 \qquad . \tag{3.76}$$

Note that this total rate consist of radiative and collisional terms, one has to describe separately. All transitions listed on page 28 have to be taken into account.

One may start with the *radiative bound-bound transitions*. The total downward rate consisting of stimulated and spontaneous transitions can expressed as

$$\begin{aligned} n_j R'_{ji} &= n_j\left(\frac{n_i}{n_j}\right)^* R_{ji} \\ &= n_j\left(\frac{n_i}{n_j}\right)^*\left[4\pi\int\frac{\alpha_{ij}(\nu)}{h\nu}\left(\frac{2h\nu_{ij}^3}{c^2}+J_\nu\right)e^{-\frac{h\nu}{kT}}\right] \qquad , \end{aligned} \tag{3.77}$$

whereas the total upward rate is written as

$$\begin{aligned} n_i R'_{ij} &= n_i B_{ij}\int\Phi_\nu J_\nu d\nu \equiv n_i B_{ij}\bar{J}_{ij} \\ &= n_i 4\pi\alpha_{ij}\frac{J_{ij}}{h\nu_{ij}} = n_i 4\pi\int\frac{\alpha_{ij}(\nu)}{h\nu}J_\nu d\nu \qquad . \end{aligned} \tag{3.78}$$

$\alpha_{ij}(\nu)$ denotes the energy absorption cross section. The other radiative processes which are important for the rate equation system are the *radiative bound-free transitions*. The total rate of photoionisations can be expressed in analogical form as

$$n_i R_{ij} = 4\pi\int_{\nu_0}^{\infty}\frac{\alpha_{ij}(\nu)}{h\nu}d\nu \tag{3.79}$$

and the total rate of radiative recombinations can be given as

$$n_i\left(\frac{n_i}{n_\kappa}\right)^* R_{ji} \equiv 4\pi\int_{\nu_0}^{\infty}\frac{\alpha_{ij}(\nu)}{h\nu}\left(\frac{2h\nu^3}{c^2}+J_\nu\right)e^{-\frac{h\nu}{kT}}d\nu \qquad . \tag{3.80}$$

Note that in the case of thermodynamic equilibrium

$$R^*_{ij}=R^*_{ji} \qquad . \tag{3.81}$$

After the discussion of radiative processes, which have to be taken into account, one must have a closer look at the collisional processes. The total number of upward *collisional bound-bound transitions* can be given in dependence of the cross section as

$$n_i C_{ij} = n_i n_e\int_{\nu_0}^{\infty}\sigma_{ij}(v)f(v)dv \qquad , \tag{3.82}$$

with the definition of the maximum speed

$$v_0 = \sqrt{\frac{2E_0}{m_e}} \quad . \tag{3.83}$$

Using detailed balancing arguments, one gets the total collisional downward rate

$$n_j C_{ji} = \left(\frac{n_i}{n_j}\right)^* n_e \int_{v_0}^{\infty} \sigma_{ij}(v) f(v) dv \quad . \tag{3.84}$$

Analogical to the photoionisation rate one may give the rate of the *collisional ionisations* or the *collisional bound-free transitions* as

$$C_{i\kappa} = 1.55 \times 10^{13} \frac{\bar{g}_i \alpha(\nu_0)}{\sqrt{T}} \frac{e^{-u_0}}{u_0} \quad . \tag{3.85}$$

Equation 3.85 is the Seaton-formula, after Seaton (1962). $\alpha(\nu_0)$ denotes the photoionisation cross section.

Another type of processes are those with two electrons involved. These are the *autoionisation* and *dielectronic recombinations*. They are important in the very hot parts of a disc, e.g. the disc corona.

Now, all the rates mentioned above can be combined together in an equation system

$$\begin{aligned} & -\sum_{i''<i} n_{i''}(R_{i''i} + C_{i''i}) \quad + \\ \left[\sum_{i''<i} \left(\frac{n_{i''}}{n_i}\right)^* (R_{ii''} + C_{ii''}) + \sum_{i'>i}^{\kappa} n_{i''}(R_{ii'} + C_{ii'})\right] & \\ -\sum_{i'>i}^{\kappa} n_{i'} \left(\frac{n_{i''}}{n_i}\right)^* (R_{i'i} + C_{i'i}) & = 0 \quad . \end{aligned} \tag{3.86}$$

To complete the rate equation system one has to invoke the particle conservation

$$\sum_{i,j} n_{ij,k} - \left(\frac{\alpha_k}{\alpha_H}\right)\left(\sum_i n_{i,H} + n_p\right) = 0 \quad . \tag{3.87}$$

The complete system can then be written down in matrix form

$$\mathcal{A}\mathbf{n} = \mathcal{B} \quad , \tag{3.88}$$

using the here listed notations.

n, a vector with $\mathcal{N}$ occupation numbers

$\mathcal{N}$, overall amount of occupation numbers

$\mathcal{A}$, Rate Matrix$\mathcal{N} \times \mathcal{N}$

$\mathcal{B}$, vector with one nonzero element (from Equation 3.87)

3.7 non-LTE Accretion Disc Models

To get a non-LTE accretion disc model, one has to solve the radiation transfer equation, the energy equation, the rate equations and the hydrostatic equation consistently. Therefore we have the non-linear equation system

$$\mathcal{M}^d(\psi)\cdot\psi^d = \mathbf{c}^d(\psi) \quad , \tag{3.89}$$

with the solution vector

$$\psi^d = (n_1,\ldots,n_{NL},N,T,n_e,J_{\nu_1},\ldots,J_{\nu_{NF}})^d \quad . \tag{3.90}$$

Note that d denotes the dependency of the equation system on the depth in the vertical direction z of the accretion disc.

The solution vector consist of the following single parts:

occupation numbers from the rate equations: $\mathbf{n}(d) = (n_1,\ldots,n_{NL})^d$

hydrostatic layering: $N(d)$

energy distribution: $T(d)$

particle conservation: n_e

radiation field from the radiation transfer: $J_\nu = (J_{\nu_1},\ldots,J_{\nu_{NF}})^d$

In that case the accelerated lambda iteration (ALI) eliminates the explicit appearance of the radiative transfer in the equation system by providing an implicit approximative solution for the radiation field. One gets the exact solution by the following iteration scheme

$$J_\nu^{(i)} = \Lambda^* S_\nu^{(i)} + \Delta J_\nu^{(i)} \quad . \tag{3.91}$$

The equation system can be solved by Newton-Raphson iteration for every depth d, shown in Figure 3.5. One uses the start approximation,

$$\psi^d = (n_1,\ldots,n_{NL},N,T,n_e,n_H)^d \tag{3.92}$$

the corrections

$$\delta\psi^d = (\delta n_1,\ldots,\delta n_{NL},\delta N,\delta T,\delta n_e,\delta n_H)^d \tag{3.93}$$

and the linearised equation system:

$$\mathcal{M}^d(\psi)\cdot\delta\psi^d = \mathbf{c}^d(\psi) \tag{3.94}$$

Note that the n_H is the particle density.

Finally there are some remarks to make on the iteration methods mentioned here. First there are a lot of modified and successive methods to the ALI method which are used in todays accretion disc and stellar atmosphere modelling, e.g. the short characteristic method used in AcDc. Some successive methods have been also implemented for the Newton-Raphson-Iteration (Koesterke, Hamann & Kosmol 1992).

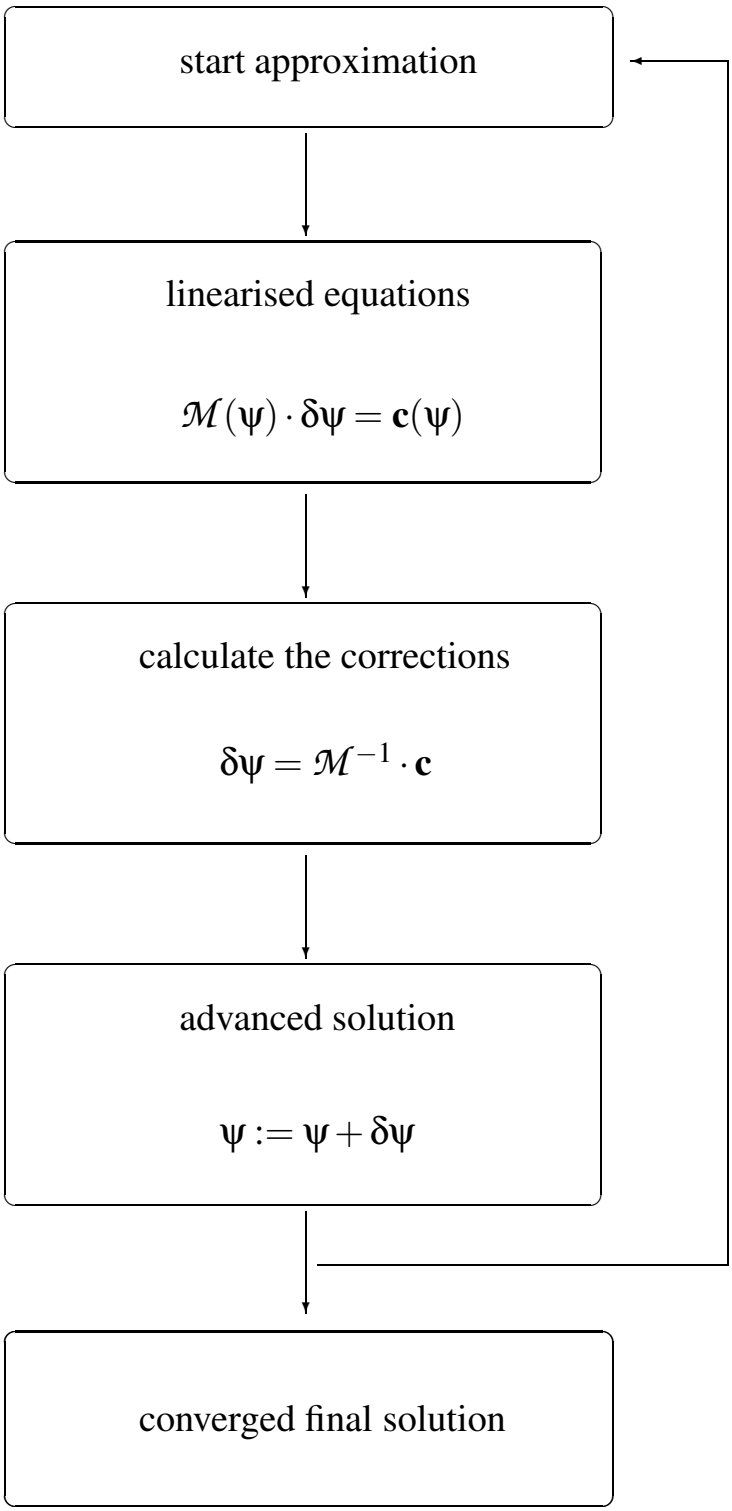

Figure 3.5: Flux chart of the Newton-Raphson-iteration

Part II

Theory of non-LTE Rate Equations

In this part of my diploma thesis, I will introduce the rate equations or equations of statistical equilibrium. In chapter 4 I will introduce the rate matrix in standard form (Mihalas 1978), which is known now for more than twenty five years.

In chapter 5 I will show how to handle and to solve the rate equation matrix with numerical methods, during the calculation of accretion disc models or stellar atmosphere models.

In chapter 6 I will show newer methods (Werner & Dreizler 1999) to solve the non-LTE rate equations. These are used in the stellar model atmosphere codes PRO2 and NGRT and in the accretion disc model code ACDC.

Chapter 4

Concept of the Rate Matrix

To calculate the occupation numbers of bound and free states of an atom in non-LTE model accretion discs, one uses the non-LTE rate equations. Usually the equations are simplified by assuming *complete redistribution* in the lines (i.e., *the emission and absorption line profiles are assumed to be identical*).

4.1 Appearance of the Matrix *A*

In a volume element of a moving medium, the number density of particles of a given state (bound or free) i of a chemical species k will change in time, according to the *net rate* at which particles are brought from other states j. This *net fluxes* of particles is generated by radiative and collisional processes and is described by

$$\frac{\partial n_{ik}}{\partial t} = -\nabla \cdot (n_{ik}\mathbf{v}) + \sum_{j \neq i} \left(n_{jk} P_{ji} - n_{ik} P_{ij} \right) \quad . \tag{4.1}$$

Furthermore one has the *equation of continuity* for every species

$$\frac{\partial N_k}{\partial t} + \nabla \cdot (N_k \mathbf{v}) = 0 \tag{4.2}$$

and the standard hydrodynamical equation of continuity

$$\frac{\partial \rho}{\partial t} + \nabla \cdot (\rho \mathbf{v}) = 0 \quad . \tag{4.3}$$

In that case the density ρ can be expressed by $\rho = \sum_k m_k N_k$. For a *steady state*, one can simplify Equation 4.1 to

$$n_{ik} \sum_{j \neq i} P_{ij} - \sum_{j \neq i} n_{jk} P_{ji} = \nabla \cdot (n_{ik}\mathbf{v}) \quad . \tag{4.4}$$

Is the accretion disc model above all *static*, one gets

$$n_{ik} \sum_{j \neq i} P_{ij} - \sum_{j \neq i} n_{jk} P_{ji} = 0 \quad . \tag{4.5}$$

Note that in these equations the subscript k is suppressed. The total rate P_{ij} in general contains both, radiative and collisional terms. It will not been shown how to handle moving media in this thesis, because in ACDC the stratification is assumed to be hydrostatic.

4.2 Radiative Transition Rates

4.2.1 Bound-Bound Transitions

As mention by Mihalas (1978), it is very useful to write down the radiative transition rates in two different formalisms. First in *Einstein transition probabilities*, which are useful to do analytical manipulations with simplified model atoms. Secondly in *energy absorption cross sections*, which can be used to write radiative bound-bound transitions (RBB) in the same way as radiative bound-free transitions (RBF). The last method is successfully used in accretion disc and stellar atmosphere modelling.

Φ_ν, absorption and emission line profiles

i, j, bound levels

n, occupation number of a level

$d\nu$, frequency interval

$d\omega$, solid angle

B_{ij},B_{ji},A_{ji}, Einstein transition probabilities or Einstein coefficients

α_{ij}, energy absorption cross sections

Now the moments of intensity are needed. They have been already defined in section 3.1.

$$\mu \equiv cos\,\Theta \tag{4.6}$$

$$J_\nu(z) = \frac{1}{2}\int_{-1}^{+1} I_\nu d\mu \tag{4.7}$$

$$H_\nu(z) = \frac{1}{2}\int_{-1}^{+1} \mu I_\nu d\mu \tag{4.8}$$

$$K_\nu(z) = \frac{1}{2}\int_{-1}^{+1} \mu^2 I_\nu d\mu \tag{4.9}$$

The number of transitions produced by the radiation field I_ν in the frequency interval $d\nu$ and the solid angle $d\omega$ is

$$n_i B_{ij} \Phi_\nu d\nu \frac{d\omega}{4\pi} = n_i \left(\frac{\alpha_{\alpha_{ij}}}{h\nu}\right) \Phi_\nu d\omega d\nu \quad . \tag{4.10}$$

In a *static* medium, Φ_ν is isotropic, so one can integrate over all angles and frequencies. Therewith the *number of absorptions* follows as

$$\begin{aligned} n_i R'_{ij} &= n_i B_{ij} \int \Phi_\nu J_\nu d\nu \equiv n_i B_{ij} \bar{J}_{ij} \\ &= n_i 4\pi\alpha_{ij} \frac{J_{ij}}{h\nu_{ij}} = n_i 4\pi \int \frac{\alpha_{ij}(\nu)}{h\nu} J_\nu d\nu \quad . \end{aligned} \tag{4.11}$$

The number of *stimulated emissions* can be written as

$$\begin{aligned} n_j B_{ji} \int \Phi_\nu J_\nu d\nu &= n_j B_{ji} \bar{J}_{ji} = n_j \left(\frac{g_i B_{ij}}{g_j}\right) \bar{J}_{ij} \\ &= n_j \left(\frac{4\pi}{h\nu_{ij}}\right) \left(\frac{g_i \alpha_{ij}}{g_j}\right) \bar{J}_{ij} \quad . \end{aligned} \tag{4.12}$$

In a final step one can write the number of *spontaneous emissions* as

$$\begin{aligned} n_j A_{ji} \int \Phi_\nu d\nu &= n_j \left(\frac{2h\nu_{ij}^3}{c^2} \right) B_{ji} \\ &= n_j \left(\frac{2h\nu_{ij}^3}{c^2} \right) \left(\frac{4\pi}{h\nu_{ij}} \right) \left(\frac{g_i \alpha_{ij}}{g_j} \right) \quad . \end{aligned} \tag{4.13}$$

Putting the pieces together, the *total downward rate* can be expressed as sum of the *stimulated emission rate* (Equation 4.12) and the *spontaneous emission rate* (Equation 4.13)

$$\begin{aligned} n_j R'_{ji} &= n_j \left(A_{ji} + B_{ji} \bar{J}_{ij} \right) \\ &= n_j \left(\frac{4\pi}{h\nu_{ij}} \right) \left(\frac{g_i \alpha_{ij}}{g_j} \right) \left[\left(\frac{2h\nu_{ij}^3}{c^2} \right) + \bar{J}_{ij} \right] \quad . \end{aligned} \tag{4.14}$$

By factoring out the occupation ratio of local thermodynamic equilibrium (see Boltzmann equation page 42)

$$\left(\frac{n_i}{n_j} \right)^* = \left(\frac{g_i}{g_j} \right) e^{-\frac{h\nu}{kT}} \quad , \tag{4.15}$$

the *total downward rate* (Equation 4.14) can be written in the following form

$$\begin{aligned} n_j R'_{ji} &= n_j \left(\frac{n_i}{n_j} \right)^* R_{ji} \\ &= n_j \left(\frac{n_i}{n_j} \right)^* \left[4\pi \int \frac{\alpha_{ij}(\nu)}{h\nu} \left(\frac{2h\nu^3}{c^2} + J_\nu \right) e^{-\frac{h\nu}{kT}} \right] \quad . \end{aligned} \tag{4.16}$$

The statistical weights are denoted by g_x. The quite strange appearance of Equation 4.16, is due to the fact that one may write the downward rate of the bound-free transitions and the downward rate of the collisional transitions in the same style. When setting up the full rate equation system, some considerable advantages are addicted.

4.2.2 Bound-Free Transitions

We now calculate the radiative transition rates from a bound level to the continuum, the so called bound-free transitions. There the photoionisation cross section $\alpha_{i\kappa}(\nu)$ and some other parameters are needed:

$\alpha_{i\kappa}(\nu)$, photoionisation cross section

i, bound level

κ, free level or continuum

B_ν, black body or Planck function

n_κ, ion density

n_e, electron density

T_e, electron temperature

Then the number of photoionisations can be calculated in the following way

$$n_i R_{i\kappa} = n_i 4\pi \int_{\nu_0}^{\infty} \frac{\alpha_{i\kappa}(\nu)}{h\nu} J_\nu d\nu \quad . \tag{4.17}$$

Using detailed balancing arguments, one may calculate the number of *spontaneous recombinations*. In thermodynamic equilibrium (TE) the number of spontaneous recombinations must be equal to the number of photoionisations. Assuming that the mean intensity in TE can expressed by a black body and a correction factor $1-e^{-\frac{h\nu}{kT}}$ for *stimulated emission*, one may calculate the number of *spontaneous recombinations* using Equation 4.17

$$(n_\kappa R_{\kappa i})^*_{\text{spon}} = n_i^* 4\pi \int_{\nu_0}^{\infty} \frac{\alpha_{i\kappa}(\nu)}{h\nu} B_\nu (1-e^{-\frac{h\nu}{kT}}) d\nu \quad . \tag{4.18}$$

Since recombination is due to collision between electrons and ions, it is proportional to the product $n_e \cdot n_\kappa$. The velocity distribution of electrons is described by their temperature.Using this together with the electron density, one may calculate the recombination rate only in dependency on *ions*. If one wants to calculate the spontaneous non-LTE recombination rate, some correction terms are needed

$$\begin{aligned}(n_\kappa R_{\kappa i})^*_{\text{spon}} &= n_\kappa \left(\frac{n_i}{n_\kappa}\right)^* 4\pi \int_{\nu_0}^{\infty} \frac{\alpha_{i\kappa}(\nu)}{h\nu} B_\nu (1-e^{-\frac{h\nu}{kT}}) d\nu \\ &= n_\kappa \left(\frac{n_i}{n_\kappa}\right)^* 4\pi \int_{\nu_0}^{\infty} \frac{\alpha_{i\kappa}(\nu)}{h\nu} \left(\frac{2h\nu^3}{c^2}\right) e^{-\frac{h\nu}{kT}} d\nu \quad .\end{aligned} \tag{4.19}$$

According to the Boltzmann law, the population of an excited level is

$$\left(\frac{n_{ijk}}{n_{0jk}}\right)^* = \left(\frac{g_{ijk}}{g_{0jk}}\right) e^{-\frac{\chi_{ijk}}{kT}} \quad . \tag{4.20}$$

For any two excited levels l and m, one may find

$$\left(\frac{n_{ljk}}{n_{mjk}}\right)^* = \left(\frac{g_{ijk}}{g_{0jk}}\right) e^{-\frac{(\chi_{ljk}-\chi_{mjk})}{kT}} = \left(\frac{g_{ijk}}{g_{0jk}}\right) e^{-\frac{h\nu_{lm}}{kT}} \quad . \tag{4.21}$$

In that case $h\nu_{lm}$ denotes the energy of a photon equal to the energy difference of the two levels.

To describe the ionisation equilibrium one uses the *Saha ionisation Equation*. Therefore one will use the parameters listet below:

$n^*_{0,0,k}$, occupation number of the ground state

$n^*_{0,1,k}$, occupation number of an excited state

n^*_e, electron number

$g^*_{0,0,k}$, Saha factor of the ground state

$g^*_{0,1,k}$, Saha factor of an excited state

$\chi^*_{I,0,k}$, energy difference between the two states

Therewith the basic appearance of the *Saha equation* is

$$n^*_{0,0,k} = n^*_{0,1,k} n^*_e \frac{1}{2} \left(\frac{h^2}{2\pi mkT} \right)^{\frac{2}{3}} \left(\frac{g_{0,0,k}}{g_{0,0,k}} \right) e^{\frac{\chi_{I,0,k}}{kT}} \quad . \tag{4.22}$$

Using Equation 4.22 and two neighbouring ionisation stages, one will get

$$n^*_{0,j,k} = n^*_{0,j+1,k} n^*_e \frac{1}{2} \left(\frac{h^2}{2\pi mkT} \right)^{\frac{2}{3}} \left(\frac{g_{0,j,k}}{g_{0,j+1,k}} \right) e^{\frac{\chi_{I,j,k}}{kT}} \quad . \tag{4.23}$$

Combining Equation 4.20 and Equation 4.23 provides the following form of the Saha equation

$$\begin{aligned} n^*_{i,j,k} &= n_{0,j+i,k} n_e \left(\frac{g_{0,0,k}}{g_{0,0,k}} \right) C_I T^{\frac{2}{3}} e^{\frac{(\chi_{I,j,k} - \chi_{i,j,k})}{kT}} \\ &\equiv n_{0,j+i,k} n_e \phi_{ijk}(T) \quad . \end{aligned} \tag{4.24}$$

From equation Equation 4.24 we can derive

$$\left(\frac{n_i}{n_\kappa} \right)^* = n_e \phi_{i\kappa}(T) \quad , \tag{4.25}$$

which shows that the spontaneous recombination rate depends on the product of electron and ion density. Furthermore it depends on a function of the temperature, which is connected to the atomic properties by the cross section.

Assuming thermodynamic equilibrium, the *stimulated recombinations* may be calculated in an analogous way

$$\left(n_\kappa R'_{\kappa i}\right)^*_{\text{stim}} = n_i^* 4\pi \int_{\nu_0}^{\infty} \frac{\alpha_{i\kappa}(\nu)}{h\nu} B_\nu (1 - e^{-\frac{h\nu}{kT}}) d\nu \quad . \tag{4.26}$$

Now, the obtained results should be generalised to the non-LTE case. To do that, one has to replace the Planck function B_ν by the mean intensity J_ν. In addition one has to use the current ion density n_κ, which leads to

$$\left(n_\kappa R'_{\kappa i}\right)_{\text{stim}} = n_i \left(\frac{n_i}{n_\kappa}\right)^* 4\pi \int_{\nu_0}^{\infty} \frac{\alpha_{i\kappa}(\nu)}{h\nu} B_\nu (1 - e^{-\frac{h\nu}{kT}}) d\nu \quad . \tag{4.27}$$

Finally the *total number of recombinations* may be calculated as sum of the *stimulated* and the *spontaneous recombination*

$$\begin{aligned} n_\kappa \left(R'_{\kappa i,\text{stim}} + R'_{\kappa i,\text{spon}}\right) &\equiv n_i \left(\frac{n_i}{n_\kappa}\right)^* R_{\kappa i} \\ &= n_i \left(\frac{n_i}{n_\kappa}\right)^* 4\pi \int_{\nu_0}^{\infty} \frac{\alpha_{i\kappa}(\nu)}{h\nu} \left(\frac{2h\nu^3}{c^2} + J_\nu\right) e^{-\frac{h\nu}{kT}} d\nu \end{aligned} \tag{4.28}$$

Comparing Equation 4.10 and Equation 4.17 suggest, that the notation should be systemised.

Doing so, one may write *all upward radiative rates* as

$$n_i R_{ij} \tag{4.29}$$

with

$$R_{ij} \equiv 4\pi \int_{\nu_0}^{\infty} \frac{\alpha_{ij}(\nu)}{h\nu} d\nu \tag{4.30}$$

and *all downward radiative rates* as

$$n_i \left(\frac{n_i}{n_\kappa}\right)^* R_{ij} \tag{4.31}$$

with

$$R_{ji} \equiv 4\pi \int_{\nu_0}^{\infty} \frac{\alpha_{ij}(\nu)}{h\nu} \left(\frac{2h\nu^3}{c^2} + J_\nu\right) e^{-\frac{h\nu}{kT}} d\nu \tag{4.32}$$

Note that in the case of thermodynamic equilibrium, it has to be

$$R^*_{ij} = R^*_{ji} \tag{4.33}$$

4.3 Collisional Transition Rates

Accretion discs in CVs and XRBs as well as stellar atmospheres are consisting of a hot plasma composed out of ions and electrons as well as neutral atoms. For this reason collisions of these particles will result in ionisations and excitations.

Since the Coulomb force is a long range interaction, collisions with charged particles are predominant. Due to the fact that the collision frequency is velocity dependent, the only species which has to be taken into account at the encountered densities, are electrons. In thermodynamic equilibrium their velocity is by a factor

$$\left(\frac{m_H A}{m_e}\right)^{\frac{1}{2}} \propto 43\sqrt{A} \tag{4.34}$$

times larger than the velocity of ions with the atomic mass A.

To discuss the collisional rate transitions the parameters and notations listed below are needed:

n, number of collisional transitions

$\sigma_{ij}(v)$, collisional transition cross section

Q_{ij}, cross section in terms of the Bohr radius

a_0, Bohr radius

v, electron velocity

Y_{ij}, net collisional bracket

E_0, threshold energy

The total number of transitions can be calculated with the following expression

$$n_i C_{ij} = n_i n_e \int_{v_0}^{\infty} \sigma_{ij}(v) f(v) dv \equiv n_i n_e q_{ij}(T) \qquad , \tag{4.35}$$

whereupon v_0 is defined by

$$v_0 = \sqrt{\frac{2E_0}{m_e}} \qquad . \tag{4.36}$$

Now, the detailed balancing arguments (see Page 42) could be used again. Doing so and using the velocity distribution for electrons in equilibrium (i.e. Maxwellian function), one may obtain the *downward rate*. Then the following relation

$$n_i^* C_{ij} = n_j^* C_{ji} \tag{4.37}$$

is correct, so one gets the total number of downward transitions as

$$n_j C_{ji} = n_j \left(\frac{n_i}{n_j}\right)^* C_{ij} = \left(\frac{n_i}{n_j}\right)^* n_e q_{ij}(T) \qquad . \tag{4.38}$$

To get the collisional cross sections, required to calculate collisional transitions rates, one may do sophisticated quantum mechanical computer calculations, as done at the Iron Project, e.g. see Nahar (2003) or one can do laboratory measurements. For further information about collisional cross sections see e.g. Massey, Burhop & Gilbody (1974).

Usually one is more interested in rates for a given cross section (see Equation 4.29). Therefore it is useful to have a closer look at $q_{ij}(T)$. Cross sections are often measured in dependence of the Bohr radius a_0. Thus one may write

$$\sigma_{ij} = \pi a_0^2 Q_{ij} \quad . \tag{4.39}$$

Q_{ij} is usually given in terms of excitation energy of particles, which leads to

$$E = \frac{1}{2} m v^2 \quad . \tag{4.40}$$

The velocity distribution of particles in thermodynamics is given by the *Maxwellian velocity distribution*

$$f(\mathbf{v}) dv_x dv_y dv_z = \left(\frac{m}{2\pi kT}\right)^{\frac{2}{3}} e^{-\frac{m(v_x^2+v_y^2+v_z^2)}{2kT}} dv_x dv_y dv_z \quad . \tag{4.41}$$

It denotes the probability to find a particle of mass m, temperature T and located in the volume $dv_x dv_y dv_z$, in the velocity range $(\mathbf{v}, \mathbf{v}+\mathbf{dv})$.

If Equation 4.38 is expressed in terms of speed, one will get

$$f(\mathbf{v}) dv = \left(\frac{m}{2\pi kT}\right)^{\frac{2}{3}} e^{-\frac{mv^2}{2kT}} 4\pi v^2 dv \quad . \tag{4.42}$$

$< v^2 >$ is the root mean square velocity, $< v_x^2 >$ is the root mean square velocity in the line of sight and v_0^2 is *most probable speed* of an particle with nucleus mass A.

Inserting Equation 4.40 and Equation 4.42 into Equation 4.35 leads to

$$q_{ij}(T) = C_0 \sqrt{T} \int_{u_0}^{\infty} Q_{ij}(ukT) u e^{-u} du \quad , \tag{4.43}$$

thereby the following substitutions are used

$$\begin{aligned} u &\equiv \frac{E}{kT} \\ u_0 &\equiv \frac{E_0}{kT} \\ C_0 &= \pi a_0^2 \sqrt{\frac{8k}{m\pi}} = 5.5 \times 10^{-11} \quad . \end{aligned} \tag{4.44}$$

Substituting $x = (u - u_0)$ and using u_0 from above one gets

$$q_{ij}(T) = C_0 \sqrt{T}\, e^{-\frac{e_0}{kT}}\, \Gamma_{ij}(T) \quad , \tag{4.45}$$

where $\Gamma_{ij}(T)$ is a function of the temperature

$$\Gamma_{ij}(T) = \int_0^{\infty} Q_{ij}\,(E_0 + xkT) \left(x + \frac{E_0}{kT}\right) e^{-x} dx \quad . \tag{4.46}$$

Since the term $\Gamma_{ij}(T)$ is varying only very slowly with the temperature, one has obtained a function, showing the following dependence

$$q_{ij}(T) \sim \sqrt{T}\, e^{-\frac{e_0}{kT}} \quad . \tag{4.47}$$

One of the biggest problems is, that most of the transitions of astrophysical interest, are in the energy range $kT \ll E_0$. There the transition rate depends extremely sensitive on Q_{ij}-values near the threshold.

All small energy approximations are losing their validity near the threshold, because of resonance effects. The computational complexity is growing more and more to get accurate results for the cross sections.

For the spectra of H I, He I and He II good experimental data are only available for transitions from ground state. The other data has to be obtained from theoretical calculations. There is a lot of work going on, at projects like the Iron Project mentioned above (see Page 45). However, in most cases, the calculations are made for heavier elements like Iron. Still a lot of work has to be done in future.

It is often very useful to express the excitation rate for transitions, which are radiatively permitted, in terms of the oscillator strength f_{ij}. Then one gets (van Regemorter 1962)

$$C_{ij} = C_0 n_e \sqrt{T} \left[14.5 f_{ij} \left(\frac{I_H}{E_0} \right)^2 \right] u_0 e^{-u_0} \, \Gamma_e(u_0) \quad , \tag{4.48}$$

where u_0 is the same substitution as above. I_H indicates the ionisation energy of hydrogen. For ions, $\Gamma_e(u_0)$ looks the following way

$$\Gamma_e(u_0) = \max\left[\bar{g}, 0.276 e^{u_0} E_1(u_0)\right] u_0 e^{-u_0} \, \Gamma_e(u_0) \quad . \tag{4.49}$$

Transition of the type $nl \rightarrow nl'$ result in $\bar{g} \approx 0.7$, whereas transition of the type $nl \rightarrow n'l'$ described by a value of 0.2. Note that for the first ionisation stage, $\Gamma_e(u_0)$ has a different form.

In general, collisional transition are not restricted by the dipole transition selection rule $\Delta l = \pm 1$. Cross section for other transitions may be in the same order of magnitude as dipole transition, despite the fact that $f_{ij} \approx 0$ in the dipole approximation.

Lotz (1968) has given the semi-empirical formula

$$\sigma_{i\kappa}(E) = \pi a_0^2 \left[2.5 \zeta \left(\frac{I_H}{E_0} \right)^2 \right] ln\left(\frac{E}{E_0} \right) \left\{ 1 - b\, e^{-c \frac{(E-E_0)}{E_0}} \right\} \left(\frac{E_0}{E} \right) \tag{4.50}$$

for collisional ionisations. This leads to a transition rate of

$$C_{i\kappa} = C_0 n_e \sqrt{T} \left[2.5 \zeta \left(\frac{I_H}{E_0} \right)^2 \right] u_0 \left[E_1(u_0) - b e^c \, u_0 \frac{E_1(u_1)}{u_1} \right] \quad . \tag{4.51}$$

In that formula ζ, b and c are empirical factors depending on the ion species. u_0 is defined in Equation 4.46 and $u_1 = u_0 + c$.

At last one can give another approximate formula, for the collisional ionisation cross section. It can be expressed in terms of the photoionisation cross section

$$C_{i\kappa} = 1.55 \times 10^{13} \frac{\bar{g}_i \, \alpha(\nu_0)}{\sqrt{T}} \frac{e^{-u_0}}{u_0} \quad . \tag{4.52}$$

Here $\alpha(\nu_0)$ denotes the photoionisation cross section. The factor $\bar{g}_i$ is about 0.1, 0.2 and 0.3 for once, twice and multi ionised atoms. Equation 4.52 is known as the Seaton-formula (Seaton 1962).

4.4 Dielectronic Recombination and Autoionisation

In atoms with many electrons the ionisation energy is defined as the energy, you will at least need to divide the atom in a free electron and an ion in ground state. Are there several electrons excited, the sum of the electron excitation energies might be larger than the value of the ionisation energy. Thus in principal it is possible to ionise the atom and that happens very often. One calls this mechanism auto-ionisation. Then one says, that the excited atom has been auto-ionised to the ion's ground state plus a free electron.

Of course the inverse process is also possible. If an atom in ground state collides with an electron, a double excited atom could be generated. Usually it will auto-ionise again. That is why this process is in general not very important. Sometimes one of the excited electrons makes a radiative transition to a lower level. Now the total energy of the ion is not high enough to auto ionise again. This process is called *dielectronic recombination*.

To describe the processes mathematical correctly, one needs the following definitions:

X, chemical species

Z, charge

n,l, quantum numbers of a state

e, electron

d,b, bound states

κ, continuum

A_a, A_s, transition probability

E, energy

$\chi_{d,\kappa}$, energy difference between the two states

g_κ, g_d, factors of statistical weight

The *dielectronic recombination* is described by the process of an electron capture

$$X^{+(Z)}(n,l) = e(E,l''+1) \rightleftharpoons X^{+(Z+1)}(n',l+1;n'',l'') \tag{4.53}$$

and the following radiative stabilisation transition

$$X^{+(Z-1)}(n',l+1;n'',l'') \rightarrow X^{+(Z+1)}(n,l;n'',l'') \quad . \tag{4.54}$$

The result is an ion in a bound state. In Mihalas (1978) one may find the example of He II and an electron colliding

$$\begin{aligned} He^+(1s) + e(E,l''+1) &\rightarrow He^0(2p;n'',l'') \\ He^0(2p;n'',l'') &\rightarrow He^0(1s;n'',l'') + h\nu \quad . \end{aligned} \tag{4.55}$$

Denoting the doubly excited state of the ion with charge Z by d. Its ground state should be denoted with κ and the final bound state of the ion with charge $Z-1$ by b. Then one can write the number of dielectronic recombinations from state d to state b as

$$n_\kappa R_{db} = n_d A_s \quad . \tag{4.56}$$

In that case A_s denotes the probability of a spontaneous stabilising transition. Usually a well approximation for the ion with the charge Z is

$$A_s = A(n^{'}, l+1; n, l) \qquad , \tag{4.57}$$

especially for large values of $n^{''}$. For weak radiation fields, one may ignore the reverse process of Equation 4.54. Using the transition probability for *autoionisation* A_a, n_d can be written in terms of the equilibrium value n_d^*

$$n_d = \frac{n_d^* A_a}{(A_a + A_s)} \qquad , \tag{4.58}$$

whereupon the equilibrium value is defined as

$$n_d^* = n_\kappa n_e \left(\frac{g_d}{g_\kappa}\right) C_I T^{-\frac{2}{3}} e^{-\frac{\chi_{d\kappa}}{kT}} \equiv n_\kappa n_e \Phi_{d\kappa}(T) \qquad . \tag{4.59}$$

In this case $\chi_{d\kappa}$ denotes the energy of state d referring to the ionisation limit. Finally one will get the number of *dielectronic recombinations*, from state d to state b as

$$n_d R_{db} = n_\kappa n_e \Phi_{d\kappa}(T) \frac{A_s A_a}{(A_a + A_s)} \qquad . \tag{4.60}$$

As already mentioned in context of radiative recombinations (see Page 44), is it useful to define a *dielectronic recombination coefficient* α_{DR} in that case, too. The recombination coefficient looks like

$$n_d R_{db} = n_\kappa n_e \alpha_{DR} \qquad . \tag{4.61}$$

It should be mentioned that the ratio of dielectronic recombinations to radiative recombinations depends only on the ratio α_{DR}/α_{RR}. Therefor it is only a function of temperature.

Dielectronic recombination is most important in very hot parts of accretion discs. For example at one million Kelvin or more the dielectronic recombination rates exceeds the radiative recombination rate by a factor of one hundred. However, for temperatures below a hundred thousand Kelvin, the radiative recombination rate is larger than the dielectronic recombination rate. One can easily see that this mechanism is most important in the coronae of solar type stars.

A second situation, dielectronic recombination is important for, is if states are hardly above the ionisation potential. A famous example for this is the $2s2p(^1P^0)3d$ state of N III, which has only a slight energetic difference to the $2s^2 3d$ state of N IV. In that case the dielectronic recombination feeds electrons in the $2s^2 3d$ state of N III. The radiative decay of this state produces the famous N III λ4636 and λ4640 emission lines of Of-stars.

4.5 Setting Up the Rate Equation Matrix

Now that all the transition processes of interest have been discussed, one should combine them in one complete equation system. This would look like Equation 4.5, involving all levels of all ionisation stages of each chemical element. The dielectronic recombination has not to be mentioned separately, because it has the same form as the radiative recombination. Therefor they may be combined together in one expression. There is also made a simplification in the notation, by the fact that one assumes that all ionisation processes are resulting in the ground state of the next ionisation stage.

In the following notation denotes i the ionisation stage. The single prime denotes the upward and the double prime the downward direction. That could be written down as

$$\begin{aligned} & -\sum_{i''<i} n_{i''}(R_{i''i}+C_{i''i}) \quad + \\ \left[\sum_{i''<i}\left(\frac{n_{i''}}{n_i}\right)^*(R_{ii''}+C_{ii''})+\sum_{i'>i}^{\kappa} n_{i''}(R_{ii'}+C_{ii'})\right] & \\ & -\sum_{i'>i}^{\kappa} n_{i'}\left(\frac{n_{i''}}{n_i}\right)^*(R_{i'i}+C_{i'i}) \quad = \quad 0 \qquad , \end{aligned} \tag{4.62}$$

whereas the single rates are defined by the following equations:

Equation 4.29 defines radiative rates

Equation 4.31 defines radiative rates

Equation 4.35 defines collisional rates

Equation 4.21 defines the LTE population ratio

Equation 4.24 defines the LTE population ratio

Now, there is still one more variable than equations. That variable is the ion density n_k. One has to find another equation to complete the rate equation system. Writing down the ionisation equation

$$\sum_{i<\kappa} n_i(R_{i\kappa}+C_{i\kappa}) - n_\kappa \sum_{i<\kappa}\left(\frac{n_i}{n_\kappa}\right)^*(R_{\kappa i}+C_{\kappa i}) = 0 \qquad , \tag{4.63}$$

one notes that Equation 4.63 gives the same results as Equation 4.62. Another physical law is needed to complete the system. In this case the particle conservation is often used. The number of all ionisation stages of every chemical species has to be equivalent to a constant number of all hydrogen atoms

$$\sum_{i,j} n_{ij,k} - \left(\frac{\alpha_k}{\alpha_H}\right)\left(\sum_i n_{i,H} + n_p\right) = 0 \qquad . \tag{4.64}$$

Alternatively one may use the charge conservation to complete the rate equation system.

After all the mathematical work, the *Rate Equation System* can be written down in the final form. There one uses these notations:

$\mathbf{n}$, a vector with $\mathcal{N}$ occupation numbers

$\mathcal{N}$, overall amount of occupation numbers

$\mathcal{A}$, Rate Matrix $\mathcal{N}\times\mathcal{N}$

$\mathcal{B}$, vector with one nonzero element (from Equation 4.64)

The general appearance of the *Rate Equation System* is

$$\mathcal{A}\mathbf{n} = \mathcal{B} \tag{4.65}$$

Generally, model atoms used for accretion disc modelling, include a large number of chemical species, e.g. H, He, C, N, O, Ne, Mg, Fe, Ni etc.. Therefore the rate equation matrix is very large and complex. To give an easy but correct example, Mihalas uses a model atom composed of hydrogen and helium. The helium abundances Y is given relative to the hydrogen abundance. Hydrogen has two ($HI\&HII$) and helium three ($HeI, HeII\&HeIII$) ionisation stages, with the levels L_H and L_0, L_+. This results in the total number of hydrogen states $M_H = L_H + 1$ and the total number of $M_{He} = L_0 + L_+ + 1$.

Denoting zero elements with 0 and nonzero elements with x, one gets the following matrix$\mathcal{A}$:

Row Number	1			L_0				M_{He}					$M_{He}+M_H$	
1	x	x	$\cdots$	x	x	0	$\cdots$	0	0	0	0	$\cdots$	0	0
2	x	x	$\cdots$	x	x	0	$\cdots$	0	0	0	0	$\cdots$	0	0
$\vdots$	$\vdots$	$\vdots$		$\vdots$	$\vdots$	$\vdots$		$\vdots$	$\vdots$	$\vdots$	$\vdots$		$\vdots$	$\vdots$
L_0	x	x	$\cdots$	x	x	0	$\cdots$	0	0	0	0	$\cdots$	0	0
L_0+1	0	0	$\cdots$	0	x	x	$\cdots$	x	x	0	0	$\cdots$	0	0
	0	0	$\cdots$	0	x	x	$\cdots$	x	x	0	0	$\cdots$	0	0
$\vdots$	$\vdots$	$\vdots$		$\vdots$	$\vdots$	$\vdots$		$\vdots$	$\vdots$	$\vdots$	$\vdots$		$\vdots$	$\vdots$
L_0+L_+	0	0	$\cdots$	0	x	x	$\cdots$	x	x	0	0	$\cdots$	0	0
M_{He}	1	1	$\cdots$	1	1	1	$\cdots$	1	1	$-y$	$-y$	$\cdots$	$-y$	$-y$
$M_{He}+1$	0	0	$\cdots$	0	0	0	$\cdots$	0	0	x	x	$\cdots$	x	x
	0	0	$\cdots$	0	0	0	$\cdots$	0	0	x	x	$\cdots$	x	x
$\vdots$	$\vdots$	$\vdots$		$\vdots$	$\vdots$	$\vdots$		$\vdots$	$\vdots$	$\vdots$	$\vdots$		$\vdots$	$\vdots$
$M_{He}+L_H$	0	0	$\cdots$	0	0	0	$\cdots$	0	0	x	x	$\cdots$	x	x
$M_{He}+M_H$	0	0	$\cdots$	0	1	1	$\cdots$	1	2	0	0	$\cdots$	0	1

Column Number

Figure 4.1: Rate matrix as an example for H and He

The rate matrix $\mathcal{A}$ contains of

$$\begin{cases} 1 to L_0 & , \text{ Equation 4.62 for } HeI \\ L_0 + 1 to L_0 + L_+ & , \text{ Equation 4.62 for } HeII \\ M_{He} & , \text{ Equation 4.64 for } HeII \\ M_{He} + 1 to M_{He} + L_H & , \text{ Equation 4.62 for } HI \end{cases}$$

The vector **n** looks like

$$\mathbf{n} = [n_1(HeI), \cdots, n_{L_0}(HeI), n_1(HeII), \cdots, n_{L_+}(HeII), \\ n(HeIII), n_1(H), \cdots, n_{L_H}(H), n_p]^T \quad , \tag{4.66}$$

whereas the vector $\mathcal{B}$ has the following appearance

$$\mathcal{B} = (0, \cdots, 0, n_e)^T \quad . \tag{4.67}$$

The temperature T, the electron number n_e and the radiation field J_ν are needed to solve Equation 4.65 as a linear equation system in **n**. In chapter 5, the standard numerical methods to solve such an equation system are introduced.

%

Chapter 5

Solving the Rate Matrix *A* by Newton-Raphson Iteration

As mentioned at the end of the last chapter (Page 52), knowing the temperature T, the electron number n_e and the radiation field J_ν, one can solve rate equation system (see Equation 4.65). As my thesis is concentrated on the rate equation system, the other equation needed to get an consistent solution for an accretion disc model are not discussed in detail here.

5.1 Linearisation of the Rate Equation System A

Considering the parameters n_e, T and J_ν are given and assuming their variations are given by δn_e, δT and δJ_ν. Then one has to calculate the *response* $\delta\mathbf{n}$ on these variations.

Starting with Equation 4.65

$$\mathcal{A}\mathbf{n} = \mathcal{B} \tag{5.1}$$

and the given values n_e, T and J_ν, one can write Equation 4.65 in terms of the new updated values as

$$(\mathcal{A}+\delta\mathcal{A})(\mathbf{n}+\delta\mathbf{n}) = (\mathcal{B}+\delta\mathcal{B}) \quad . \tag{5.2}$$

By neglecting the terms of second order, one may write down this equation in the form

$$\mathcal{A}\mathbf{n} - \mathcal{B} = -\delta\mathbf{n}\mathcal{A} - \mathbf{n}\delta\mathcal{A} + \delta\mathcal{B} \quad . \tag{5.3}$$

Now one has to find expressions for the terms $\delta\mathcal{A}$ and $\delta\mathcal{B}$. Therefore one may use the following equation:

$$\delta\mathcal{A} = \frac{\partial\mathcal{A}}{\partial T}\delta T + \frac{\partial\mathcal{A}}{\partial n_e}\delta n_e + \sum_{\nu=1}^{N_F}\frac{\partial\mathcal{A}}{\partial J_\nu}\delta J_{nu} \quad . \tag{5.4}$$

Note that in Equation 5.4 the radiation field has a discrete form. Instead of integrating the radiation field, one has to sum.

Using $\mathbf{n}$, n_e, T and J_ν as variables, Equation 5.4 can be solved. This method is known as the *Method of complete Linearisation*.

It turns out to be more useful when J_ν is eliminated out of the equation system. This can be done by expressing J_ν in terms of n_e, T and J_ν,

$$\begin{aligned} J_\nu &= f(\mathbf{n}, T, n_e) \\ J_\nu^d \sim S_\nu^d &= S_\nu^d(\mathbf{n}, T, n_e) \end{aligned} \quad . \tag{5.5}$$

In that case, the index d again denotes the depth. S_ν is the source function, which has been already defined in Equation 3.35.

The source function can be defined in a alternative way, too. Then the opacity caused by the scattering on free electrons is given by a own factor σ_ν. The source function then can be written as:

$$S_\nu^d = \frac{\eta_\nu^d}{\kappa_\nu^d + \sigma_\nu^d} \quad . \tag{5.6}$$

Going straight on with the linearisation, one may write down Equation 5.4 in the form

$$\delta\mathcal{A} = \frac{\partial\mathcal{A}}{\partial T}\delta T + \frac{\partial\mathcal{A}}{\partial n_e}\delta n_e + \sum_{\nu=1}^{N_F}\frac{\partial\mathcal{A}}{\partial S_\nu}\delta S_\nu \quad . \tag{5.7}$$

Equation 5.7 is called the *Method of advanced Λ-Operators*. For δS_ν one may write

$$\delta S_\nu = \frac{\partial S_\nu}{\partial T}\delta T + \frac{\partial S_\nu}{\partial n_e}\delta n_e + \sum_{j=1}^{NL_{\mathrm{ALL}}}\frac{\partial S_\nu}{\partial n_j}\delta n_j \quad . \tag{5.8}$$

In analogy to $\delta\mathcal{A}$ in Equation 5.7 one gets $\delta\mathcal{B}$ as follows

$$\delta\mathcal{B} = \frac{\partial\mathcal{B}}{\partial T}\delta T + \frac{\partial\mathcal{B}}{\partial n_e}\delta n_e + \sum_{\nu=1}^{N_F}\frac{\partial\mathcal{B}}{\partial S_\nu}\delta S_\nu = \frac{\partial\mathcal{B}}{\partial n_e}\delta n_e \quad , \tag{5.9}$$

because of the appearance of Equation 4.67. Now, putting together Equation 5.3, Equation 5.7 and Equation 5.9, one gets the linearised statistical equation system

$$\begin{aligned} \mathcal{A}\mathbf{n} - \mathcal{B} = -\delta\mathbf{n}\mathcal{A} \quad &- \quad \delta T\left[-\frac{\partial\mathcal{A}}{\partial T}\mathbf{n} - \sum_{\nu=1}^{N_F}\mathbf{n}\frac{\partial\mathcal{A}}{\partial S_\nu}\frac{\partial S_\nu}{\partial T}\right] \\ &+ \quad \delta n_e\left[\frac{\partial\mathcal{A}}{\partial n_e}\mathbf{n} - \sum_{\nu=1}^{N_F}\mathbf{n}\frac{\partial\mathcal{A}}{\partial S_\nu}\frac{\partial S_\nu}{\partial n_e}\right] \\ &+ \quad \sum_{j=1}^{NL_{\mathrm{ALL}}}\delta n_j\left[-\sum_{\nu=1}^{N_F}\mathbf{n}\frac{\partial\mathcal{A}}{\partial S_\nu}\frac{\partial S_\nu}{\partial n_j}\right] \quad . \end{aligned} \tag{5.10}$$

The equation system gives a *response* on the modifications δT and δn_e. It is obvious that the variables are coupled in a complex manner. Any change in the radiation field J_ν at any frequency ν will cause modifications on the occupation number of a arbitrary level l and it doesn't matter if the photon matches to a transition of this level or not.

To solve the linearised rate equation system, one needs the derivations $\frac{\partial}{\partial n_e}$, $\frac{\partial}{\partial T}$, $\frac{\partial}{\partial n_j}$ and $\frac{\partial}{\partial S_\nu}$ of the rate matrix $\mathcal{A}$, the solution vector $\mathcal{B}$ and the source function S_ν. Note that all derivations can be done analytically. Therfore the numerical solution of the linearised rate equation system will reach a higher level of accuracy and stability.

Last but not least some words on why one uses the non-LTE rate equations instead of the LTE rate equations. The reason can be found in the long range effects of photons. Aberations from the LTE will occur every time, the temperature is high and the density is low. If the conditions are the other way round (e.g. deep inside of stars) one can use the LTE equations unconsidered.

5.2 The Derivations of Rate Equation Matrix $\mathcal{A}$

5.2.1 The partial Derivation: $\frac{\partial}{\partial S_\nu}\mathcal{A}$

In principle this is the numerically most computing intensive part of the whole iterative disc calculation. This is due to the fact that one has to derive every matrix element for every frequency point in every depth and every iteration step. The only way to get rid of this problem is to eliminate the source function. Therefore one will substitute it by the local variables n_i, n_e and T. The exact description for the source function is

$$J_\nu = \Lambda S_\nu \quad , \tag{5.11}$$

but with that another problem will occur. The Lambda operator Λ is not a local operator. Better one uses the advanced form

$$J_\nu = \Lambda^* S_\nu + \Delta J_\nu \quad , \tag{5.12}$$

with the local lambda operator Λ^*. Here ΔJ_ν denotes the correction of the mean intensity during the last iteration step.

The next step is to substitute J_ν by using Equation 5.12. This has to be done for the radiative rates only, because the derivations are zero for non-radiative rates.

It suggest itself, to start the work with the *number of absorptions*. For the numerical calculation one has to discretise Equation 4.11. Therefore the transition $\nu \longrightarrow \nu_k$ with $k = 1 \ldots NF$ is made, where NF is the maximum number of frequency points used. Substituting the integral by a sum and introduce the summation weights w_k, one gets

$$n_i R_{ij} = n_i 4\pi \sum_{k=1}^{N_F} \frac{\alpha_{ij}(\nu_k)}{h\nu_k} J_{\nu_k} w_k \quad . \tag{5.13}$$

Then by inserting Equation 5.12 into Equation 5.13 one may get the final equation

$$n_i R_{ij} = n_i 4\pi \sum_{k=1}^{N_F} \frac{\alpha_{ij}(\nu_k)}{h\nu_k} w_k \left[\Lambda^* S_{\nu_k} + \Delta J_{\nu_k}\right] \quad . \tag{5.14}$$

Equation 5.14 can be derived partially $\frac{\partial}{\partial S_{\nu_k}}$, which provides the next equation

$$\begin{aligned} n_i \frac{\partial \mathcal{A}_{ij}}{S_{\nu_k}} &= -n_i \frac{\partial}{S_{\nu_k}} (R_{ij} + C_{ij}) \\ &= -\frac{\partial R_{ij}}{S_{\nu_k}} = -n_i 4\pi \frac{\alpha_{ij}(\nu_k)}{h\nu_k} w_k \Lambda^* \quad . \end{aligned} \tag{5.15}$$

Analogically the other radiative rates can be handled. Doing so, one will find for Equation 4.16

$$\begin{aligned} n_j \frac{\partial \mathcal{A}_{ij}}{S_{\nu_k}} &= -n_i \frac{\partial}{S_{\nu_k}} (R_{ji} + C_{ji}) \\ &= -n_j \frac{\partial R_{ji}}{S_{\nu_k}} = n_j \left(\frac{n_i}{n_j}\right)^* \left[4\pi \sum_{k=1}^{N_F} \frac{\alpha_{ij}(\nu_k)}{h\nu_k} \Lambda^* e^{-\frac{h\nu_k}{kT}}\right] \end{aligned} \tag{5.16}$$

and for Equation 4.28

$$\begin{aligned} n_\kappa \frac{\partial \mathcal{A}_{i\kappa}}{S_{\nu_k}} &= -n_\kappa \frac{\partial}{S_{\nu_k}} \left(R_{\kappa i,\mathrm{stim}} + R_{\kappa i,\mathrm{spon}} \right) \\ &= -n_i \left(\frac{n_i}{n_\kappa} \right)^* \frac{\partial R_{\kappa i}}{S_{\nu_k}} = -n_i \left(\frac{n_i}{n_\kappa} \right)^* \left[4\pi \sum_{k=1}^{N_F} \frac{\alpha_{i\kappa}(\nu_k)}{h\nu_k} \Lambda^* e^{-\frac{h\nu_k}{kT}} \right] \quad . \end{aligned} \tag{5.17}$$

To provide all derivation, which are needed, the first step is to calculate the partial derivations $\frac{\partial}{\partial S_\nu}\mathcal{A}$. In the next subsection 5.2.2 as a second step the partial derivations $\frac{\partial}{\partial n_e}\mathcal{A}$ is attended.

5.2.2 The partial Derivation: $\frac{\partial}{\partial n_e}\mathcal{A}$

For the calculation of this derivation, one has to consider all collisional ionisation rates and all recombination rates, namely the collisional recombination rates and the radiative recombination rates. The collisional ionisation rates are concerned by the expression

$$C_{ij} = n_e \cdot \Omega_{ij} \quad , \tag{5.18}$$

whereas the recombination rates are involved, because of the ion density

$$\left(\frac{n_i}{n_j} \right) = n_e \cdot \phi_i \quad . \tag{5.19}$$

The downward transition rates have not to be considered. This is because the distribution in that case is given by the Boltzmann equation, where the electron density is not involved in, unlike the Saha equation used in Equation 5.19. In principle all line transition rates have to be considered as well, but not in practice. This is due to the fact, that the electron density is fundamental for the Stark broadening of the lines, but for the calculation of the disc structure the exact line profile is not important. One will use a Doppler profile with a characteristic temperature ($\frac{3}{4} \cdot T_{\mathrm{eff}}$). If one wants to do line formation calculation this is of course no longer true.

For the following calculation of the derivation, l denotes the ionisation stage, whereas i and j are the identifiers of the levels involved

$$\frac{\partial \mathcal{A}_{ij}}{\partial n_e} = \begin{cases} -\Omega_{ji} & j < i & i = 1, NL(l) \\ -\left(\frac{n_i}{n_j} \right)^* \Omega_{ij} & j > i & \\ -\phi_i^* \left(R_{ji} + 2 n_e \Omega_{ij} \right) & j > i & j = \mathrm{cont}^* \, (\mathrm{recomb.}) \\ \sum\limits_{m<i} \left(\frac{n_m}{n_i} \right)^* \Omega_{mi} + \sum\limits_{m>i}^{\mathrm{cont.}} \Omega_{im} & j = i & \\ \sum\limits_{m=\mathrm{LTE(l-1)}} \phi_{l-1,m} & j = \mathrm{groundstates} & \\ -Y_k \sum\limits_{m=\mathrm{LTE(H)}} \phi_m & j = \mathrm{NL_{ALL}} & \\ q(l-1) \sum\limits_{m=\mathrm{LTE(l-1)}} \phi_{l-1,m} & j = \mathrm{groundstates} & \quad . \end{cases} \tag{5.20}$$

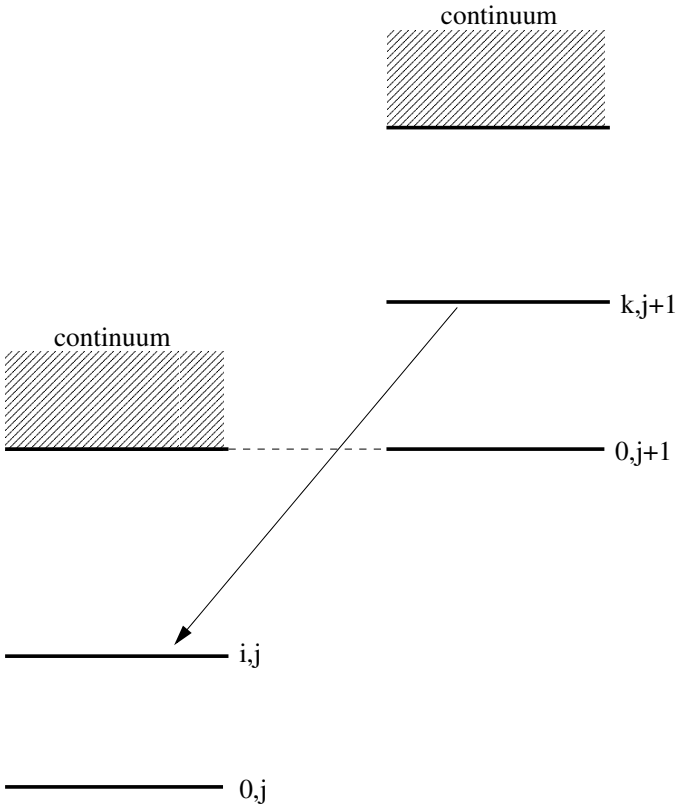

Figure 5.1: Recombination from an excited level shown as a Grotrian diagram

Now one special case has to be discussed. If there is a recombination from an excited level, the Saha factor ϕ_i has to be modified. This case is shown as a Grotrian diagram in Figure 5.1. To get the new Saha factor one has to make a transition like the following ones. Note that the first index denotes the level and the second index denotes the ionisation stage.

$$\phi_{i,l} \longrightarrow \phi_{i,l} \cdot \frac{\phi_{0,l+1}}{\phi_{j,l+1}} \tag{5.21}$$

Using the definition of the LTE occupation number n^*_{ij} and the definition of the Saha factor $\phi_{ij\to 0,l+1}$, one can easily see that there is a problem with recombinations from an excited level

$$n^*_{ij} = n_e n_{0,j+1} \phi_{ij\to 0,j+1} \Longrightarrow \frac{n^*_{ij}}{n_{0,j+1}} = n_e \phi_{ij\to 0,j+1} \tag{5.22}$$

$$\phi_{ij\to 0,j+1} = \frac{g_{i,j}}{g_{0,j+1}} \frac{1}{2} \left(\frac{h^2}{2\pi m k T} \right) e^{\frac{h\nu_{ij\to 0,j+1}}{kT}} \quad . \tag{5.23}$$

Combining the equations Equation 5.22 and Equation 5.23, one will find, that the ratio of occupation numbers in LTE case is not the same as the ratio of the LTE occupation numbers in non-LTE case.

$$\left(\frac{n_{ij}}{n_{k,j+1}} \right)^* \neq \frac{n^*_{ij}}{n^*_{k,j+1}} \tag{5.24}$$

This is true for all recombinations from excited levels. One has to find a new expression for the ration of the occupation numbers in the LTE case $\left(\frac{n_{ij}}{n_{0,j+1}}\right)^*$. By using the definition of the Saha equation and the definition of the Boltzmann equation, one may write down the following relation

$$\left(\frac{n_{ij}}{n_{k,j+1}}\right)^* = \left(\frac{n_{ij}}{n_{0,j+1}}\right)^* \cdot \left(\frac{n_{0,j+1}}{n_{K,j+1}}\right)^* \tag{5.25}$$

$$= n_e \phi_{ij\to 0,j+1} \cdot \frac{g_{0,j+1}}{g_{k,j+1}} e^{\frac{h\nu_{0,j+1\to k,j+1}}{kT}} \quad . \tag{5.26}$$

The energy difference between the to levels k and 0 can be given as the difference between the ionisation energies of the two involved ionisation stages. Using the knowledge about this energy difference and Equation 5.25, one may express the searched ratio by the Saha factors

$$\left(\frac{n_{ij}}{n_{k,j+1}}\right)^* = n_e \phi_{i,j\to 0,j+1} \cdot \frac{\phi_{0,j+1\to 0,j+2}}{\phi_{k,j+1\to 0,j+2}} \tag{5.27}$$

$$= n_e \phi_{ij} \frac{\phi_{0,j+1}}{\phi_{k,j+1}} \quad . \tag{5.28}$$

The factor modifying the former Saha factor in Equation 5.22, arises from the occupation balance between two neighbouring ionisation stages. The greatest advantage of writing down this relation in the form of Equation 5.27 or Equation 5.22 is, that the occupation numbers of levels of neighbouring ionisation stages are given consistently.

5.2.3 The partial Derivation: $\frac{\partial}{\partial T}\mathcal{A}$

Because the temperature appears explicitly in most of the equations the rate matrix $\mathcal{A}$ consisting of, deriving the rate matrix system is a demanding work. One has to take into account the

- line or RBB transition rates
- continuum or RBF transition rates
- collisional transition rates, CBB, CBF, etc.

The derivation of the cross section appearing in the radiative bound-bound rate provides the fact, that absorption and emission lines are only broadened by Doppler effect

$$\frac{\partial}{\partial T}\sigma_{ij}(\nu) = \sigma_{ij}(\nu)\frac{1}{2T}\left[\left(\frac{\Delta\nu}{\Delta\nu_D}\right)^2 - 1\right] \quad . \tag{5.29}$$

In the case of the radiative bound-free transition rates, the cross section does not depend on the temperature. This makes the whole calculation a lot more simple

$$\frac{\partial \mathcal{A}_{ij}}{\partial T} = \begin{cases} -n_e \frac{\partial \Omega_{ji}}{\partial T} - \frac{\partial R_{ij}}{\partial T} & j < i \quad i = 1, NL(l) \\ -\left(\frac{n_i}{n_j}\right)^* \left[-(R_{ji}+C_{ij})\frac{h\nu_{ij}}{kT^2} + \right. & \\ \qquad \left. \int \sigma_{ij}\left(J_\nu + \frac{2h\nu^3}{c^2}\right) e^{-\frac{h\nu}{kT}} d\nu + n_e \frac{\partial \Omega_{ji}}{\partial T}\right] & j > i \\ -\left(\frac{n_i}{n_j}\right)^* \left[\frac{1}{T}\left(-\frac{3}{2} - \frac{h\nu_i}{kT}\right)(R_{ji}+C_{ij}) + \right. & \\ \qquad \left. \int \sigma_{ij}\left(J_\nu + \frac{2h\nu^3}{c^2}\right) e^{-\frac{h\nu}{kT}} d\nu + n_e \frac{\partial \Omega_{ji}}{\partial T}\right] & j > i \quad j = continuum \\ -\sum_{m<i} \frac{\partial \mathcal{A}_{mi}}{\partial T} - \sum_{m>i} \frac{\partial \mathcal{A}_{mi}}{\partial T} + n_e \frac{\partial \Omega_{i,cont.}}{\partial T} & j = i \\ -\frac{n_e}{T} \sum_{m=LTE(l-1)} \phi_{l-1,m}\left(\frac{3}{2} + \frac{h\nu_{lm}}{kT}\right) & j = groundstates \\ Y_k \frac{n_e}{T} \sum_{m=LTE(H)} \phi_m \left(\frac{3}{2} + \frac{h\nu_m}{kT}\right) & j = NL_{\mathrm{ALL}} \\ -q(l-1)\frac{n_e}{T} \sum_{m=LTE(l-1)} \phi_{l-1,m}\left(\frac{3}{2} + \frac{h\nu_m}{kT}\right) & j = groundstates \quad . \end{cases} \tag{5.30}$$

Note that collisional transition rates can be expressed analytically too, which makes the numerical calculation more stable and a lot of faster.

5.3 Solving the Rate Equation System

For the calculation of an accretion disc model, one has to solves the radiation transfer equation, the energy equation, the rate equation and the hydrostatic equation consistently with the ALI method (Werner 1986; Werner & Dreizler 1999). This non-linear equation system may be written in matrix notification (see section 3.7)

$$\mathcal{M}^d(\psi)\cdot\psi^d = \mathbf{c}^d(\psi) \qquad . \tag{5.31}$$

The upper index d denotes the depth dependency of the equation system. The solution vector of the equation system is given as follows

$$\psi^d = (n_1,\ldots,n_{NL},N,T,n_e,J_{\nu_1},\ldots,J_{\nu_{NF}})^d \qquad . \tag{5.32}$$

It contains the occupation numbers from the rate equations $(n_1,\ldots,n_{NL})^d$ and radiation field $(J_{\nu_1},\ldots,J_{\nu_{NF}})^d$, as well as the hydrostatic layering $N(d)$, the energy distribution $T(d)$ and at last the particle conservation n_e.

The rate equation system is just a subset of equations in the non-linear equation system one has to solve. The other equations have to be linearised in the same way as it has been done in section 5.1 for the rate equations. Therefor one will need some more derivations. Namely the derivations $\frac{\partial S_k}{\partial n_j}$, $\frac{\partial S_k}{\partial n_e}$ and $\frac{\partial S_k}{\partial T}$.

The major task of the accelerated lambda iteration (ALI) is to eliminate the explicit appearance of the radiation field in the equation system by providing an implicit approximative solution for the radiation field. Therefore the following approach for the radiation field is used to get the exact solution by iteration.

$$J_\nu^{(i)} = \Lambda^* S_\nu^{(i)} + \Delta J_\nu^{(i)} \qquad . \tag{5.33}$$

The whole iteration process is shown as a diagram in Figure 5.2. As a start approximation normally a LTE model is applied.

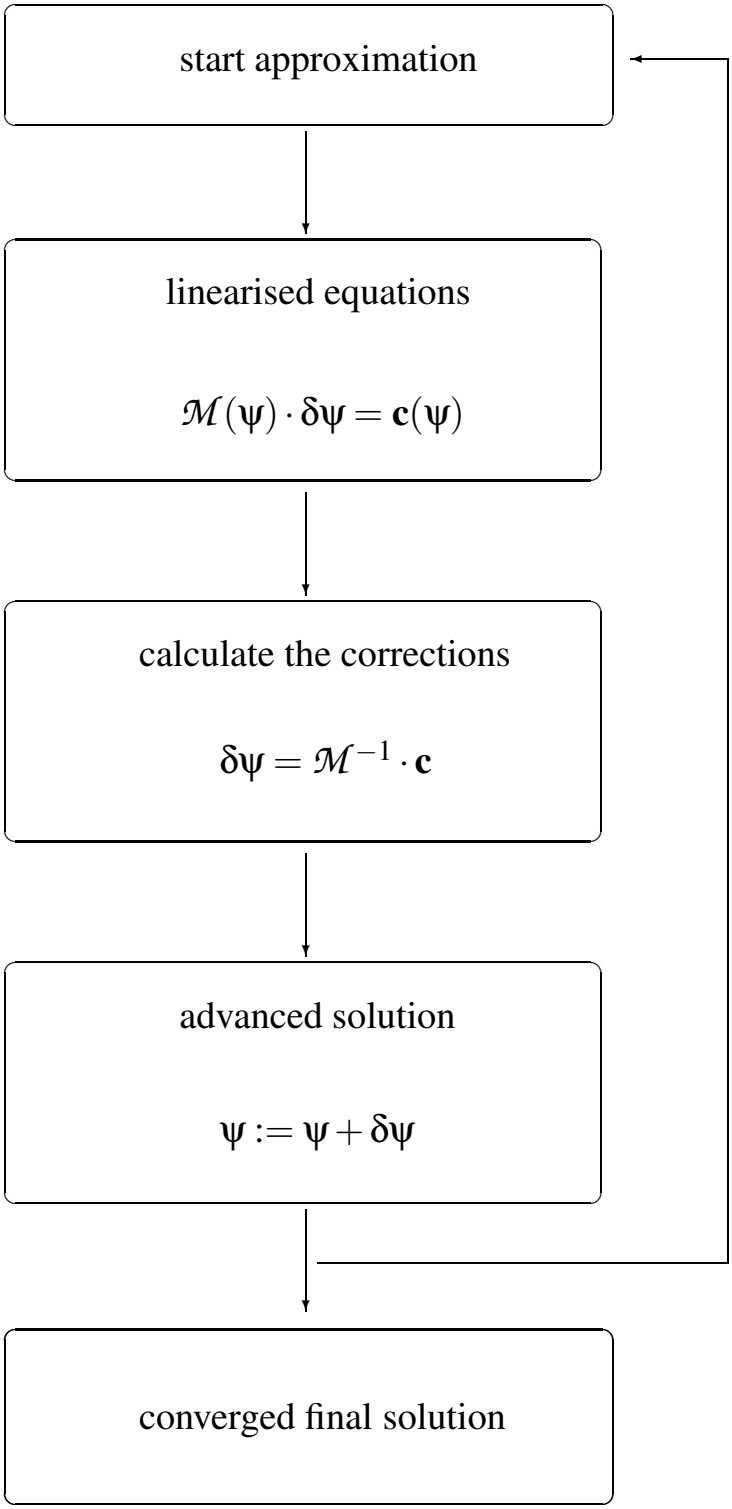

Figure 5.2: Flux chart of the accelerated lambda iteration

Chapter 6

New Solution Technique

6.1 Solution Technique used in AcDc

By increasing the number of chemical species and ionisation stages, the rate matrix $\mathcal{A}$ grows more and more. The demand of memory during the numerical calculation of the accretion disc model increases heavily. The other problem is that a very huge matrix will need a lot of time to be inverted.

Therefore in the ACDC non-LTE accretion disc model code and in the non-LTE stellar atmosphere code NGRT on which ACDC is based on, a modified method to solve the rate matrix system is used.

As discussed in section 4.5, in classical atmosphere modelling the rate matrix is set up for all levels of every ionisation stage of all involved chemical species. To avoid the problems mentioned above a basic idea is, to set up the rate matrix only for the ionisation stages of on single chemical species. Then the rate matrix would be much smaller and easier to handle. In Figure 6.1 an example of a rate matrix is shown according to Figure 4.1. During the iteration all the rate matrices for the

$$
\begin{array}{ll}
\textit{Row} & \\
\textit{Number} & \\
M_{He} & \begin{pmatrix} 1 & -y & -y & \cdots & -y & -y \end{pmatrix} \\
M_{He}+1 & \begin{pmatrix} 0 & x & x & \cdots & x & x \end{pmatrix} \\
 & \begin{pmatrix} 0 & x & x & \cdots & x & x \end{pmatrix} \\
\vdots & \begin{pmatrix} \vdots & \vdots & \vdots & & \vdots & \vdots \end{pmatrix} \\
M_{He}+L_H & \begin{pmatrix} 0 & x & x & \cdots & x & x \end{pmatrix} \\
M_{He}+M_H & \begin{pmatrix} 2 & 0 & 0 & \cdots & 0 & 1 \end{pmatrix} \\
 & \begin{array}{cccccc} M_{He} & & & & & M_{He}+M_H \end{array}
\end{array}
$$

Column Number

Figure 6.1: Rate matrix as an example for He

single chemical species can be solved in the same manner as discussed for in the classical case in section 5.3. This opens up the possibility to handle chemical species with a lot more ionisation stages than hydrogen and helium.

6.2 Outlook

As a further step to reduce the amount of computing power and memory use, one can set up the a separate rate matrix for every single ionisation stage. This feature is basically provided by the ACDC code, but not yet supported by the depth dependent model atom. It would be one of the future steps to implement the DEPTOM for this method, too.

Part III

The Depth Dependent Model Atom DEPTOM

Chapter 7

The DEPTOM in the AcDc Model Disc Code

The chapter will provide general overview over the depth dependent model atom, hereafter called DEPTOM. The newly developed routines are described as well, as the changes to routines of the ACDC accretion disc model code.

7.1 Why develop a Depth Dependent Model Atom?

First one has to discuss the need to develop a depth dependent model atom. In accretion discs the temperature varies over a large range (a few 10 000 K up to a few 100 000 K). This leads to the fact, that in the hot parts of the disc, the lower ionisation stages are barely occupied, whereas the other way round in the cooler parts of the disc the occupations numbers of the higher ionisation stages are very small. Such extremely small occupation numbers (e.g. O VIII has sometimes an occupation number $\sim 10^{-150}$) causes strong numerical problems since they are numerical almost identical to zero.

The goal of this diploma thesis was to develop a numerical mechanism which identifies the weakly occupied ions and deactivates them in the further iterative process of the accretion disc calculation. This stabilises the whole numerical calculation. It also allows the use of a consistent model atom, which has not to be adapted separately for every disc ring.

7.2 The Basic Ideas of the Depth Dependent Model Atom

Here the basic ideas of DEPTOM are shown and a short overview over some of the problems implementing the DEPTOM is given.

First one has to monitor the occupation numbers of all ionisation stages involved in the calculation. In every iteration step the occupation numbers are compared to a lower limit, which can be set by the user. If the occupation number of a specific ionisation stage is below that limit the stage will be marked. A specific ionisation stage will not be switched off until the occupation numbers are several times below the limit. This is necessary to avoid problems with numerical fluctuation during the iteration process.

Once an ionisation stage has been switched off, all levels assigned to it, have to be cut out of the rate matrix. Due to the fact that the rate matrix has to be inverted at the end of the iteration step, to calculate the occupation numbers, the ionisation stage cannot be set to zero.

If one wants to invert the rate matrix, the matrix must not have columns or rows containing only zeros. This can be seen at the following formulae for matrix inverting

$$\mathcal{A}^{-1} = \frac{1}{det\,(\mathcal{A})}\mathcal{A}_{\mathrm{adj}} = \frac{1}{det\,(\mathcal{A})}\mathcal{A}_{\chi\psi} \qquad . \tag{7.1}$$

Note that $\mathcal{A}_{\mathrm{adj}}$ is the so called adjoint matrix, consisting of the adjoint elements. These adjoint elements satisfy the relation

$$\sum_{\psi=1}^{n} a_{\chi\psi}\mathcal{A}_{\zeta\psi} = 0 \qquad (\chi,\zeta \text{ fixed}; \quad \zeta \neq \psi) \qquad . \tag{7.2}$$

As shown above, it is impossible to invert matrices with columns and rows composed completely of zeros. Therefore it is not possible to set the columns and rows of an specific ionisation stage simply to zero when the stage is deactivated. One has to cut the rows and columns out of the rate matrix $\mathcal{A}$ and combine the remnant of the matrix to a new smaller rate matrix (see Figure 7.1). Which can then be used in the further iterative process.

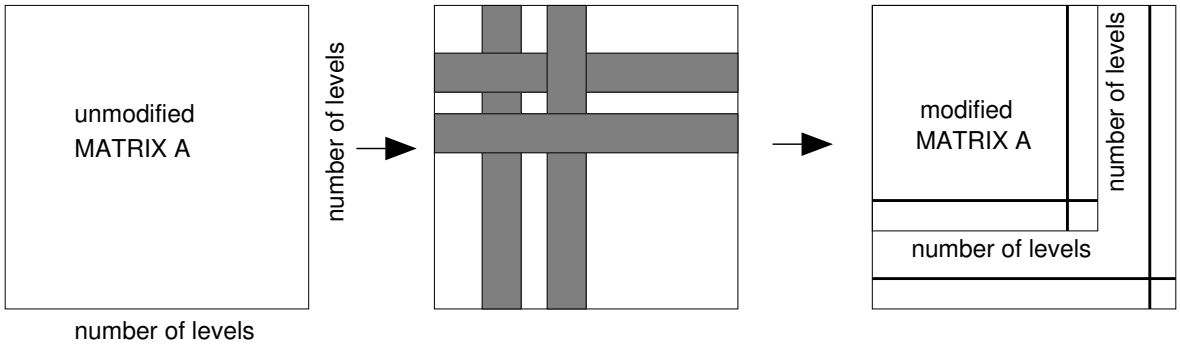

Figure 7.1: Cutting ionisation stages out of the rate matrix $\mathcal{A}$. The grey fields denotes the cut out ionisation stage. The black bars denote the old and new position of a specific level, before and after cutting out the ionisation stages.

But cutting out ionisation stages, causes some new problems. Reducing the rate matrix means, that levels will change their position in the matrix. The loop counter system, used in the code, will not work any more. One has to adjust the loop counters in the routines (see Figure 7.1), to ensure that the levels and the associated transitions are still matching together.

Another thing to keep in mind is the fact that in the model atoms used for accretion disc modelling the last ionisation stage of a chemical element is used as the closure. Thus the last active ionisation stage is the new closure of the model atom for a specific chemical specie. Therefore it should consist of only the ground state. This requires different rules for cutting out ionisation stages at the upper end and the lower end of the model atom.

Another major problem appears when one is calculating irradiated accretion disc models. Ionisation stages with an occupation number well below the limit, in a not or only weakly irradiated accretion disc model, might get occupied stronger and stronger when the temperature rises due to the irradiation. Then they should be reactivated for the further iteration process. But monitoring the deactivated ionisation stages is not trivial, due the fact that their occupation numbers are not calculated correctly.

The easiest way to solve the problem is to reset the DEPTOM every several iteration steps and keep it deactivated for a few steps. Then the occupation numbers are able to relax. Resetting the DEPTOM is done by the heat cycle loop. This is not a very elegant way and time should be spent to solve that problem more elegantly in future work.

7.3 The Subroutine DEPTOM

The deptom subroutine is together with the controlling subroutines depcon (see section 7.4) and set_amat_depcon (see section 7.5) the heart of the depth dependent model atom. Both subroutines are placed in the subroutine se_solve, but both run directly in the ALI-iteration loop.

The user of ACDC has the free choice to use DEPTOM or not. One can set the on / off switch in a control card. The default status is off. All new control cards for ACDC, which are implemented with DEPTOM, are listed in Appendix A.

The first step which is done in the deptom subroutine is to check whether DEPTOM is active or not. After that the so called occupation density is calculated. This simply is the occupation number of an ionisation stage normalised by dividing by the overall particle number. This occupation density is then compared to a lower limit. The user of ACDC can provide the limit, otherwise the code will use 10^{-20} as a default value.

Because of numerical fluctuations, especially at the beginning of the iteration, it is not useful to deactivate a specific ionisation stage, if it is only sometimes below the limit. Therefore a kind of damping factor for DEPTOM was created. If the occupation density of an ionisation stage is below the limit the stage gets a mark in the so called bad-array. Therein all ionisation stages in all depths are listed. Now the damping factor tells the code how often one ionisation stage should be marked before it is finally deactivated. All this is done in a loop for all involved ionisation stages.

As a reminiscence to the fact that the procedures described here are somewhat complex, they are shown graphically in a kind of flux chart in Figure 7.2 and Figure 7.3.

If one of the ionisation stages has been marked more often than the value set by the DEPTOM damping factor, the code has to check at which position of the full model atom this ionisation stage is found. This is very important for the further proceeding. If the ionisation stage is at the lower end of the model atom, it is simply deactivated by setting the activation flag in DEPTOM flag array to zero. The flag array contains the whole activation information for every ionisation stage in every depth. The array is used to determine later what to do with transitions with a specific ionisation stage involved in. Afterwards the entry in the bad-array is reset to zero.

If the ionisation stage is at the upper end of the model atom, it is deactivated too, but then one needs a new closure for the model atom. This is done by reducing the next ionisation stage below the one deactivated to the ground state. Therefore the entry in the flag array is set to a value of two.

The case when the ionisation stage is found in the middle of the model atom, is treated as a unphysical case. Then it is handled like an ionisation stage at the upper end and all stages above are deactivated. For this reason one has to check the status of the ionisation stages above and below the one considered here.

The last step in the deptom routine is to print out the bad-mark array and the flag array to the standard output file. In Figure 7.4 a DEPTOM flag array is shown as an example. The user can watch DEPTOM, which is useful because all parameters of DEPTOM can be changed, during the code is running. This is to optimise the performance of the code.

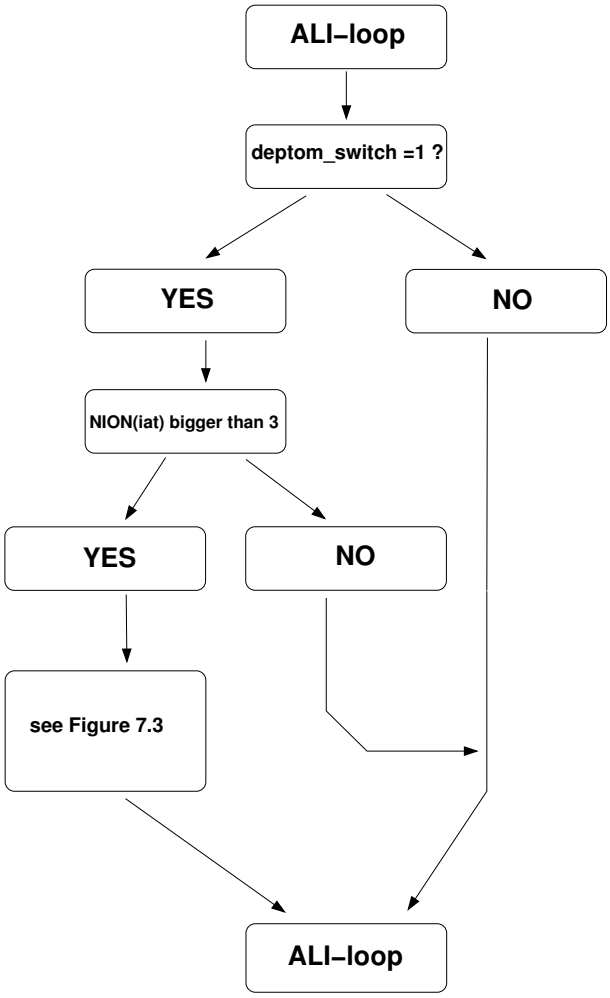

Figure 7.2: Flux chart of the depth dependent model atom: part 1. Note that NION(iat) denotes the number of ionisation stages of a specific atom.

7.4 The Subroutine DEPCON

The depcon subroutine is a small but quite important part of the DEPTOM. Therein all active levels are counted to get the new dimension of the rate matrix $\mathcal{A}$. The second and also very important function of this subroutine is to adjust the level counter to ensure that later on transitions and levels will still match together.

The first step in this subroutine is to check if DEPTOM is switched on. Then the subroutine steps atom by atom through the ionisation stages and checks the status of it. If the stage is active all levels are added, if it is reduced to ground state only one level is added and if it is deactivated no level is added.

During the summation of the levels, the current number of levels is compared to the original number of levels for every ionisation stage. The difference between the level numbers is stored in a correction array, which is used to adjust the level counter in the further iteration. In that way one

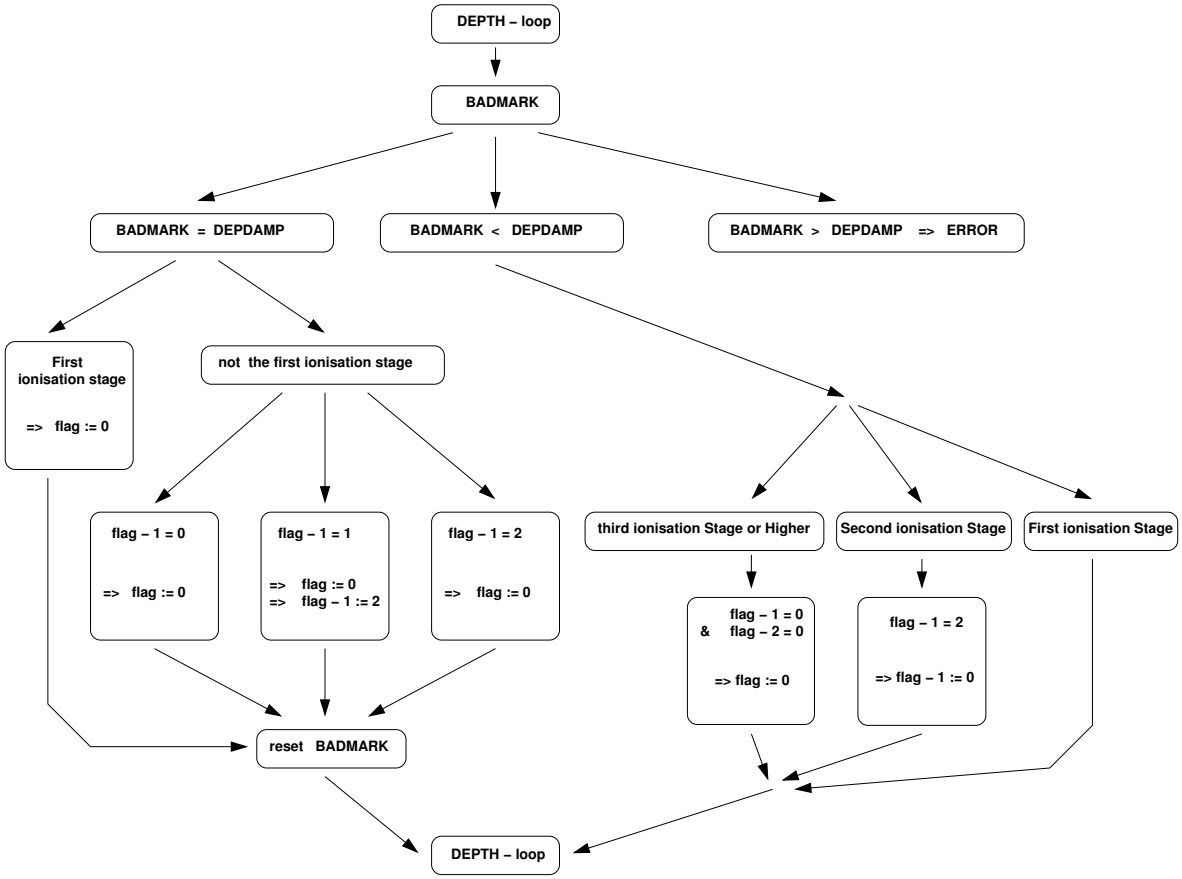

Figure 7.3: Flux chart of the depth dependent model atom: part 2. Note that flag denotes the activation flag of an specific ionisation stage and DEPDAMP denotes the damping factor of the DEPTOM (see section 7.3)

can provide a mismatch of levels and transitions, when setting up the rate matrix $\mathcal{A}$ in the subroutine set_amat_depcon (see section 7.5).

7.5 The Subroutine SET_AMAT_DEPCON

In the original subroutine set_amat the rate matrix $\mathcal{A}$ is set up. There are all the different transition prepared in, e.g. RBB-transitions and so on (Part II).

In the revised subroutine set_amat_depcon, there is a case differentiation made for every type of transitions. Hereby is checked, which case applies for the status of an associated ionisation stage. If the ionisation stage to which the transition belongs, is activated, all possible transition will be executed.

If the ionisation stage is reduced to ground state or if it is deactivated completely no transition will be executed. This is not completely correct, but a save alternative to handle the transitions from and to the ground state of model atom closures. Here some future work has to be done concerning the correct handling of transitions involving those ground states.

At the end of the subroutine set_amat_depcon the LTE populations are added to each ground state. This is done in order to get the particle conservation in section 7.6 right.

7.6 The Subroutine SE_SOLVE

The two DEPTOM controlling units depcon and set_amat_depcon are located in the subroutine se_solve. Therefore some more changes had to be made when implementing DEPTOM.

First the complete number of levels given by the used model atom is calculated. Afterwards, if DEPTOM is active, the subroutine depcon is called. The next step is to allocate the array for the rate matrix, which is set up by the subroutine set_amat. If DEPTOM is active, the subroutine set_amat_depcon is used, otherwise the original set_amat will be used.

Now ACDC solves the rate equations by matrix inversion, to get the occupation numbers . Therefor the code uses the matinv subroutine of the LAPACK math routines package (Anderson et al. 1991), which itself uses the BLAS package (Lawson et al. 1979). Thereby the occupation numbers of deactivated levels are set to 10^{-33}. This is the lower limit of a float number and equivalent to a numerical zero. Note that in the case of the closure of the model atom, only the ground state is used. All the occupation numbers of the other levels in this ionisation stage are set to 10^{-33}.

7.7 The Main Programme ACCDISC

Due to the fact, that the ALI iteration loop runs in the main program, some changes had to be made there, too. First, before the ALI loop starts, the DEPTOM arrays and the heat cycle loop counter have to be initialised. To control the initialisation DEPTOM arrays are printed to standard output. When the call of the subroutine changeinput (see section 7.8) is made, DEPTOM arrays and the heat cycle loop counter have to reinitialised.

As already mentioned in section 7.2, DEPTOM has to be reseted from time to time. This is necessary to include ionisation stages, which have been under occupied in the past, but getting occupied stronger due to the irradiation of the accretion disc. The main program accdisc contains a feature that DEPTOM is reseted at the end of the so called heat cycle. The length of the heat cycle can be set by the user of ACDC. It is also necessary to keep DEPTOM damped stronger in that case, thus the damping factor is set to 10 automatically.

The next step is to call the subroutine se_solve, which contains the controlling sections of DEPTOM, the subroutines depcon and set_amat_depcon. During testing of DEPTOM the se_solve subroutine was also placed at the end of the main program. But it turned out to be less stable.

At the end of the ALI loop one finds the deptom subroutine (see section 7.3) itself. It is placed best here, because before there is something to regulate, at least one iteration step has to be performed.

The last act done in the main program is to write all the output files to disk. Then the final DEPTOM flag array will be written to the standard output file and to a single deptom output file (see Figure 7.4).

7.8 The Subroutines RDINPUT2 and CHANGEINPUT

At last I would like to describe the input subroutines rdinput2 and changeinput. They scan through the INPUT file, which is written by the job start shell script, searching for known keywords. Then they write those control cards into the appropriate variables. Every parameter, which can be set in DEPTOM has to be implemented here.

The subroutine rdinput2 has the function to read the control cards at the beginning of the iteration. It reads the switch to activate DEPTOM and the switch, which tells DEPTOM if the deptom arrays should be printed out every iteration. The final deptom array will be printed at the end of the final

iteration in any case. The damping parameter, controlling how fast DEPTOM will act and the length of the heat cycle are also read here. The last parameters read by rdinput2, are the lower limits for the occupation numbers of the ionisation stages for all chemical species used for the calculation. The correct usage of DEPTOM parameters is given in Appendix A.

The changeinput subroutine does basically the same as rdinput2 does. It re-reads the INPUT file during the iteration, to provide the possibility to change parameters interactively. The changeinput subroutine is less extensive than the rdinput2, because not all parameters used in ACDC are allowed to be changed interactively.

All DEPTOM parameters can be changed interactively, to provide a more flexible handling. This turned out to be very useful, when one wants to use another model atom, as used for the LTE calculations.

```
        *** DEPTOM FLAG ARRAY in LAST Iteration
        ***
***  Masse des Zentralobjektes (Msol) :      0.14000000E+01
***  Radius des Zentralobjektes (cm) :       0.10000000E+07
***  Ringabstand (cm):                       0.12000000E+10
***  Akkretionsrate (Msol/y):                0.20000000E-09
***  Reynoldszahl:                          10000.00
***  Viskositaetskoeffizient zeta0:             0.000
***  Viskositaetskoeffizient zeta1:             0.010
***  Effektivtemperatur (Kelvin):           40805.45
*************************************************************************
```

* depth	log m	T	H1	H2	HE1	HE2	HE3	C2	C3	C4	C5	NE3	NE4	NE5	NE6	NE7	MG3	MG4	MG5	MG6	MG7	O2	O3	O4	O5	O6	O7	O8	O9
1	-6.500	597164.7	1	1	0	1	1	0	1	1	1	0	1	1	2	0	0	1	2	0	0	0	0	0	1	2	0	0	0
2	-6.413	585539.5	1	1	0	1	1	0	1	1	1	0	1	1	2	0	0	1	2	0	0	0	0	0	1	2	0	0	0
3	-6.326	582450.7	1	1	0	1	1	0	1	1	1	0	1	1	2	0	0	1	2	0	0	0	0	0	1	2	0	0	0
4	-6.240	578764.0	1	1	0	1	1	0	1	1	1	0	1	1	2	0	0	1	2	0	0	0	0	0	1	2	0	0	0
5	-6.153	574339.7	1	1	0	1	1	0	1	1	1	0	1	1	2	0	0	1	2	0	0	0	0	0	1	2	0	0	0
6	-6.066	569205.1	1	1	0	1	1	0	1	1	1	0	1	1	2	0	0	1	2	0	0	0	0	0	1	2	0	0	0
7	-5.979	563218.1	1	1	0	1	1	0	1	1	1	0	1	1	2	0	0	1	2	0	0	0	0	0	1	2	0	0	0
8	-5.892	556214.2	1	1	0	1	1	0	1	1	1	0	1	1	2	0	0	1	2	0	0	0	0	0	1	2	0	0	0
9	-5.806	548211.9	1	1	0	1	1	0	1	1	1	1	1	1	2	0	0	1	2	0	0	0	0	0	1	2	0	0	0
10	-5.719	538841.1	1	1	0	1	1	0	1	1	1	1	1	1	2	0	0	1	2	0	0	0	0	1	1	2	0	0	0
11	-5.632	528096.5	1	1	0	1	1	0	1	1	1	1	1	1	2	0	0	1	2	0	0	0	0	1	1	2	0	0	0
12	-5.545	516153.5	1	1	0	1	1	0	1	1	1	1	1	1	2	0	0	1	2	0	0	0	0	1	1	2	0	0	0
13	-5.458	502830.5	1	1	0	1	1	0	1	1	1	1	1	1	2	0	0	1	2	0	0	0	0	1	1	2	0	0	0
14	-5.372	488316.0	1	1	1	1	1	0	1	1	1	1	1	1	2	0	0	1	2	0	0	0	0	1	1	2	0	0	0
15	-5.285	472737.6	1	1	1	1	1	0	1	1	1	1	1	1	2	0	0	1	2	0	0	0	0	1	1	2	0	0	0
16	-5.198	456340.7	1	1	1	1	1	0	1	1	1	1	1	1	2	0	0	1	2	0	0	0	0	1	1	2	0	0	0
17	-5.111	439661.4	1	1	1	1	1	0	1	1	1	1	1	1	2	0	0	1	2	0	0	0	0	1	1	2	0	0	0
18	-5.024	422812.7	1	1	1	1	1	0	1	1	1	1	1	1	2	0	0	1	2	0	0	0	0	1	1	2	0	0	0
19	-4.938	406366.9	1	1	1	1	1	0	1	1	1	1	1	1	2	0	1	1	2	0	0	0	0	1	1	2	0	0	0
20	-4.851	390194.9	1	1	1	1	1	0	1	1	1	1	1	1	2	0	1	1	2	0	0	0	0	1	1	2	0	0	0
21	-4.764	374549.5	1	1	1	1	1	0	1	1	1	1	1	1	2	0	1	1	2	0	0	0	0	1	1	2	0	0	0
22	-4.677	359398.8	1	1	1	1	1	0	1	1	1	1	1	1	2	0	1	1	2	0	0	0	0	1	1	2	0	0	0
23	-4.590	344734.9	1	1	1	1	1	0	1	1	1	1	1	1	2	0	1	1	2	0	0	0	0	1	1	2	0	0	0
24	-4.504	330680.5	1	1	1	1	1	0	1	1	1	1	1	1	2	0	1	1	2	0	0	0	0	1	1	2	0	0	0
25	-4.417	317127.6	1	1	1	1	1	0	1	1	1	1	1	1	2	0	1	1	2	0	0	0	0	1	1	2	0	0	0
26	-4.330	303912.8	1	1	1	1	1	0	1	1	1	1	1	1	2	0	1	1	2	0	0	0	0	1	1	2	0	0	0
27	-4.243	291424.9	1	1	1	1	1	0	1	1	1	1	1	1	2	0	1	1	2	0	0	0	0	1	1	2	0	0	0
28	-4.156	279451.7	1	1	1	1	1	0	1	1	1	1	1	1	2	0	1	1	2	0	0	0	1	1	1	2	0	0	0
29	-4.069	267777.6	1	1	1	1	1	1	1	1	1	1	1	1	2	0	1	1	2	0	0	0	1	1	1	2	0	0	0
30	-3.983	256125.1	1	1	1	1	1	1	1	1	1	1	1	1	2	0	1	1	2	0	0	0	1	1	1	2	0	0	0
31	-3.896	243953.4	1	1	1	1	1	1	1	1	1	1	1	1	2	0	1	1	2	0	0	0	1	1	1	2	0	0	0
32	-3.809	232672.0	1	1	1	1	1	1	1	1	1	1	1	1	2	0	1	1	2	0	0	0	1	1	1	2	0	0	0
33	-3.722	221293.6	1	1	1	1	1	1	1	1	1	1	1	2	0	0	1	1	2	0	0	0	1	1	1	2	0	0	0
34	-3.635	204886.0	1	1	1	1	1	1	1	1	1	1	1	2	0	0	1	1	2	0	0	0	1	1	1	2	0	0	0
35	-3.549	187985.4	1	1	1	1	1	1	1	1	1	1	1	2	0	0	1	1	2	0	0	0	1	1	1	2	0	0	0
36	-3.462	165814.7	1	1	1	1	1	1	1	1	1	1	1	2	0	0	1	1	2	0	0	0	1	1	1	2	0	0	0
37	-3.375	141995.8	1	1	1	1	1	1	1	1	1	1	1	2	0	0	1	1	2	0	0	0	1	1	1	2	0	0	0
38	-3.288	110681.5	1	1	1	1	1	1	1	1	1	1	1	2	0	0	1	1	2	0	0	0	1	1	1	2	0	0	0
39	-3.201	67056.9	1	1	1	1	1	1	1	1	1	1	1	2	0	0	1	1	2	0	0	0	1	1	1	2	0	0	0
40	-3.115	59510.5	1	1	1	1	1	1	1	1	1	1	1	2	0	0	1	1	2	0	0	0	1	1	1	2	0	0	0
41	-3.028	55586.4	1	1	1	1	1	1	1	1	1	1	1	2	0	0	1	1	2	0	0	0	1	1	1	2	0	0	0
42	-2.941	51445.2	1	1	1	1	1	1	1	1	1	1	1	2	0	0	1	1	2	0	0	0	1	1	1	2	0	0	0
43	-2.854	47331.4	1	1	1	1	1	1	1	1	1	1	1	2	0	0	1	1	2	0	0	0	1	1	1	2	0	0	0
44	-2.767	44767.0	1	1	1	1	1	1	1	1	1	1	1	2	0	0	1	1	2	0	0	0	1	1	1	2	0	0	0
45	-2.681	43627.0	1	1	1	1	1	1	1	1	1	1	1	2	0	0	1	1	2	0	0	0	1	1	1	2	0	0	0
46	-2.594	42939.6	1	1	1	1	1	1	1	1	1	1	1	2	0	0	1	1	2	0	0	0	1	1	1	2	0	0	0
47	-2.507	42306.8	1	1	1	1	1	1	1	1	1	1	1	2	0	0	1	1	2	0	0	0	1	1	1	2	0	0	0
48	-2.420	41580.0	1	1	1	1	1	1	1	1	1	1	1	2	0	0	1	1	2	0	0	0	1	1	1	2	0	0	0
49	-2.333	40772.0	1	1	1	1	1	1	1	1	1	1	1	2	0	0	1	1	2	0	0	0	1	1	1	2	0	0	0
50	-2.247	40152.7	1	1	1	1	1	1	1	1	1	1	1	2	0	0	1	1	2	0	0	0	1	1	1	2	0	0	0
51	-2.160	39732.4	1	1	1	1	1	1	1	1	1	1	1	2	0	0	1	1	2	0	0	0	1	1	1	2	0	0	0
52	-2.073	39356.2	1	1	1	1	1	1	1	1	1	1	1	2	0	0	1	1	2	0	0	0	1	1	1	2	0	0	0
53	-1.986	38930.1	1	1	1	1	1	1	1	1	1	1	1	2	0	0	1	1	2	0	0	0	1	1	1	2	0	0	0
54	-1.899	38428.1	1	1	1	1	1	1	1	1	1	1	1	2	0	0	1	1	2	0	0	0	1	1	1	2	0	0	0
55	-1.813	37883.1	1	1	1	1	1	1	1	1	1	1	1	2	0	0	1	1	2	0	0	0	1	1	1	2	0	0	0
56	-1.726	37379.4	1	1	1	1	1	1	1	1	1	1	1	2	0	0	1	1	2	0	0	0	1	1	1	2	0	0	0
57	-1.639	37017.1	1	1	1	1	1	1	1	1	1	1	1	2	0	0	1	1	2	0	0	0	1	1	1	2	0	0	0
58	-1.552	36875.0	1	1	1	1	1	1	1	1	1	1	1	2	0	0	1	1	2	0	0	0	1	1	1	2	0	0	0
59	-1.465	36983.5	1	1	1	1	1	1	1	1	1	1	1	2	0	0	1	1	2	0	0	0	1	1	1	2	0	0	0
60	-1.379	37335.0	1	1	1	1	1	1	1	1	1	1	1	2	0	0	1	1	2	0	0	0	1	1	1	2	0	0	0
61	-1.292	37874.9	1	1	1	1	1	1	1	1	1	1	1	2	0	0	1	1	2	0	0	0	1	1	1	2	0	0	0
62	-1.205	38554.7	1	1	1	1	1	1	1	1	1	1	1	2	0	0	1	1	2	0	0	0	1	1	1	2	0	0	0
63	-1.118	39351.0	1	1	1	1	1	1	1	1	1	1	1	2	0	0	1	1	2	0	0	0	1	1	1	2	0	0	0
64	-1.031	40290.8	1	1	1	1	1	1	1	1	1	1	1	2	0	0	1	1	2	0	0	0	1	1	1	2	0	0	0
65	-0.945	41398.6	1	1	1	1	1	1	1	1	1	1	1	2	0	0	1	1	2	0	0	0	1	1	1	2	0	0	0
66	-0.858	42690.6	1	1	1	1	1	1	1	1	1	1	1	2	0	0	1	1	2	0	0	0	1	1	1	2	0	0	0
67	-0.771	44144.1	1	1	1	1	1	1	1	1	1	1	1	2	0	0	1	1	2	0	0	0	1	1	1	2	0	0	0
68	-0.684	45768.2	1	1	1	1	1	1	1	1	1	1	1	2	0	0	1	1	2	0	0	0	1	1	1	2	0	0	0
69	-0.597	47621.4	1	1	1	1	1	1	1	1	1	1	1	2	0	1	1	2	0	0	0	1	1	1	1	2	0	0	0
70	-0.511	49877.0	1	1	1	1	1	1	1	1	1	1	1	2	0	1	1	2	0	0	0	1	1	1	1	2	0	0	0
71	-0.424	52556.6	1	1	1	1	1	1	1	1	1	1	1	2	0	1	1	2	0	0	0	1	1	1	1	2	0	0	0
72	-0.337	55538.8	1	1	1	1	1	1	1	1	1	1	1	2	0	1	1	2	0	0	0	1	1	1	1	2	0	0	0
73	-0.250	58075.3	1	1	1	1	1	1	1	1	1	1	1	2	0	1	1	1	2	0	0	0	1	1	1	2	0	0	0
74	-0.163	60224.2	1	1	1	1	1	1	1	1	1	1	1	2	0	1	1	1	2	0	0	0	1	1	1	2	0	0	0
75	-0.077	62850.0	1	1	1	1	1	1	1	1	1	1	1	2	0	1	1	1	2	0	0	0	1	1	1	2	0	0	0
76	0.010	66054.9	1	1	1	1	1	1	1	1	1	1	1	2	0	1	1	1	2	0	0	0	1	1	1	2	0	0	0
77	0.097	70269.3	1	1	1	1	1	1	1	1	1	1	1	1	1	1	1	1	2	0	0	0	1	1	1	2	0	0	0
78	0.184	75058.0	1	1	1	1	1	1	1	1	1	1	1	1	1	1	1	1	1	1	0	0	1	1	1	2	0	0	0
79	0.271	80693.7	1	1	1	1	1	1	1	1	1	1	1	1	1	1	1	1	1	1	0	0	1	1	1	2	0	0	0
80	0.357	86250.7	1	1	1	1	1	1	1	1	1	1	1	1	1	1	1	1	1	1	0	0	1	1	1	2	0	0	0
81	0.444	91767.1	1	1	1	1	1	1	1	1	1	1	1	1	1	1	1	1	1	1	0	0	1	1	1	2	0	0	0
82	0.531	96467.2	1	1	1	1	1	1	1	1	1	1	1	1	1	1	1	1	1	1	0	0	1	1	1	2	0	0	0
83	0.618	102131.6	1	1	1	1	1	1	1	1	1	1	1	1	1	1	1	1	1	1	0	0	1	1	1	2	0	0	0
84	0.705	106346.1	1	1	1	1	1	1	1	1	1	1	1	1	1	1	1	1	1	1	0	0	1	1	1	2	0	0	0
85	0.792	112276.7	1	1	1	1	1	1	1	1	1	1	1	1	1	1	1	1	1	1	0	0	1	1	1	2	0	0	0
86	0.878	115191.6	1	1	1	1	1	1	1	1	1	1	1	1	1	1	1	1	1	1	0	0	1	1	1	2	0	0	0
87	0.965	121105.6	1	1	1	1	1	1	1	1	1	1	1	1	1	1	1	1	1	1	0	0	1	1	1	2	0	0	0
88	1.052	121110.2	1	1	1	1	1	1	1	1	1	1	1	1	1	1	1	1	1	1	0	0	1	1	1	2	0	0	0
89	1.061	121110.0	1	1	1	1	1	1	1	1	1	1	1	1	1	1	1	1	1	1	0	0	1	1	1	2	0	0	0
90	1.139	120977.4	1	1	1	1	1	1	1	1	1	1	1	1	1	1	1	1	1	1	0	0	1	1	1	2	0	0	0

Figure 7.4: Example of a DEPTOM array

Part IV

Using and Testing the new AcDc Code

Chapter 8

Models for 4U 1626-67 and 4U 0614+091 calculated with the new AcDc Code

8.1 The Ultra Compact Binary System 4U 1626-67 (KZ Tr A)

Finally some models for the ultra compact x-ray binary system 4U 1626-67 (KZ Tr A), which is one of six known ultra compact binary systems, showing a hydrogen and helium free disc spectrum, were computed. The system consists of a 7.66s X-ray pulsar and a white dwarf companion. The primary star (neutron star) has a mass of about $1.4\,M_\odot$ and the secondary (white dwarf) of about $0.02\,M_\odot$ (Chakrabarty 1998). The distance separating the two stars is about 300 000 km (Schulz et al. 2001) and the orbital period is about 42 min (Middleditch et al. 1981). The inner boundary of the accretion disc is at a distance of 6 500 km (Schulz et al. 2001) from the centre, where the disc is truncated by the strong magnetic field of the neutron star. The field strength is about 3×10^{12} G on the surface, derived by Orlandini et al. (1998) by analysis of electron cyclotron resonance lines. The outer boundary is defined by the tidal radius at a distance of about 200 000 km (Schulz et al. 2001) from the centre. For the X-ray luminosity Chakrabarty (1998) derived $7 \times 10^{36} \lesssim L_x \lesssim 5 \times 10^{37}$erg s^{-1}, corresponding to a distance of 1 kpc, leading to an accretion rate of about $2 \times 10^{-10}\,M_\odot\,\mathrm{yr}^{-1}$.

8.2 The Ultra Compact Binary System 4U 0614+091

The ultra compact LMXB 4U 0614+091 was discovered by the UHURU survey in the 1970's. Swank et al. (1978) identified the source as a type I X-ray burster. Based on a model for the X-ray bursts, Brandt et al. (1992) suggest a distance of 3 kpc for 4U 0614+091. The inclination angle of

element	N_k/N_H	mass fraction β_k (%)	number fraction (%)
H	1.0	$91.17 \cdot 10^{-6}$	$1.0 \cdot 10^{-3}$
He	$1.0 \cdot 10^{3}$	$38.16 \cdot 10^{-2}$	1.4
C	$1.5 \cdot 10^{4}$	17.19	21.4
O	$5.4 \cdot 10^{4}$	82.43	77.1

Table 8.1: Composition of model atom 1 used for the calculations of 4U 1626-67's and 4U 0614+091's accretion disc

element	N_k/N_H	mass fraction β_k (%)	number fraction (%)
H	1.0	$58.76 \cdot 10^{-6}$	$1.0 \cdot 10^{-3}$
He	$1.0 \cdot 10^{3}$	$23.32 \cdot 10^{-6}$	1.0
C	$1.5 \cdot 10^{4}$	10.50	15.0
Ne	$1.5 \cdot 10^{4}$	17.65	15.0
Mg	$1.5 \cdot 10^{4}$	21.26	15.0
O	$5.4 \cdot 10^{4}$	50.36	54.0

Table 8.2: Composition of model atom 2 used for the calculations of 4U 1626-67's and 4U 0614+091's accretion disc models

ring no.	radius r / [km]	height z / [km]	irrad. angle β [°]	T_{eff}
1	6 500	94.2	1.00	64 454
2	7 500	109.6	1.00	57 936
3	8 500	125.3	1.00	52 775
4	10 000	147.6	1.00	46 751
5	12 000	176.6	1.00	40 805
6	15 000	221.3	1.00	34 544
7	19 000	267.3	1.00	28 953
8	25 000	377.6	1.00	23 585
9	35 000	547.0	1.00	18 339
10	50 000	820.4	1.00	14 044
11	70 000	1213.4	1.00	11 918
12	100 000	1840.8	1.00	8 359

Table 8.3: Parameters of an accretion disc model for 4U 1626-67 and 4U 0614+091, calculated with model atom 1

the system should be less than 60° (Piraino et al. 1999).

Since there are not many system parameters known of the ultra compact LMXB 4U 0614+091, we assumed the same parameters as for 4U 1626-67, given above. Therefore we used the same accretion disc models for both LMXB systems.

8.3 Parameters of 4U 1626-67's and 4U 0614+091's Disc Model

The following approach was chosen to calculate an accretion disc model for 4U 1626-67 and 4U 0614+091. We calculated the vertical structure of twelve concentric rings of the disc with AcDc. The radii of the disc rings were chosen in a way, that the radial temperature distribution was divided in equidistant steps. For the irradiated disc models we assumed irradiation angles, defined by the difference of the radii and heights of two neighbouring rings. This is shown in the sketch of the disc in Figure 8.1 and Figure 8.2. The disc height is calculated under the assumption of an α-disc structure (Shakura & Sunyaev 1973), using the accretion rate, the Reynolds number and the mass of the central compact object as parameters. The characteristic data of the accretion disc model are given in Table 8.3.

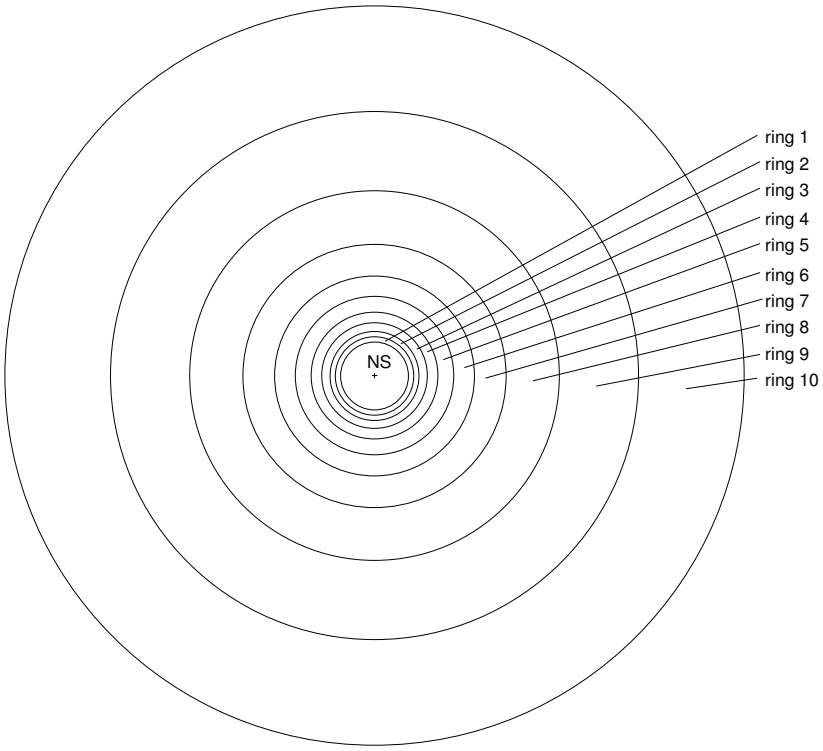

Figure 8.1: View from above on the accretion disc model of 4U 1626-67 and 4U 0614+091

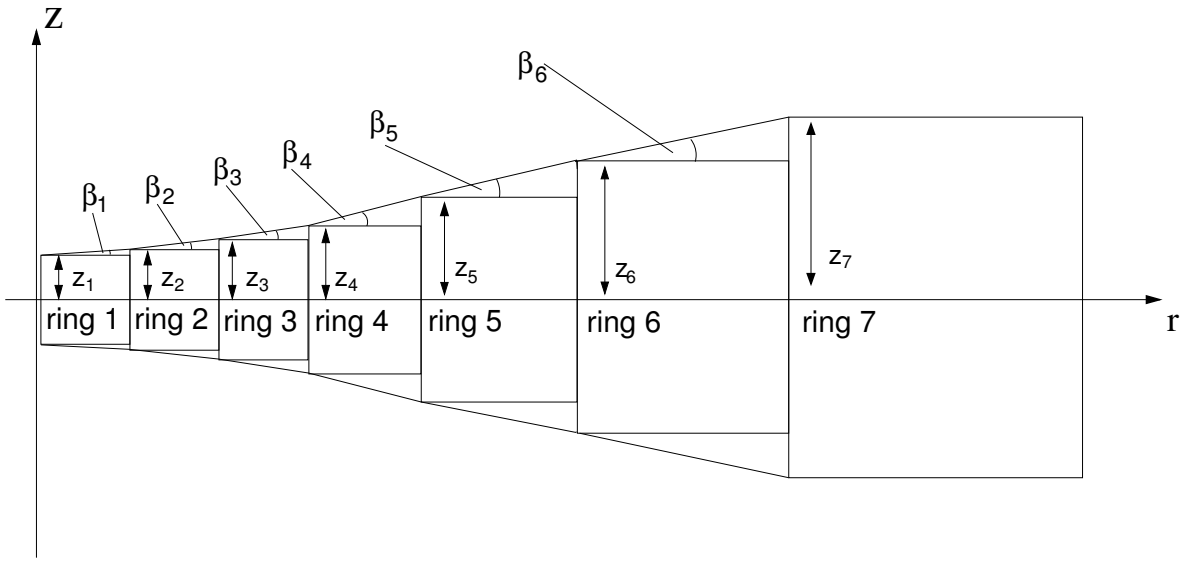

Figure 8.2: Cut through the z-r-plane of 4U 1626-67's and 4U 0614+091's accretion disc model

8.4 LTE Accretion Disc Models

As a first step, a set of LTE accretion disc models is calculated, using AcDc-LTE (Nagel 2003), which were used as starting models.

As it turned out, useful LTE-models were obtained, if approximately one hundred iterations were done with AcDc-LTE. However, the LTE models are then still not fully converged. Because of the large temperature range in the accretion disc, it was not possible to use only one model atom (see Table 8.4) for all LTE disc ring models. Thus for the disc models including Ne and Mg, rings number

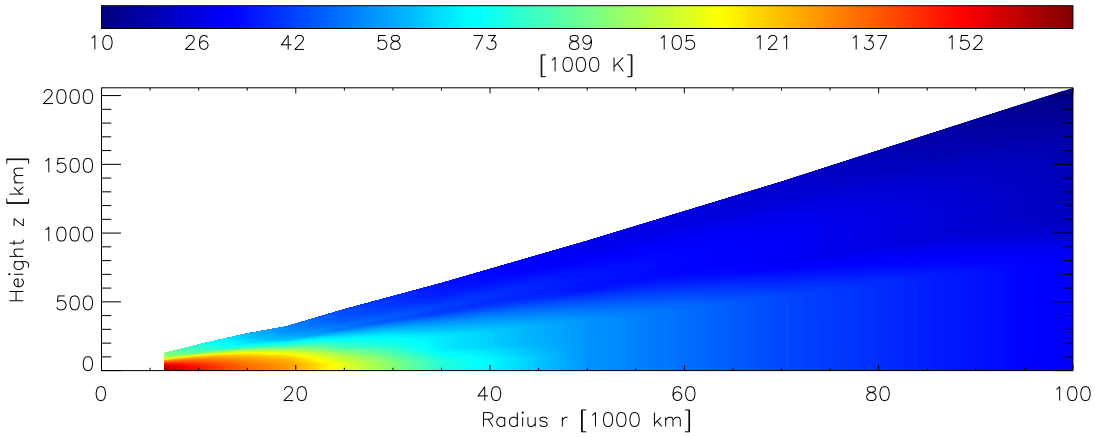

Figure 8.3: Temperature structure of the LTE disc model containing rings 1 - 16

one to six were calculated using model atom 2. The following three disc rings were calculated with the slightly modified model atom number 3. In that case the highest ionisation stages of Ne, Mg and O were removed from the model atom. The rings number ten to thirteen were calculated with model atom number 4.

A second accretion disc model was calculated with the smaller model atom number 2. With it it was possible to calculate the whole set of LTE ring models with the same model atom. The content of the different model atoms is shown in Table 8.4. Using this model atom it was possible to calculate a LTE disc model consisting of 16 rings. The disc model ranges from the corotation radius at 6 500 km, the inner edge of the disc, out to the tidal radius at 200 000 km. However the effective temperature of the rings number 13 to 16 is that low, that they are strongly influenced by physics not included in AcDc yet. Therefore it is not useful to calculate non-LTE models for that region.

The resulting disc model temperature structure is shown in Figure 8.3 as 2D colour coded contour plot. All other plots for the LTE disc model, namely the structure and the spectra of every disc ring and the spectra of the whole disc, are shown in Appendix B. Note that in the 2D Plot the structure is plotted in geometric stratification, whereas in Figure B.3 and Figure B.4 the structure for each ring is plotted separately in units of mass column. Table 8.1 gives an overview of the chemical composition used for the accretion disc models of the ultra-compact LMXBs 4U 1626-67 and 4U 0614+091.

8.5 non-LTE Accretion Disc Models

The next step was to calculate a non-irradiated non-LTE accretion disc model for 4U 1626-67 and 4U 0614+091. It was calculated with the AcDc non-LTE accretion disc model code. The disc rings

	species	ionisation stage								
model atom 1	H	I	II							
	He	I	II	III						
	C		II	III	IV	V				
	O			III	IV	V	VI			
model atom 2	H	I	II							
	He	I	II	III						
	C			III	IV	V				
	O				IV	V	VI	VII	VIII	IX
	Ne			III	IV	V	VI	VII		
	Mg			III	IV	V	VI	VII		
model atom 3	H	I	II							
	He	I	II	III						
	C			III	IV	V				
	O				IV	V	VI	VII		
	Ne			III	IV	V	VI	VII		
	Mg			III	IV	V	VI	VII		
model atom 4	H	I	II							
	He	I	II	III						
	C			III	IV	V				
	O				IV	V	VI			
	Ne			III	IV	V	VI			
	Mg			III	IV	V	VI			

Table 8.4: Ionisation stages of the model atom used for the calculations of 4U 1626-67's and 4U 0614+091's accretion disc models

were not irradiated and DEPTOM was activated, with a limit of 10^{-25}.

The disc height of the converged non-LTE disc models is in all cases smaller than the height of the LTE disc models. This fact is a clear evidence that the LTE disc models were not converged.

It was found that disc rings beyond 50 000 km are optically thin. This leads to line transitions of the model atom being in emission. The continuum is therefore on a low level compared to the continuum of irradiated disc ring models. Hence some conclusions can be drawn concerning the geometry of the discs in the two LMXBs (see section 8.7).

In Figure 8.4 the 2D temperature structure plot of the non-LTE disc model is shown (see section 8.4). The other plots of the non-irradiated non-LTE disc model are shown in Appendix C.

8.6 Irradiated non-LTE Accretion Disc Models

The last step was to calculate irradiated non-LTE accretion disc models for 4U 1626-67 and 4U 0614+091. For the irradiation angle one degree was assumed for all disc rings. This is truly not the case in a real system, due to the fact that the surface of an accretion disc should have a concave shape. However, the exact luminosity of the central source is not known and might vary about a factor of ten. Therefore it is not necessary to determine the irradiation angle with high accuracy.

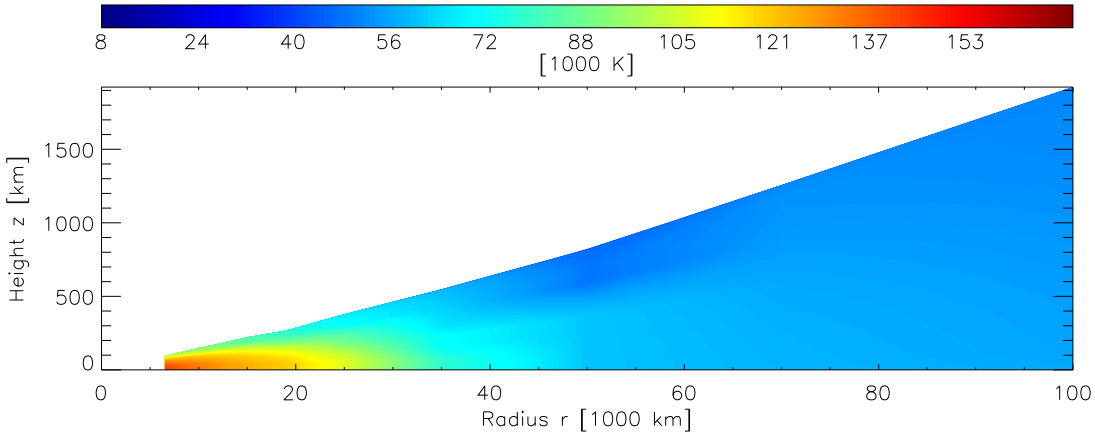

Figure 8.4: Temperature structure of a non-irradiated disc model in the z-r-plane

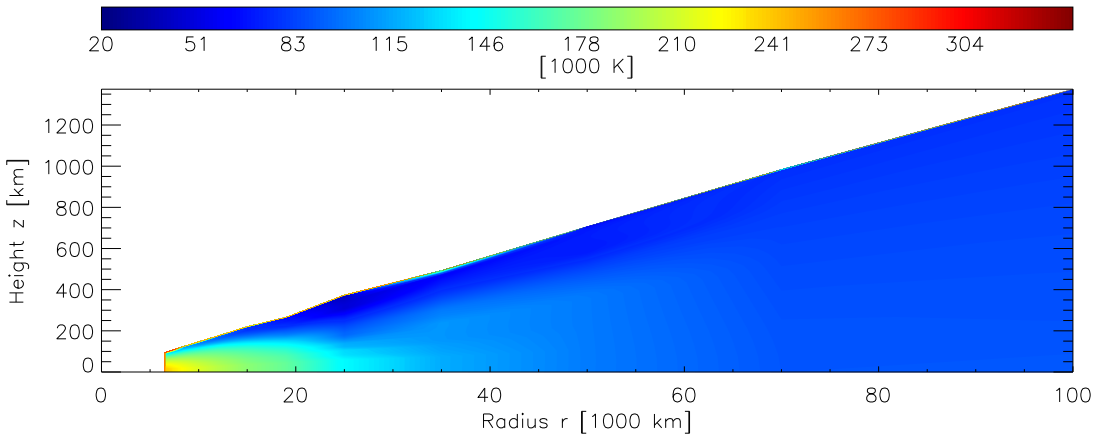

Figure 8.5: Temperature structure of an irradiated disc model in the z-r-plane

Irradiating the whole disc with an irradiation angle of one degree, the outer parts of the disc turned out to be optically thick again. The consequences of that behaviour are discussed in section 8.7.

In Figure 8.5 the temperature structure of the irradiated disc model is shown. All other plots of the irradiated disc model are presented in Appendix D.

8.7 Comparing the Disc Models with observed Spectra

In this section some fits of disc models to single features of observed spectra of 4U 1626-67 and 4U 0614+091 are discussed.

Due to the fact that many features in accretion discs are barely or not identifiable, because of e.g. rotation broadening, nobody could definitely show that the discs in ultra compact LMXB systems are hydrogen and helium free until today. Nevertheless, lots of evidences, like the short binary period, suggests that the secondaries in those systems have to be at least extreme hydrogen and helium poor.

We were able to show that the upper limit of the hydrogen abundance in the accretion discs of both ultra compact binary systems could be set to 10^{-6}. Some more work is in progress to obtain a more accurate limit to the hydrogen abundance. It is eligible to give a upper limit for the helium abundance in the same manner. This is one of the next steps to be done in our work.

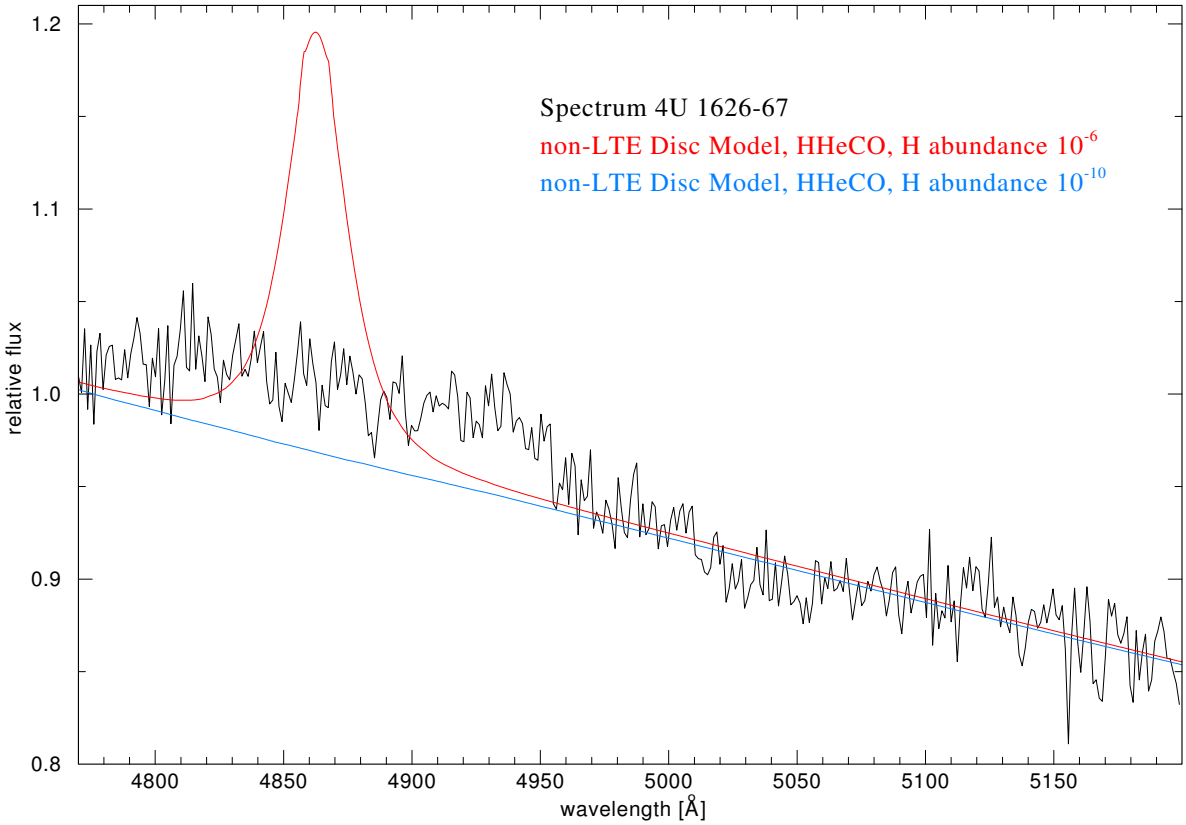

Figure 8.6: Comparing the H_β line of two models with different H abundance to the spectrum of 4U 1626-67

One of the C II features in the optical spectrum of 4U 0614+091 could be explained by an emission line emerged in the outer, optically thin parts of the disc. However, the C II emission line in the synthetic spectra matches the features in the observed spectra not very well. Some more work has to be done to obtain a spectrum of a weakly irradiated outer disc. The weakly irradiated spectrum might fit the feature in a better way.

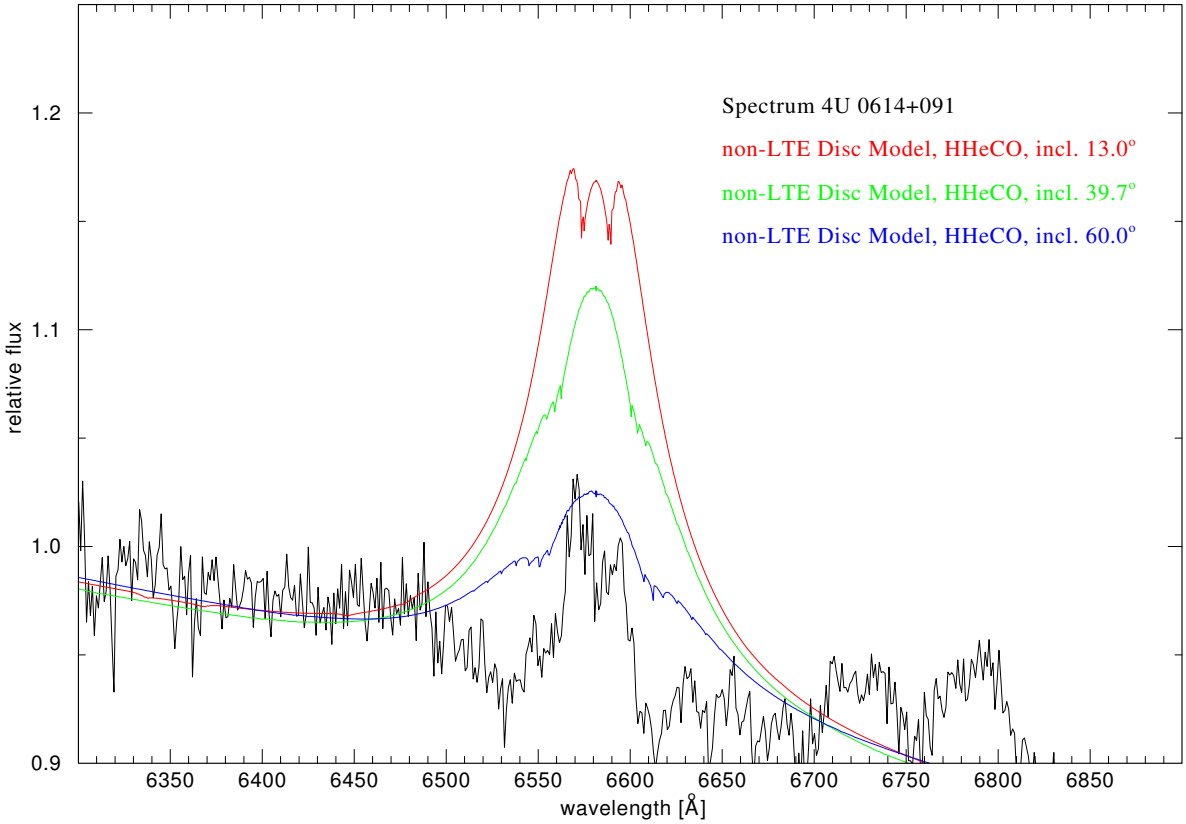

Figure 8.7: Comparing a C II feature in the spectrum of 4U 0614+091 with a disc model for different inclination angles

The emission line features in the UV, however, can only be explained with quite strong irradiation of at least the inner parts of the accretion disc. As an example a fit to an O V emission line at 1370 Å is shown. But there are some more features in the UV range, which are likely to be produced by the irradiation of the disc.

This draws the following picture of accretion discs in those ultra compact LMXB systems. The inner parts are strongly irradiated, whereas the outer parts are weakly or not irradiated. The reason for this could be a bulge in the disc caused by the strong irradiation of the inner disc, which leads to an expansion of the disc. This bulge shadows the outer parts of the disc.

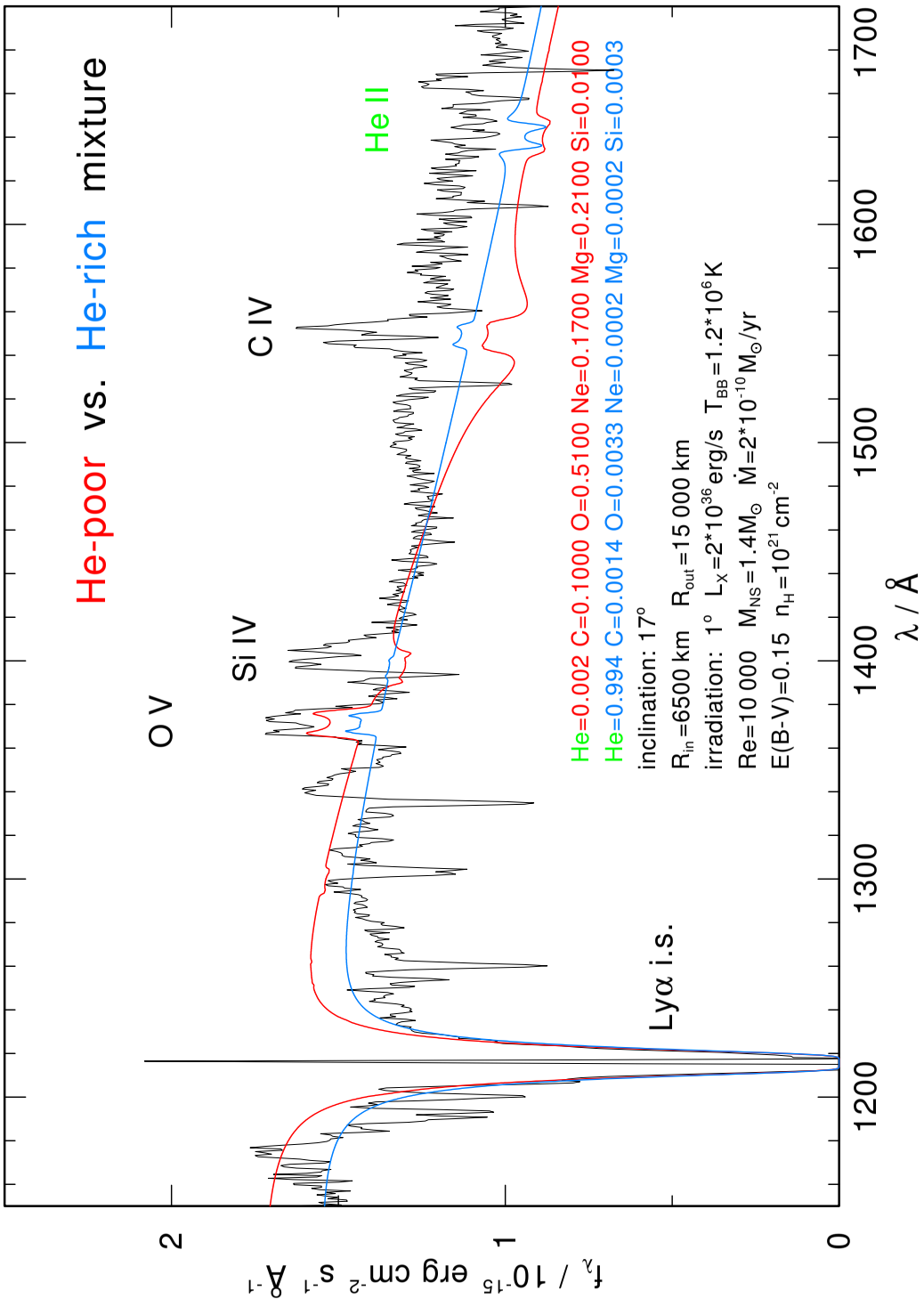

Figure 8.8: Fit to a O V feature in the UV range of the observed spectrum from 4U 1626-67 (Nagel 2003)

Chapter 9

Summary and Conclusions

During the work presented in this thesis DEPTOM, a depth dependent model atom, was developed and implemented in AcDc. DEPTOM compares the atomic occupation numbers of every ionisation stage to a lower limit. Underpopulated ionisation stages, failing this test several times, will be deactivated. However, setting the corresponding rate equations to zero, makes the rate matrix no longer invertible. The relevant rate equations have to be cut out. Thereby the corelation between atomic levels and the associated transitions has to be assured.

There was a lot of progress in accretion disc modelling during the last year, partially effected by implementing DEPTOM. Now it is possible to calculate the whole accretion disc model with a consistent model atom. This was not the case in the past, due to the large range of temperatures appearing in the disc. The disc model e.g. of 4U 1626-67 consist of twelve single model rings, reaching from 6 500 km to 100 000 km, which is equivalent to an effective temperature range from 8 500 K up to 65 000 K. Therewith the outer parts of the disc, which are mainly responsible for the optical emission are modelled. These parts are seem to be responsible for some of the emission features seen in the optical range of spectra from ultra compact LMXBs.

The structure of accretion disc models calculated with the updated code, seems to be smoother than further models. The ripples in the structure caused by under populated ionisation stages are gone and the calculation is numerical more stable.

However, there is still a long way to go. They ionisation processes in excited levels of the new model atom closure should be handled more carefully, by redirecting them to the ground state of the last ionisation stage. The heating cycle should be replaced by a mechanism calculating the atomic LTE population numbers of all ionisation stages, to monitor the population numbers of the deactivated ionisation stages. Then it would be possible to reactivate ionisation stages in which the population numbers have grown stronger due to e.g. irradiation.

Moreover, there are still some problems remaining. The calculation respond very sensitively to the composition of a specific model atom. Changing the model atom of an non-LTE disc model is still quite difficult.

Finally the radiative transfer and the equation of hydrostatic equilibrium should be expanded to multi dimensions to consider effects like radiation transfer in radial direction and convection. Some more physics, e.g. comptonisation, disc winds, should be implement in AcDc. There is some work on that going on in a PhD. thesis.

Part V

Appendix

Appendix A

New Control Commands for AcDc

`USE DEPTH DEPENDENT MODEL ATOM 1`
Switch the depth dependent model atom on

`USE DEPTH DEPENDENT MODEL ATOM 0`
Switch the depth dependent model atom off

`PRINT DEPTOM ARRAYS 1`
Activates the printing of the deptom badmark array. By selecting 1, 2, ... one can determine that the deptom flag array is printed every ALI iteration, every second ALI iteration and so on.

`PRINT DEPTOM ARRAYS 0`
Deactivates the printing of the deptom badmark array, the deptom flag array and the deptom limits to the standard output file

`DEPTOM DAMPING FACTOR 3`
Sets the factor to control how quick the DEPTOM reacts. The damping factor must be between 1 and 100 and the default value is 3.

`DEPTOM LIMIT C 1.0E-20`
set the deptom limit for carbon. This will also work for all elements of the model atom, with more than two ionisation stages (`HE, N, O, NE, MG ....`).
The limit must be larger than 1.0E-250

`HEATING CYCLE 100`
Sets the length of the heat cycle, which specifies how often the DEPTOM is reseted when calculating an irradiated model. The factor must be larger than 1, the default value is 100.

`HEATING CYCLE 0`
Deactivates the resets of the DEPTOM.

At the moment there is no explicit User's Guide to the Accretion Model Disc Code AcDc, one may find some instructions in Nagel (2003). Because of its affinity to the other codes of the Tübingen NLTE Model Atmosphere Package, most of AcDc's features are mentioned in the User's Guide to the Tübingen NLTE Model Atmosphere Package.

Appendix B

Plots of LTE Accretion Disc Models

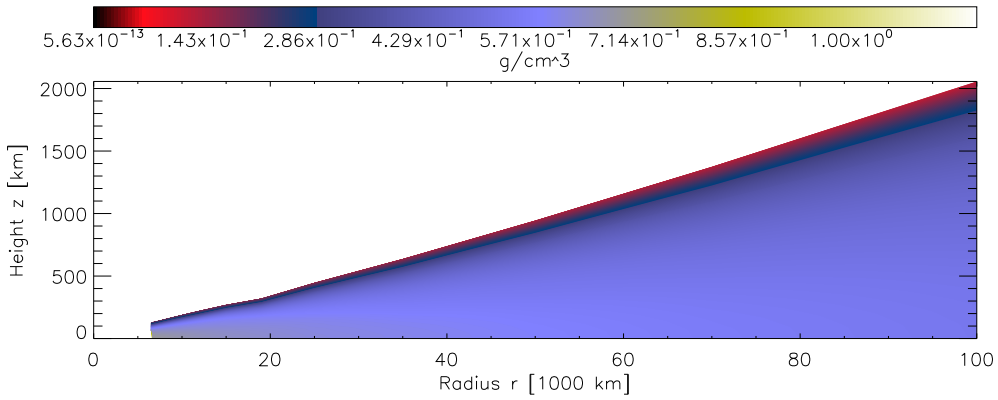

Figure B.1: Density structure of a LTE disc model containing rings 1 - 16

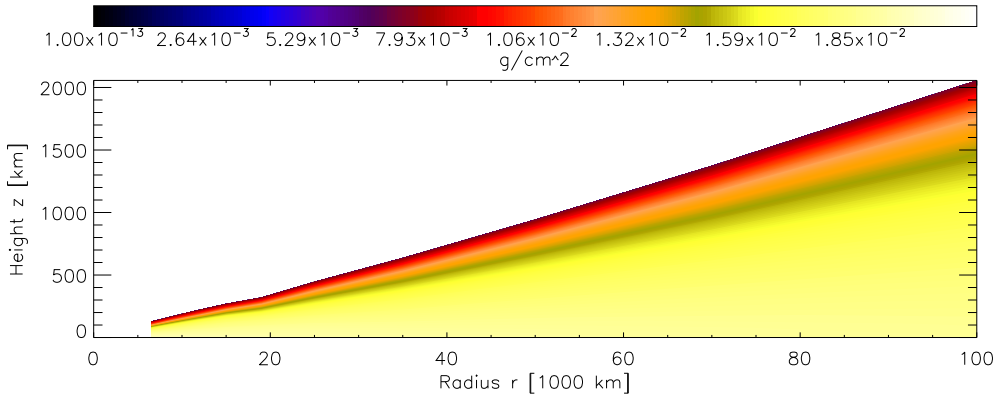

Figure B.2: Column mass structure of a LTE disc model containing rings 1 - 16

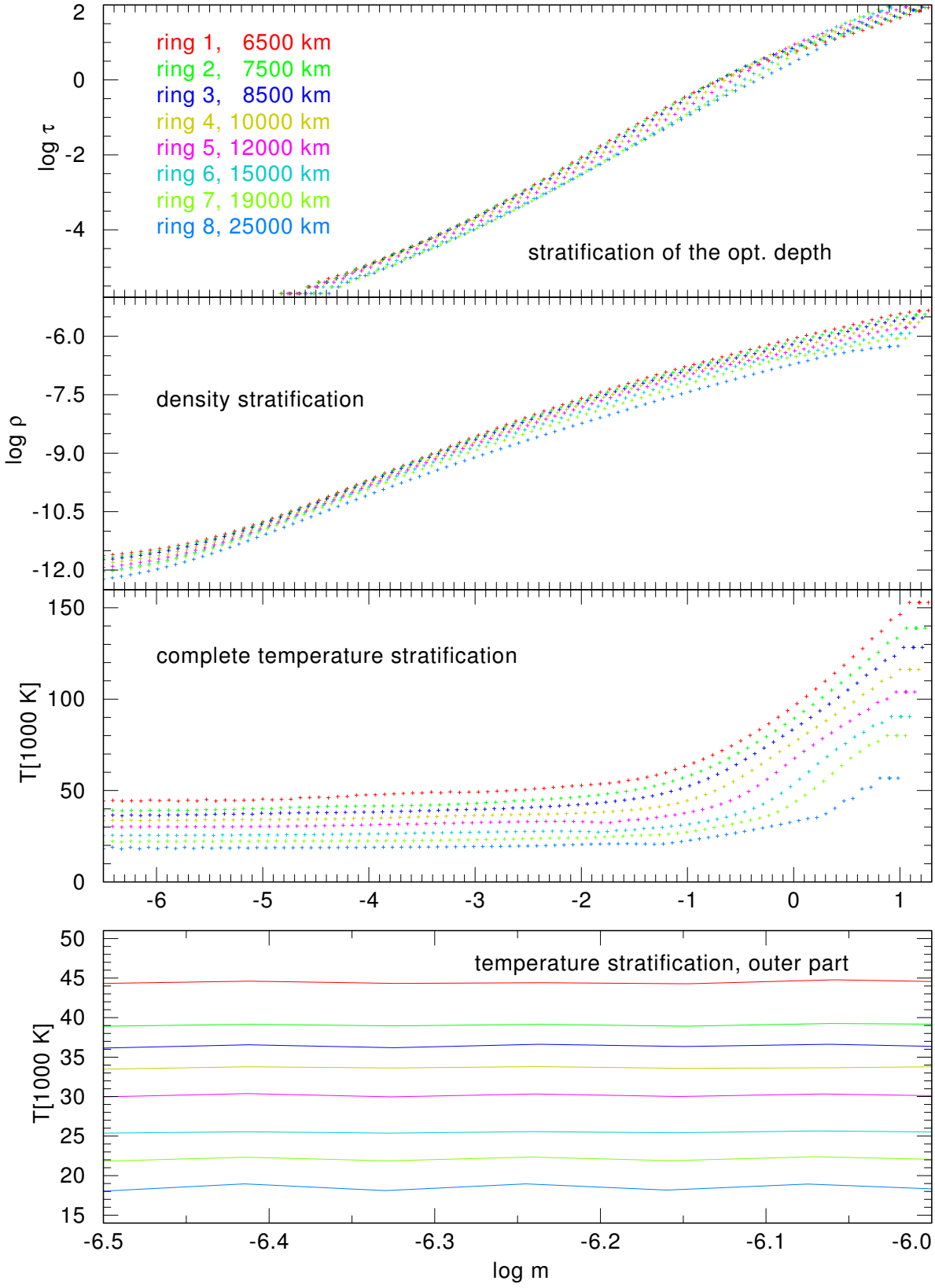

Figure B.3: Stratification of LTE models for the rings 1 - 8

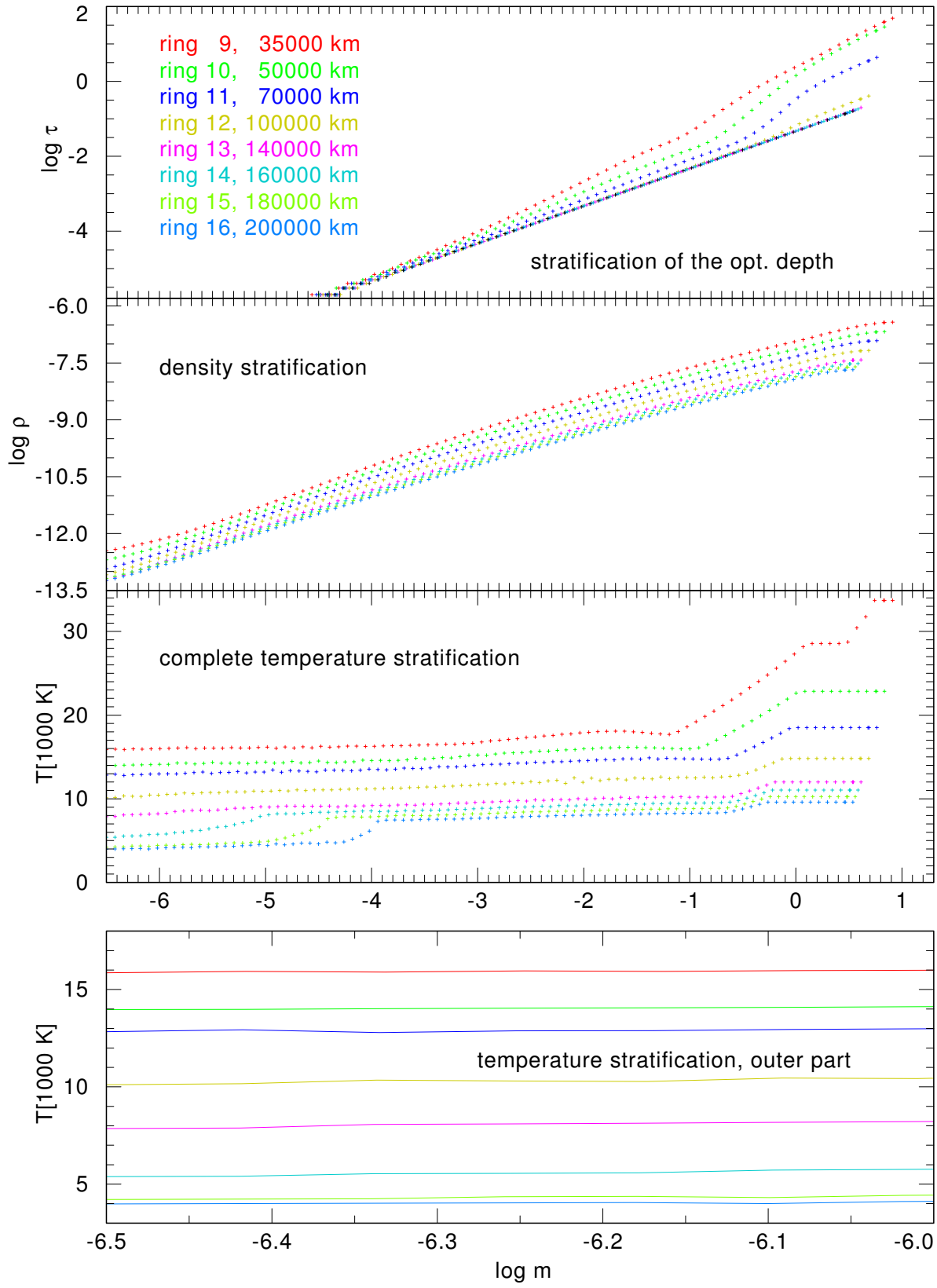

Figure B.4: Stratification of LTE models for the rings 7 - 13

Appendix C

Plots of non-irradiated non-LTE Accretion Disc Models

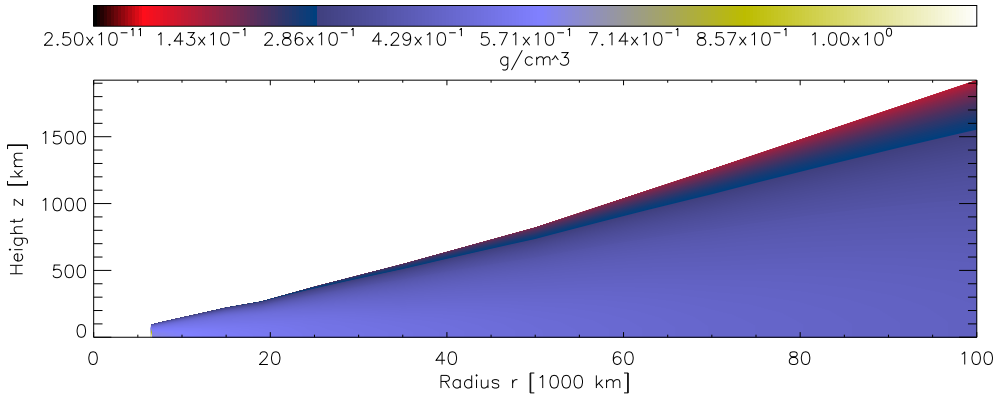

Figure C.1: Density structure of non-irradiated disc model in the z-r-plane

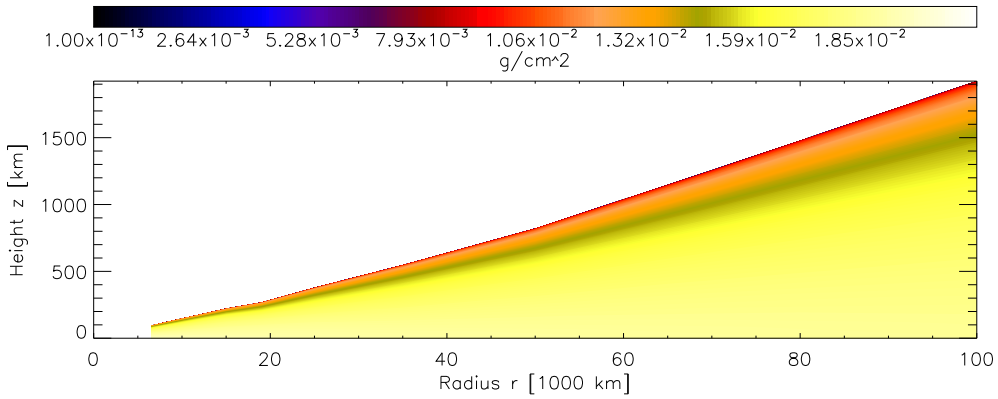

Figure C.2: Column mass structure of non-irradiated disc model in the z-r-plane

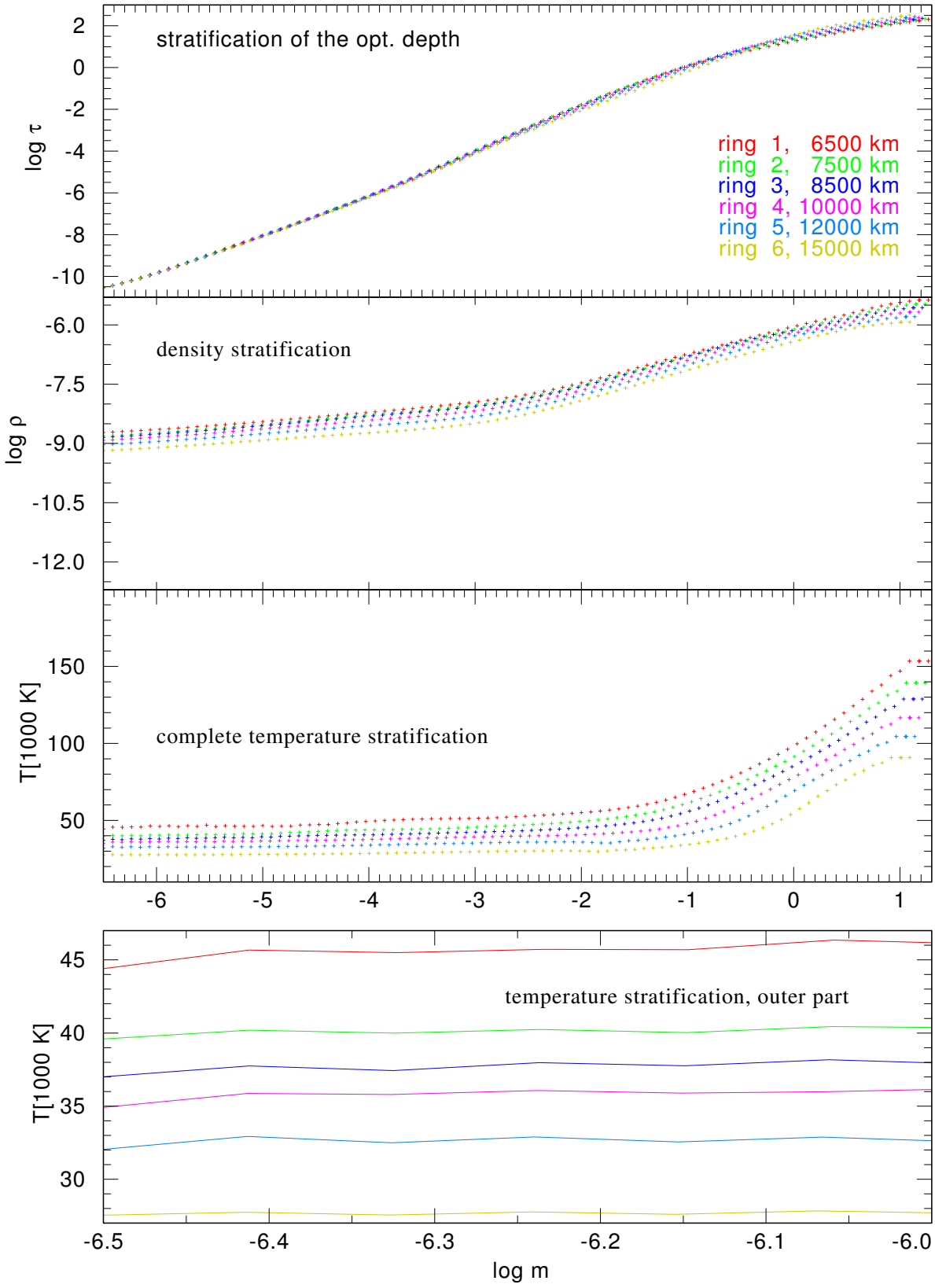

Figure C.3: Stratification of non-LTE models for the rings 1 - 6

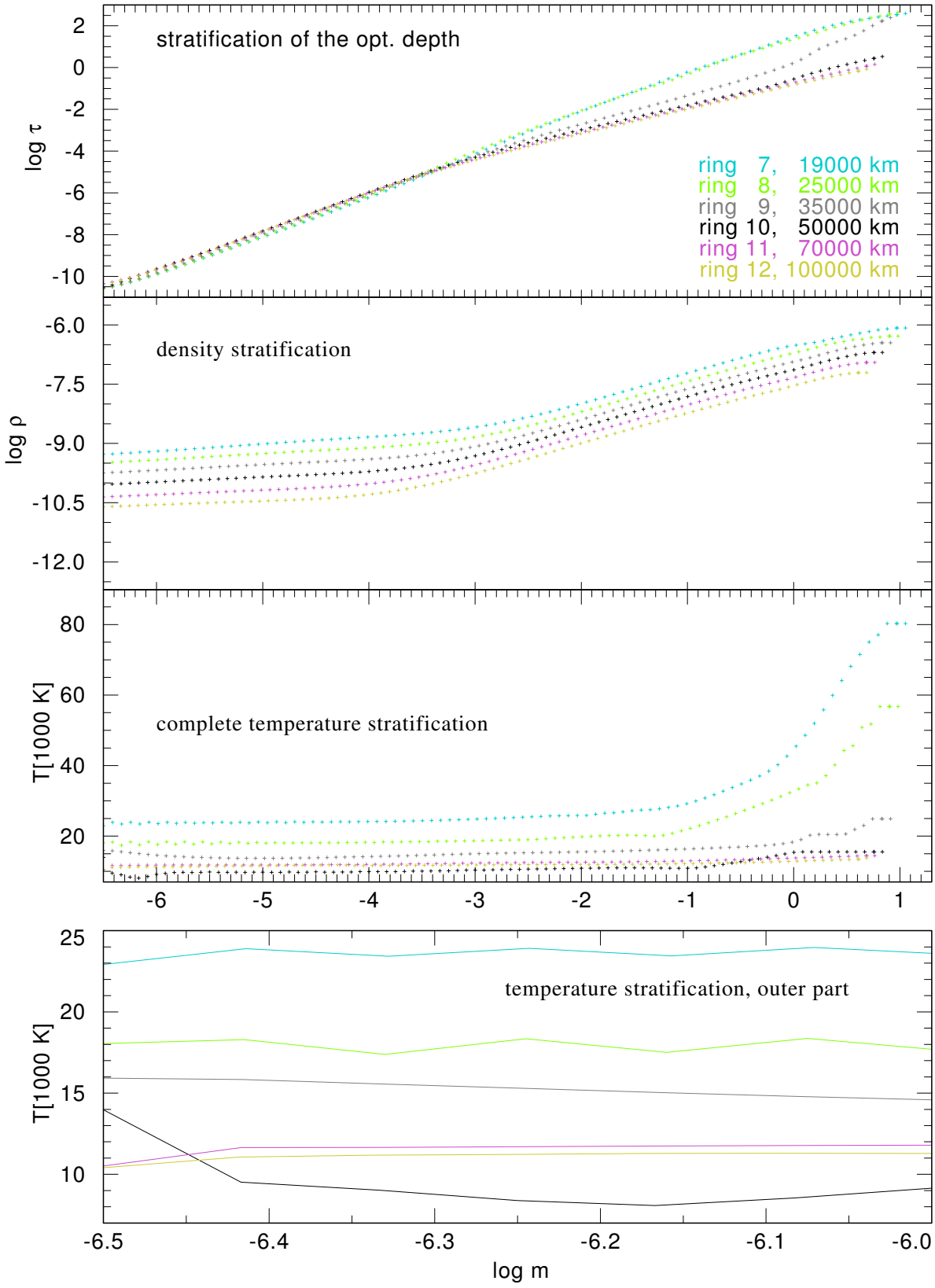

Figure C.4: Stratification of non-LTE models for the rings 7 - 12

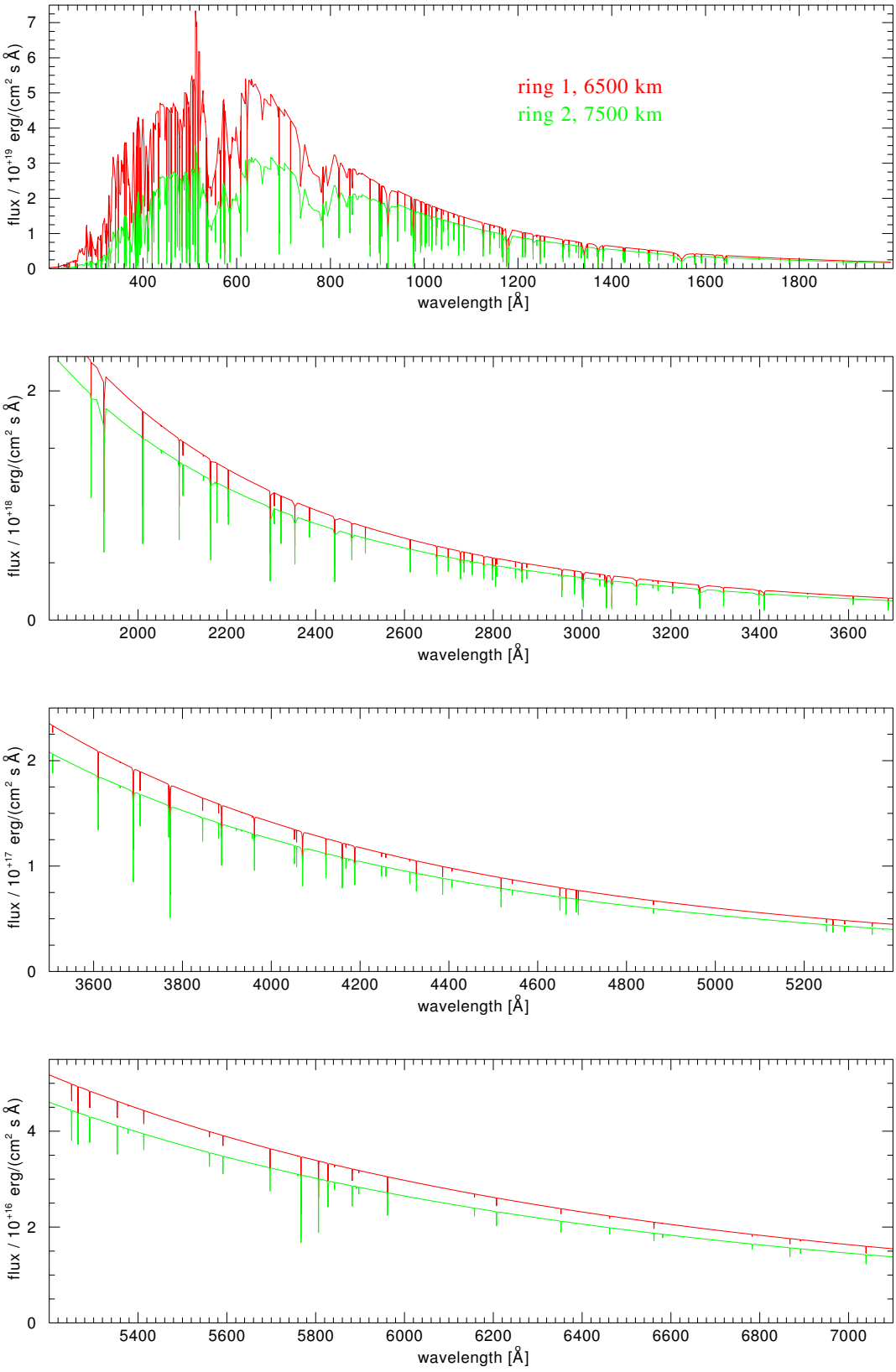

Figure C.5: Spectrum of non-irradiated non-LTE models for the rings 1 and 2

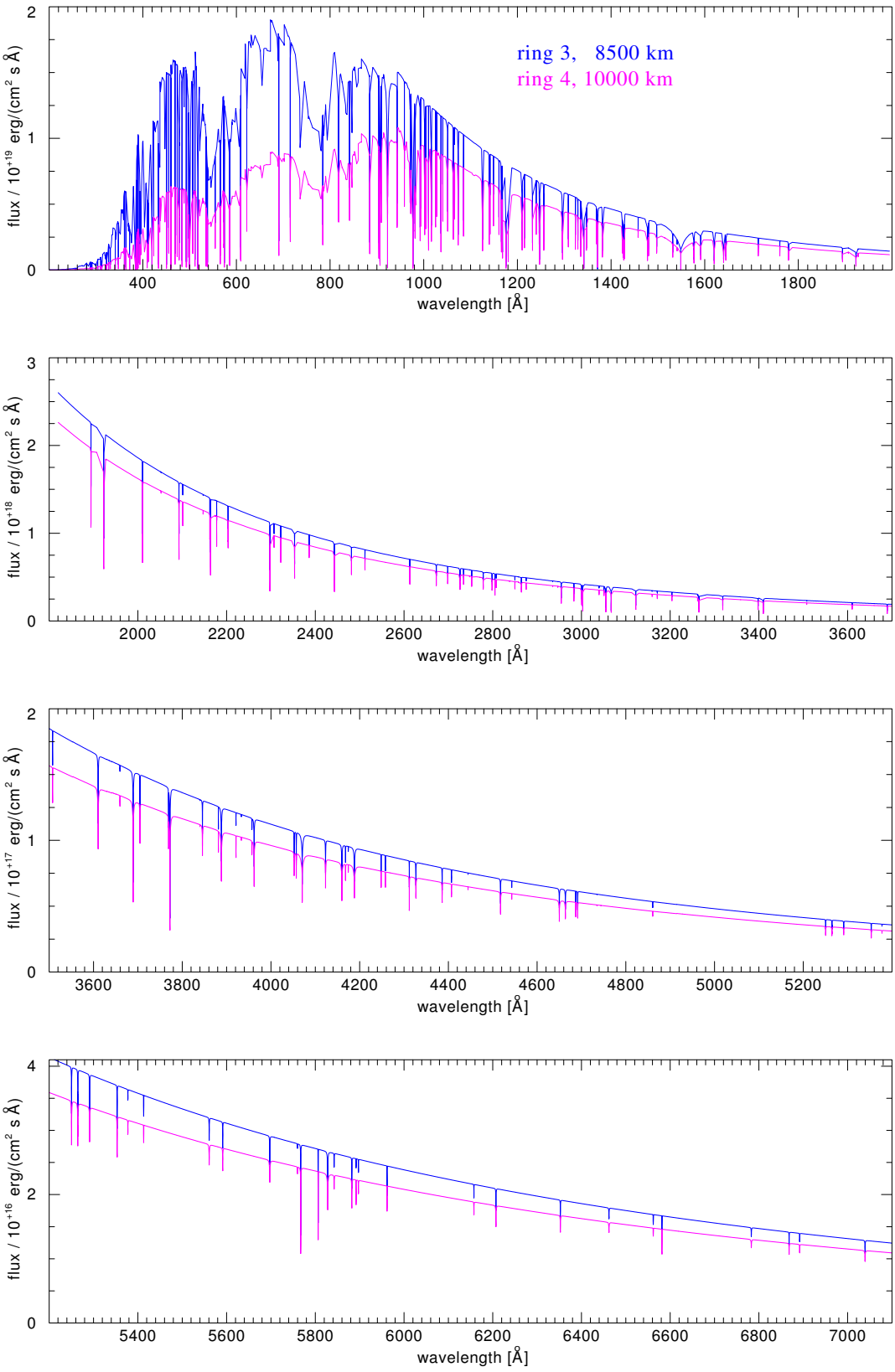

Figure C.6: Spectrum of non-irradiated non-LTE models for the rings 3 and 4

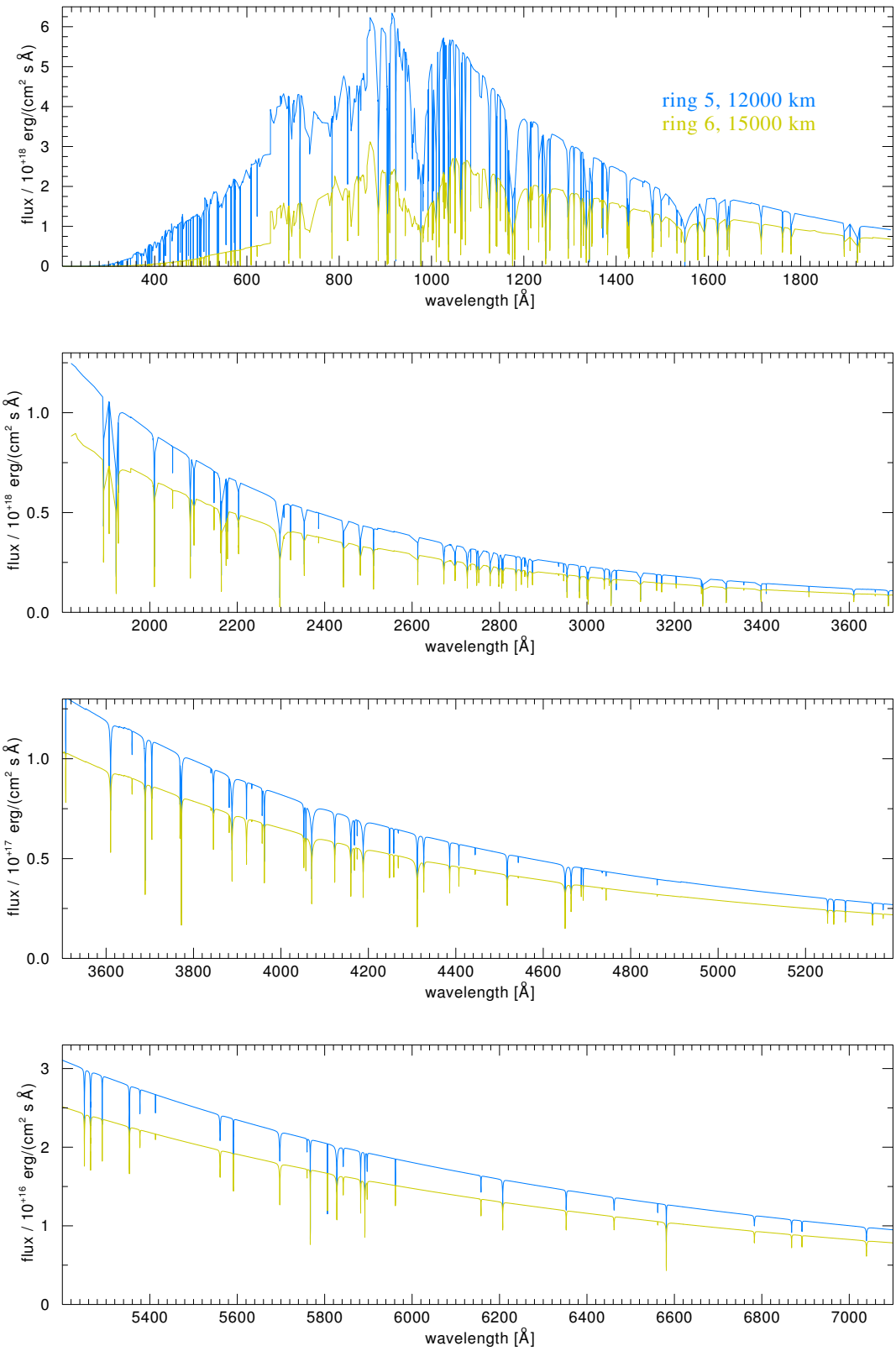

Figure C.7: Spectrum of non-irradiated non-LTE models for the rings 5 and 6

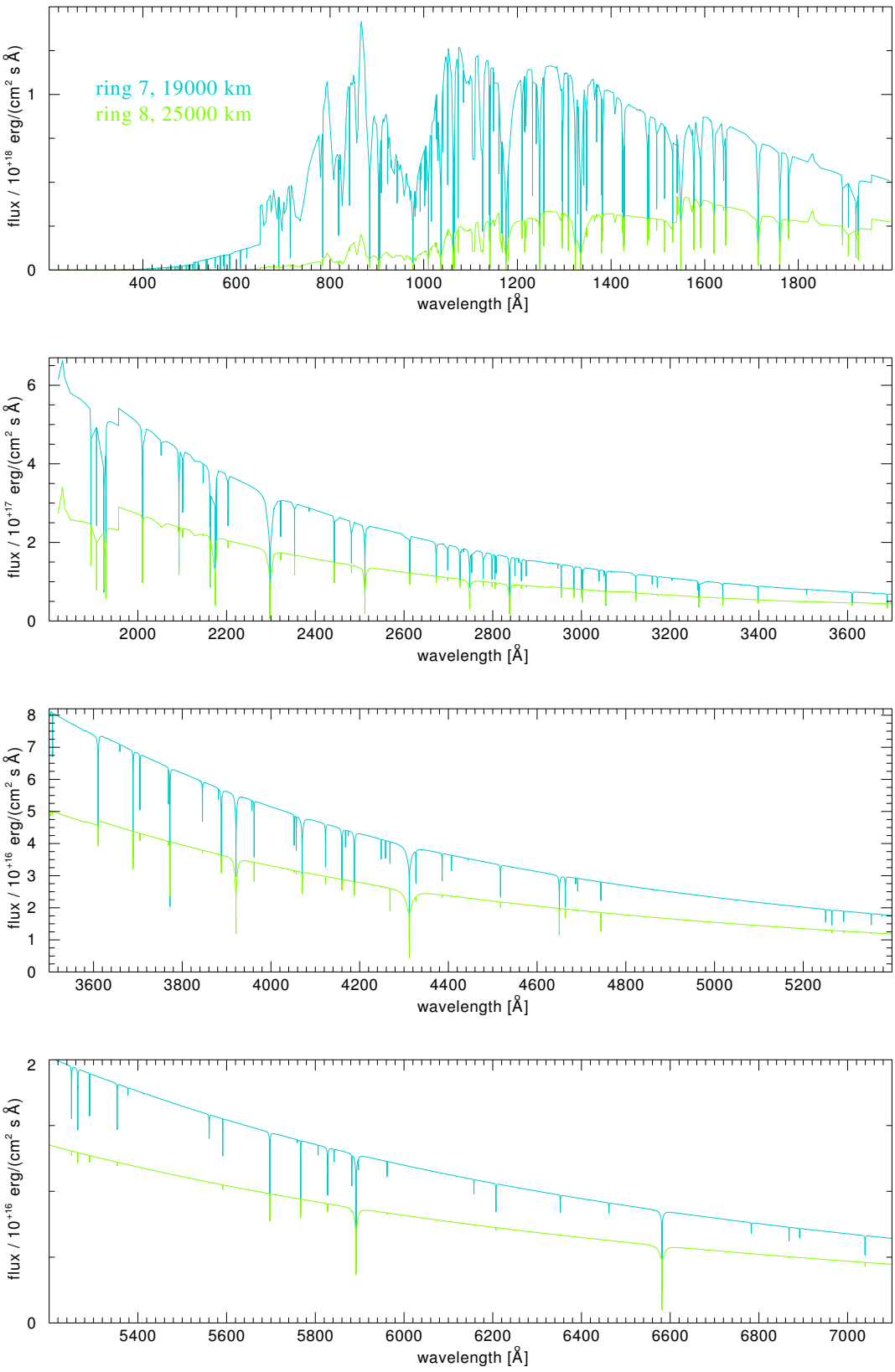

Figure C.8: Spectrum of non-irradiated non-LTE models for the rings 7 and 8

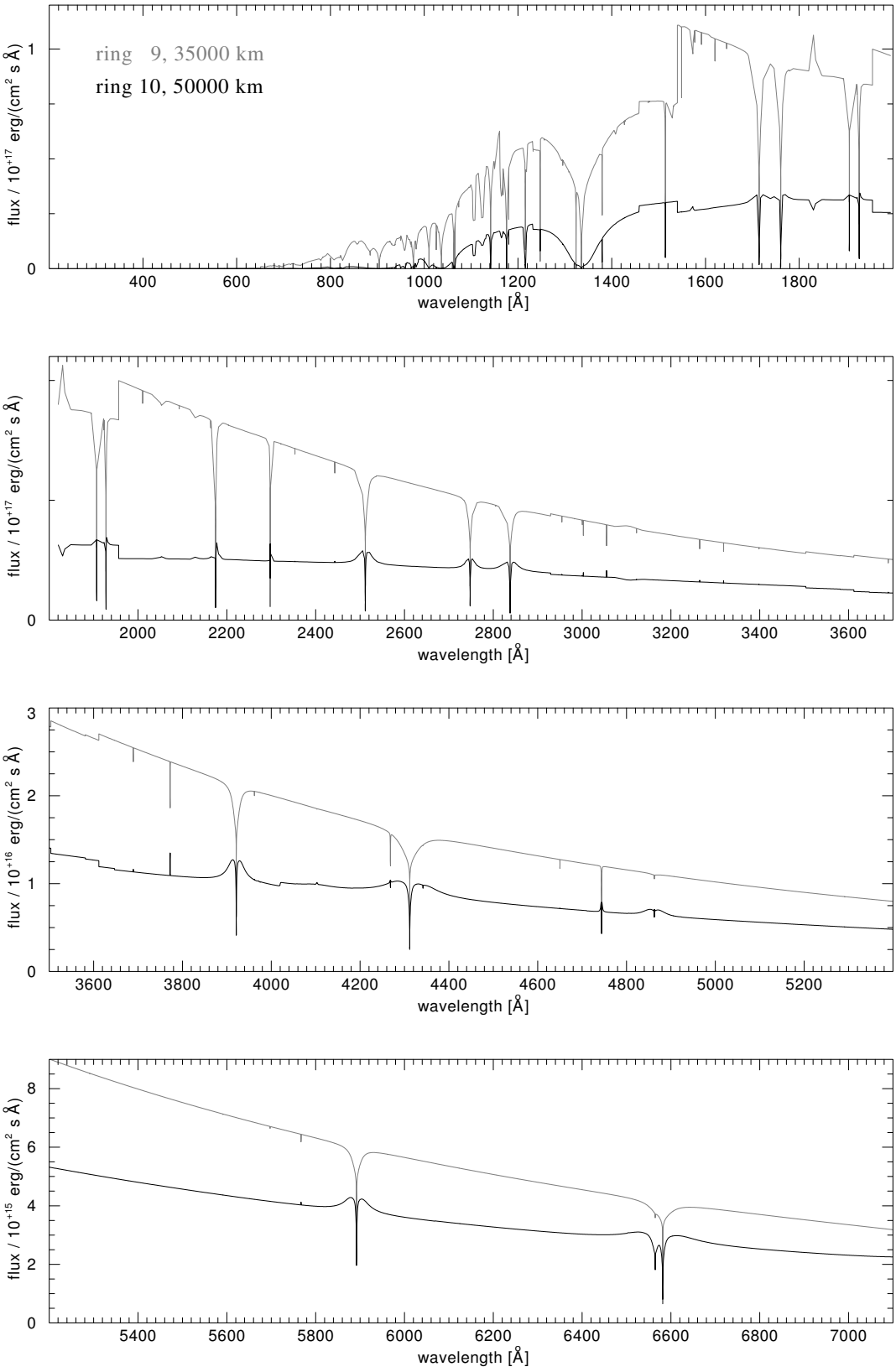

Figure C.9: Spectrum of non-irradiated non-LTE models for the rings 9 and 10

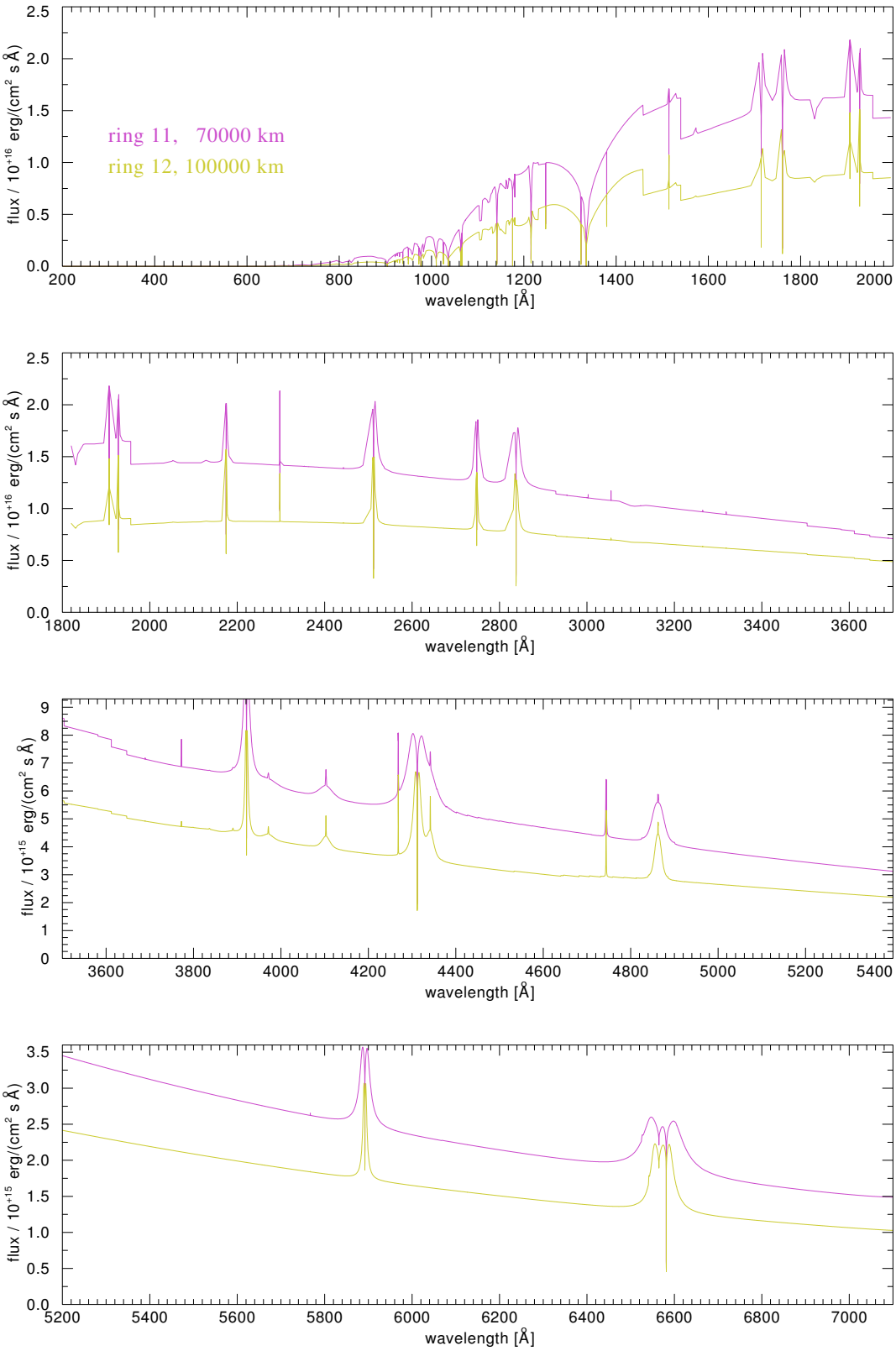

Figure C.10: Spectrum of non-irradiated non-LTE models for the rings 11 and 12

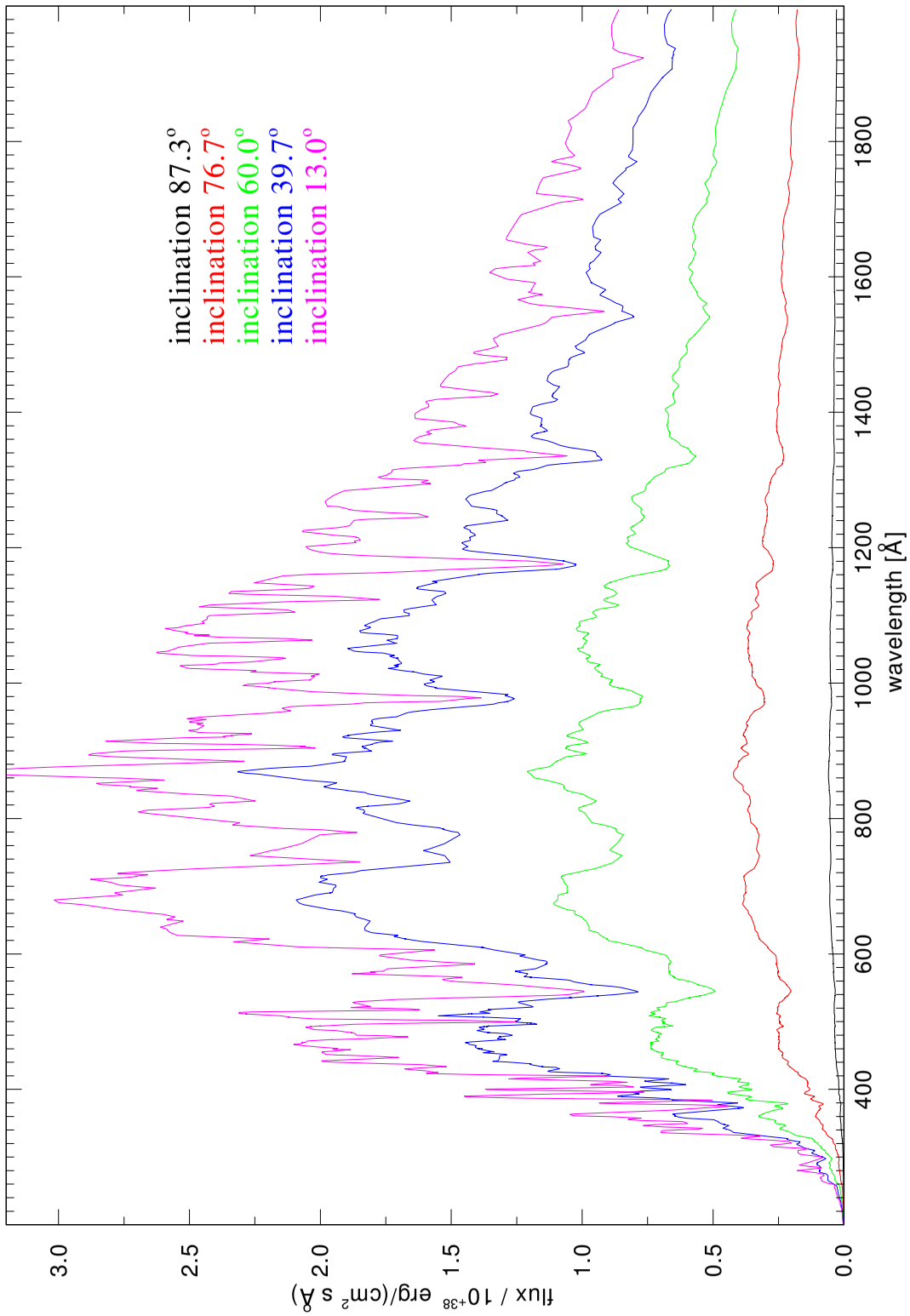

Figure C.11: Spectrum of a non-irradiated non-LTE accretion disc model, part 1

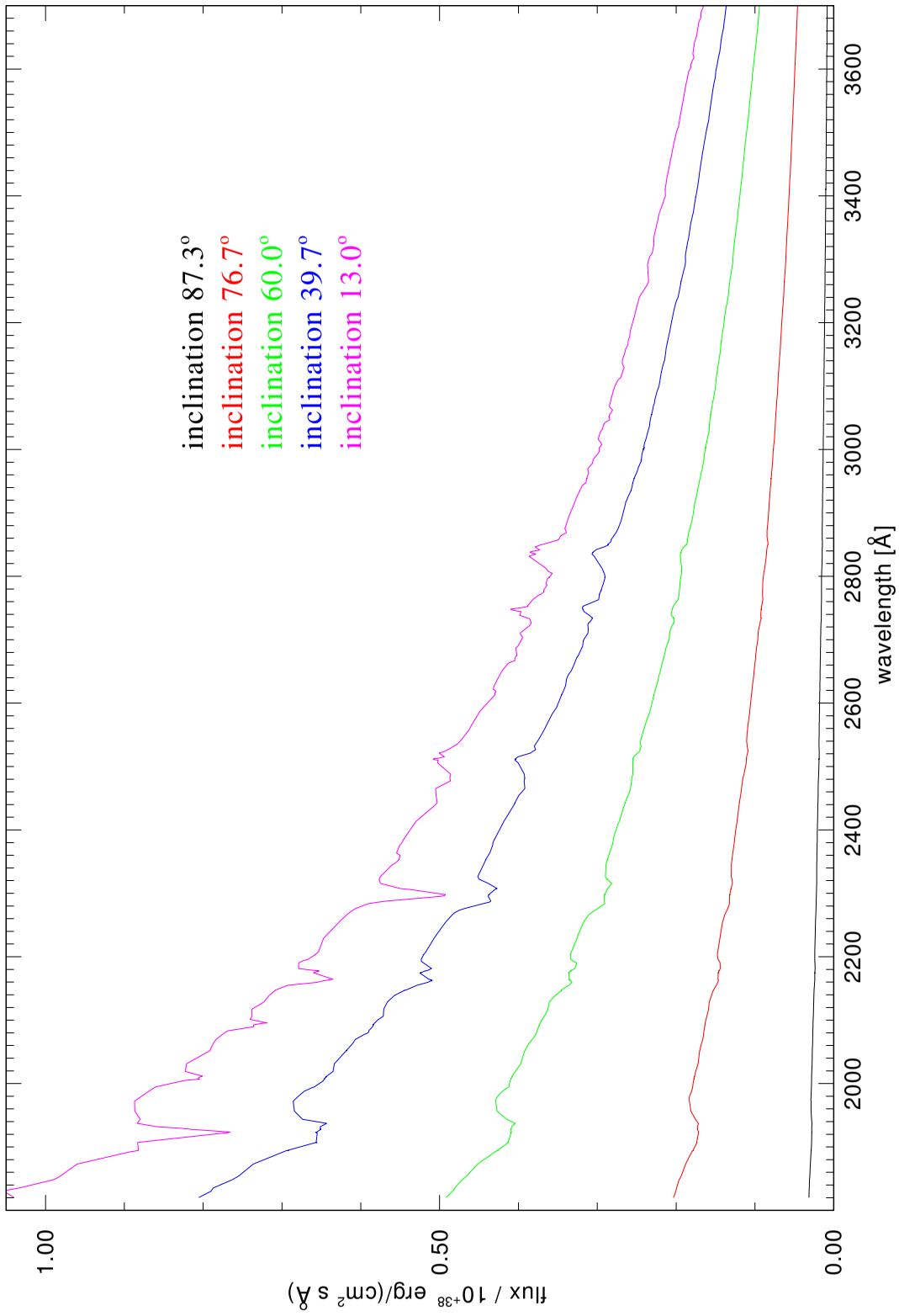

Figure C.12: Spectrum of a non-irradiated non-LTE accretion disc model, part 2

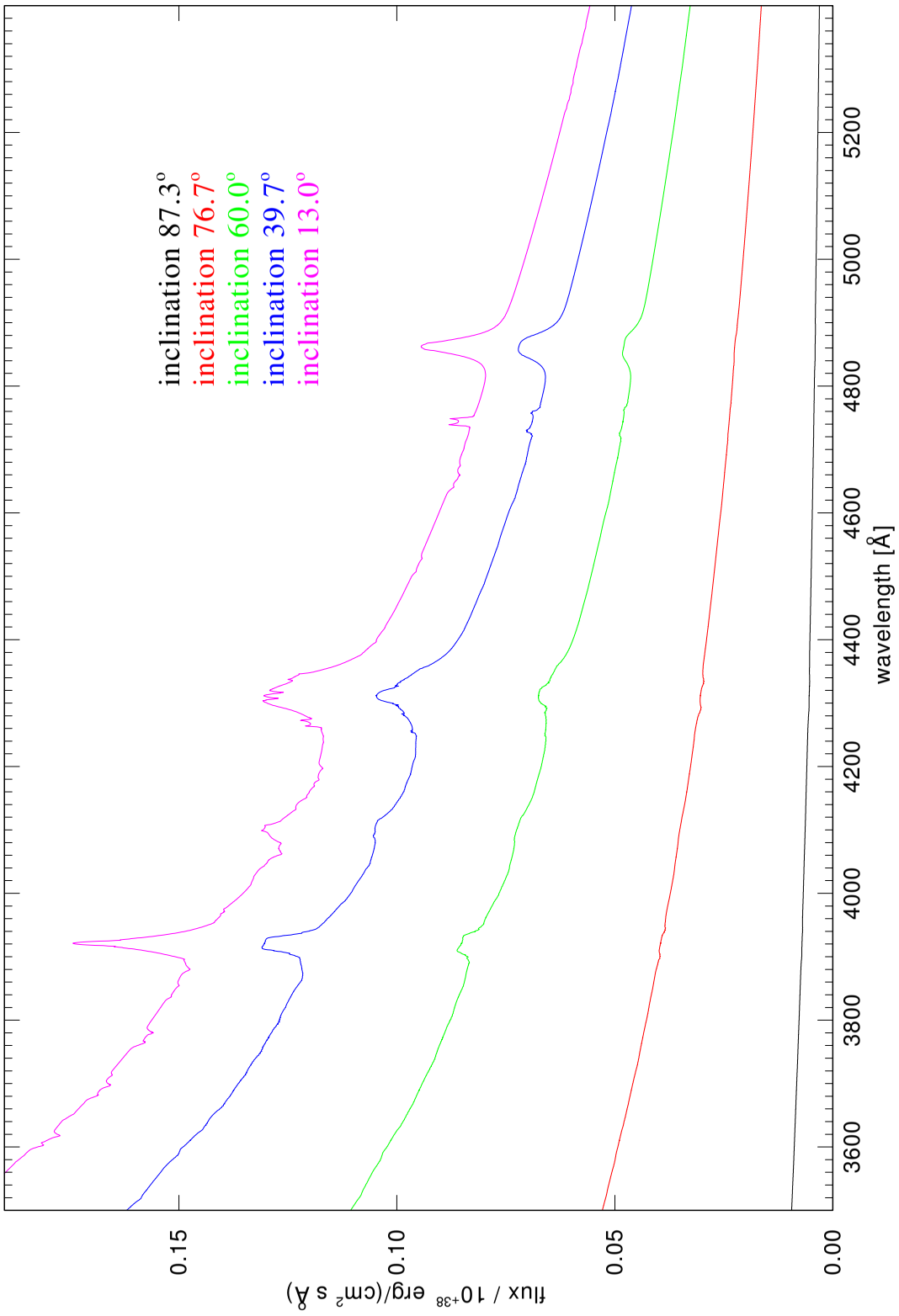

Figure C.13: Spectrum of a non-irradiated non-LTE accretion disc model, part 3

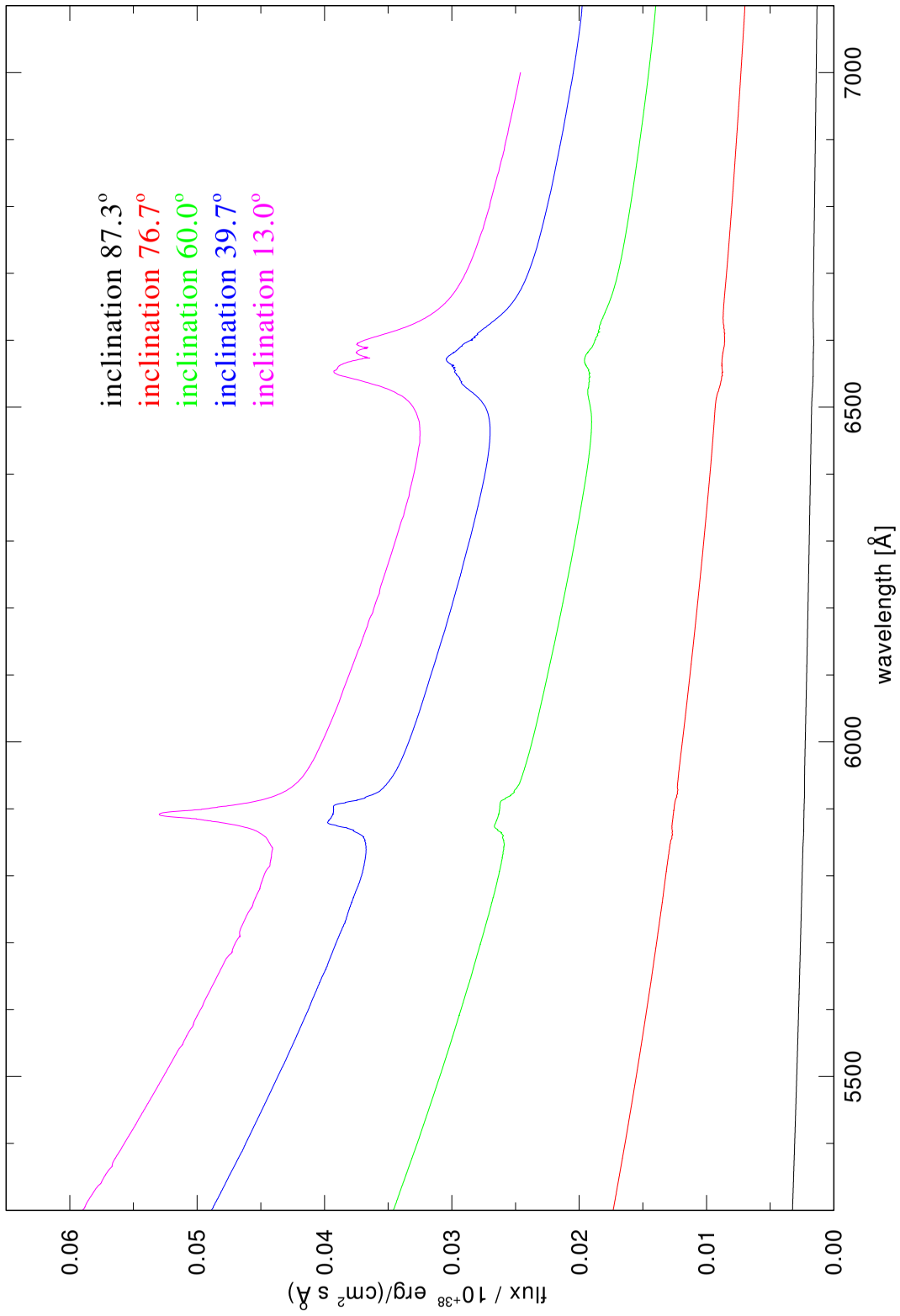

Figure C.14: Spectrum of a non-irradiated non-LTE accretion disc model, part 4

Appendix D

Plots of irradiated non-LTE Accretion Disc Models

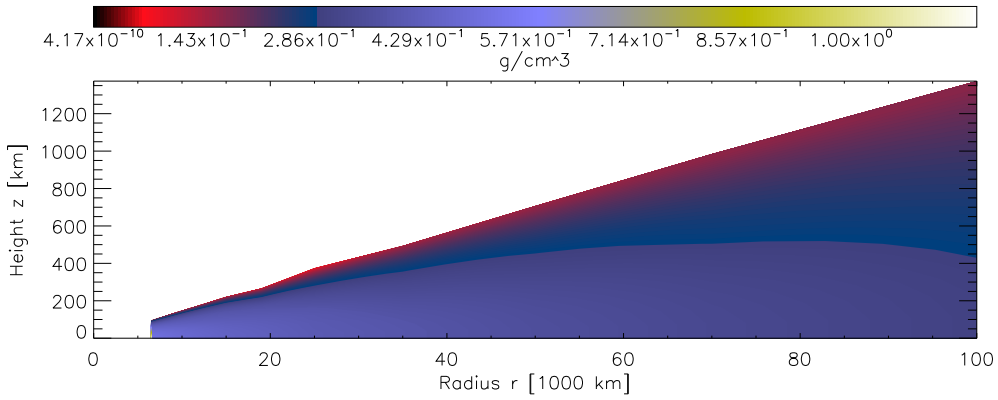

Figure D.1: Density structure of irradiated disc model in the z-r-plane

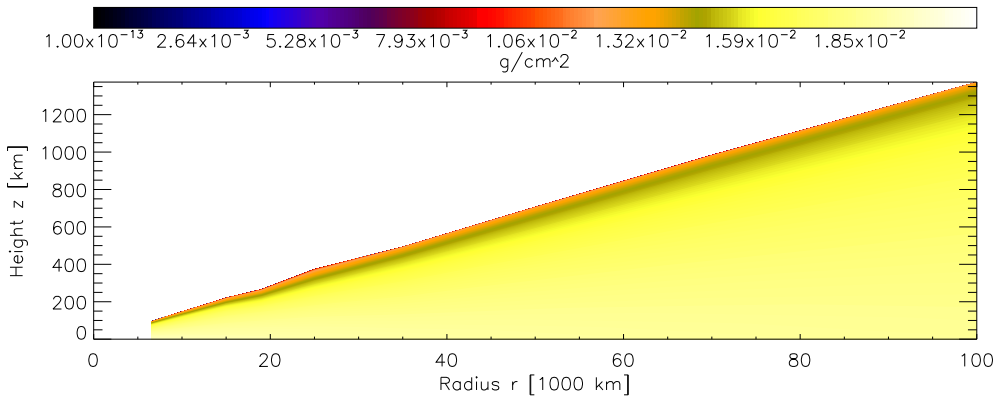

Figure D.2: Column mass structure of irradiated disc model in the z-r-plane

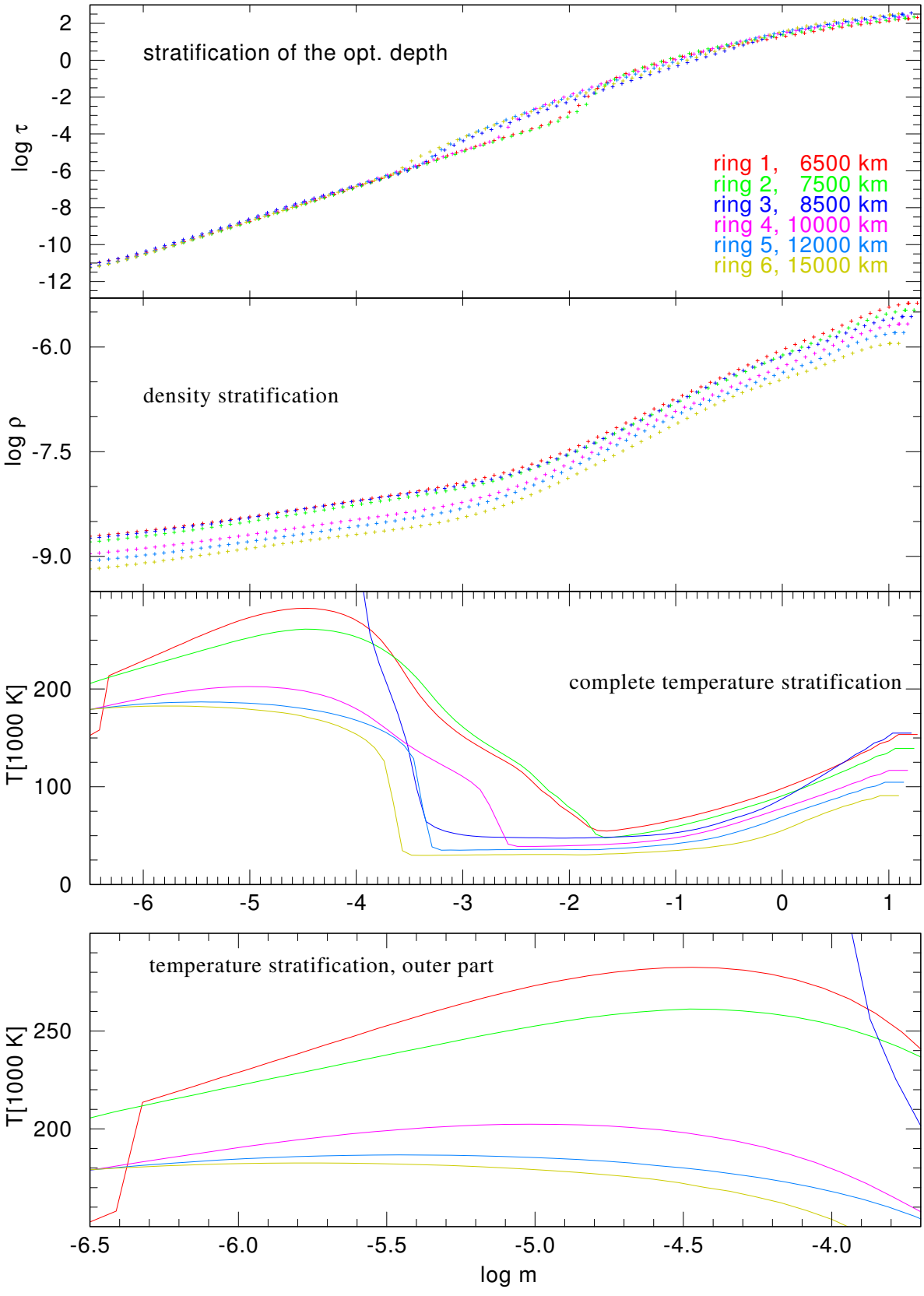

Figure D.3: Stratification of irradiated non-LTE models for the rings 1 - 6

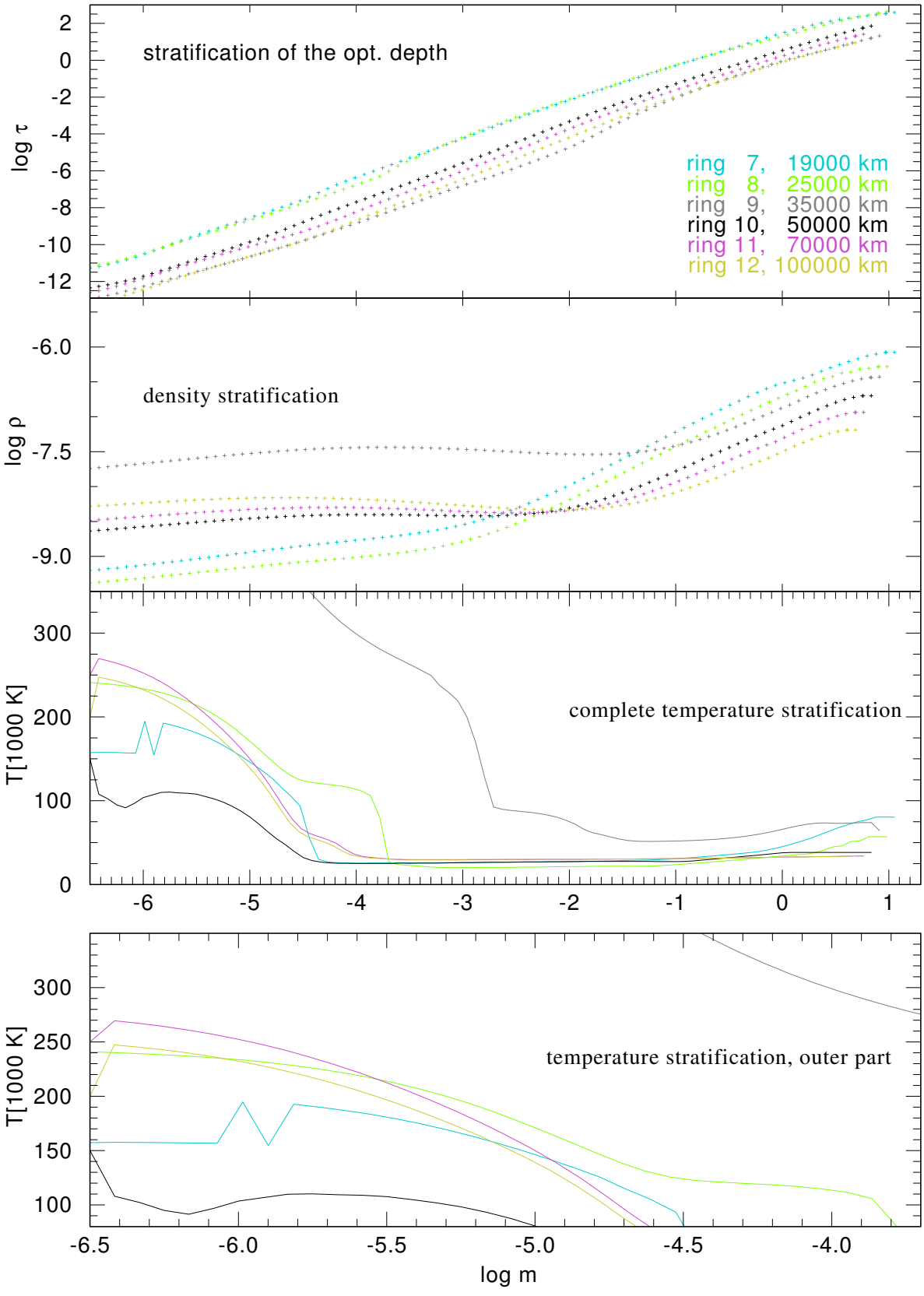

Figure D.4: Stratification of irradiated non-LTE models for the rings 7 - 12

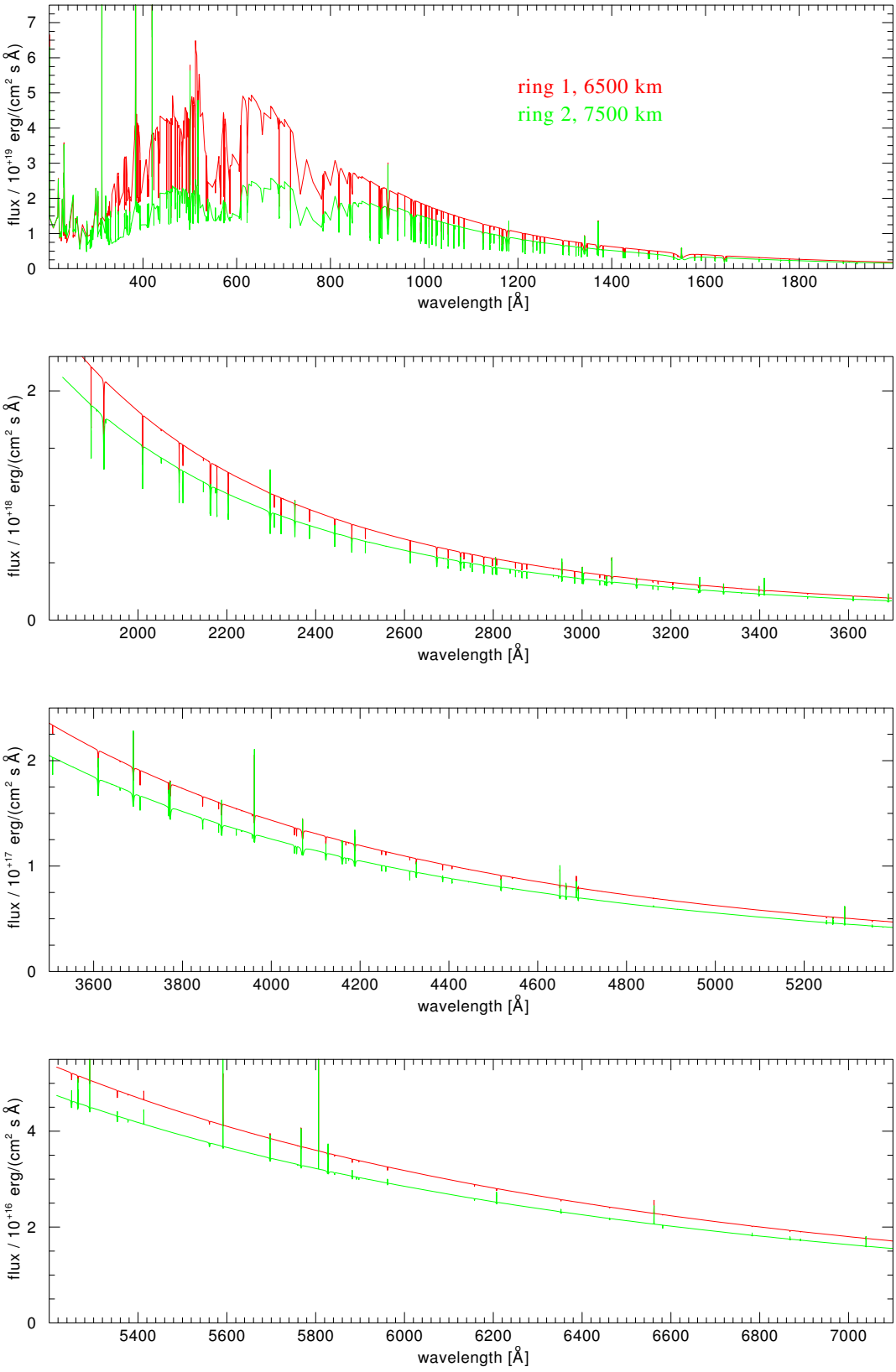

Figure D.5: Spectrum of irradiated non-LTE models for the rings 1 and 2

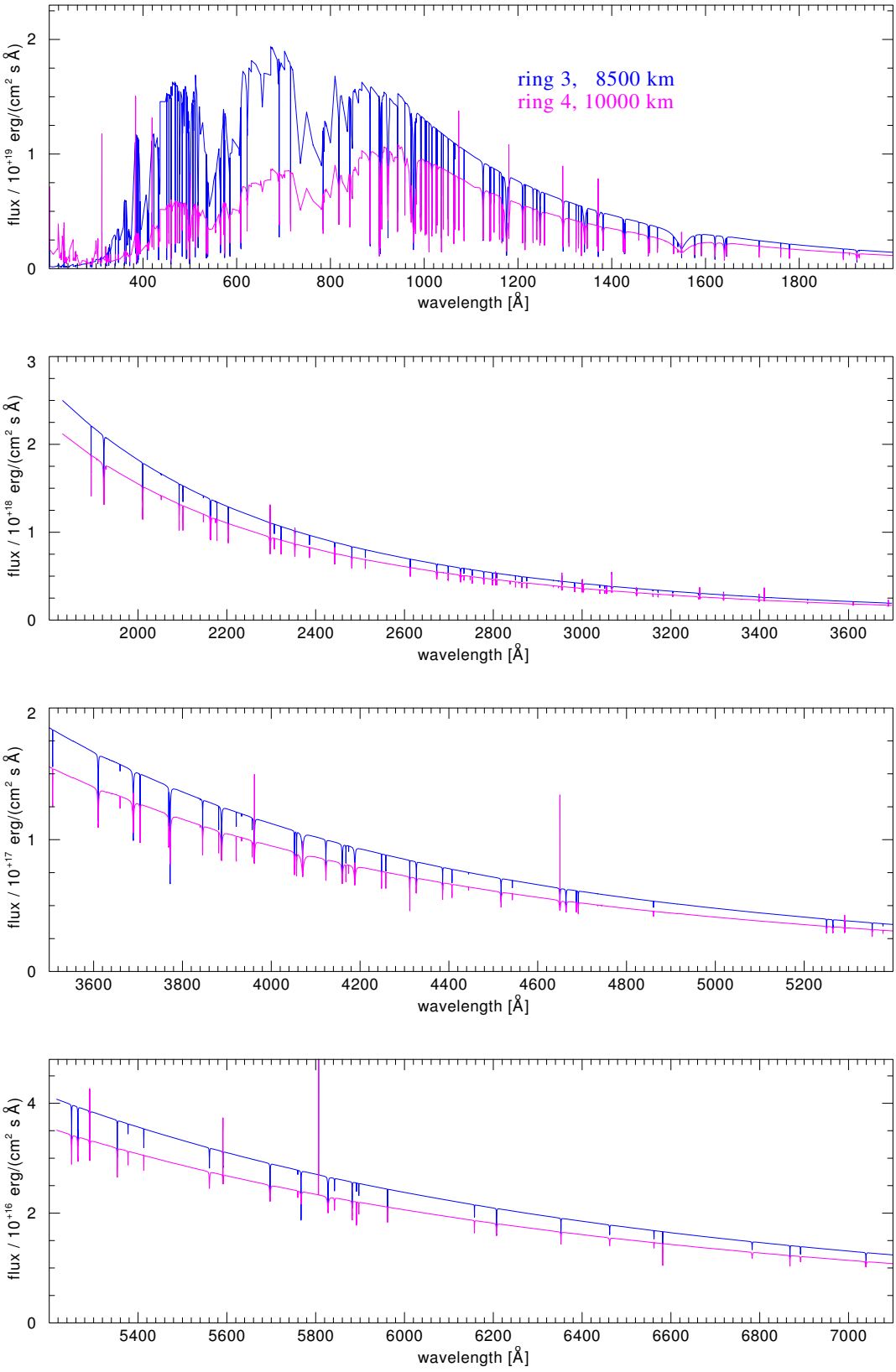

Figure D.6: Spectrum of irradiated non-LTE models for the rings 3 and 4

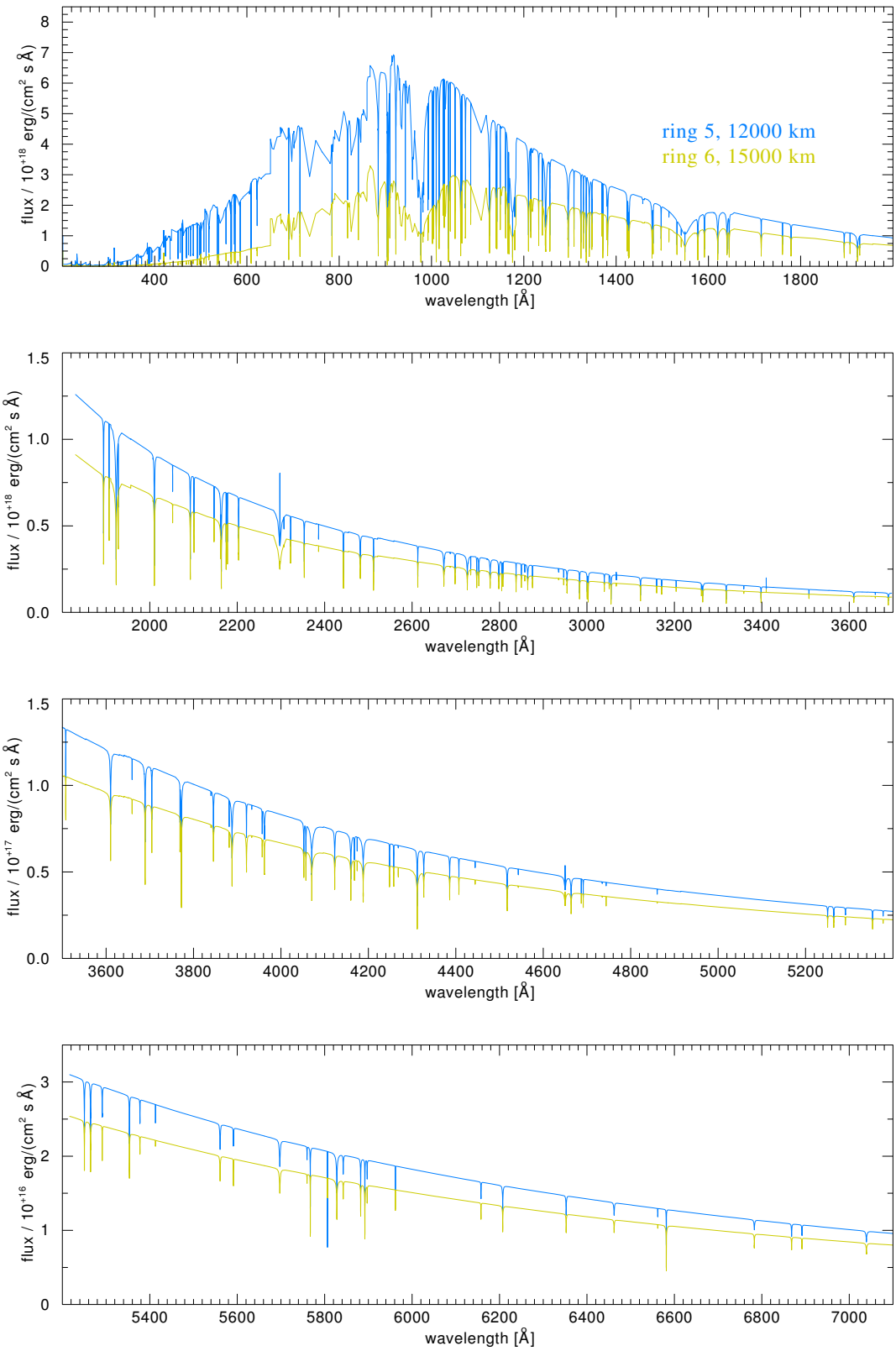

Figure D.7: Spectrum of irradiated non-LTE models for the rings 5 and 6

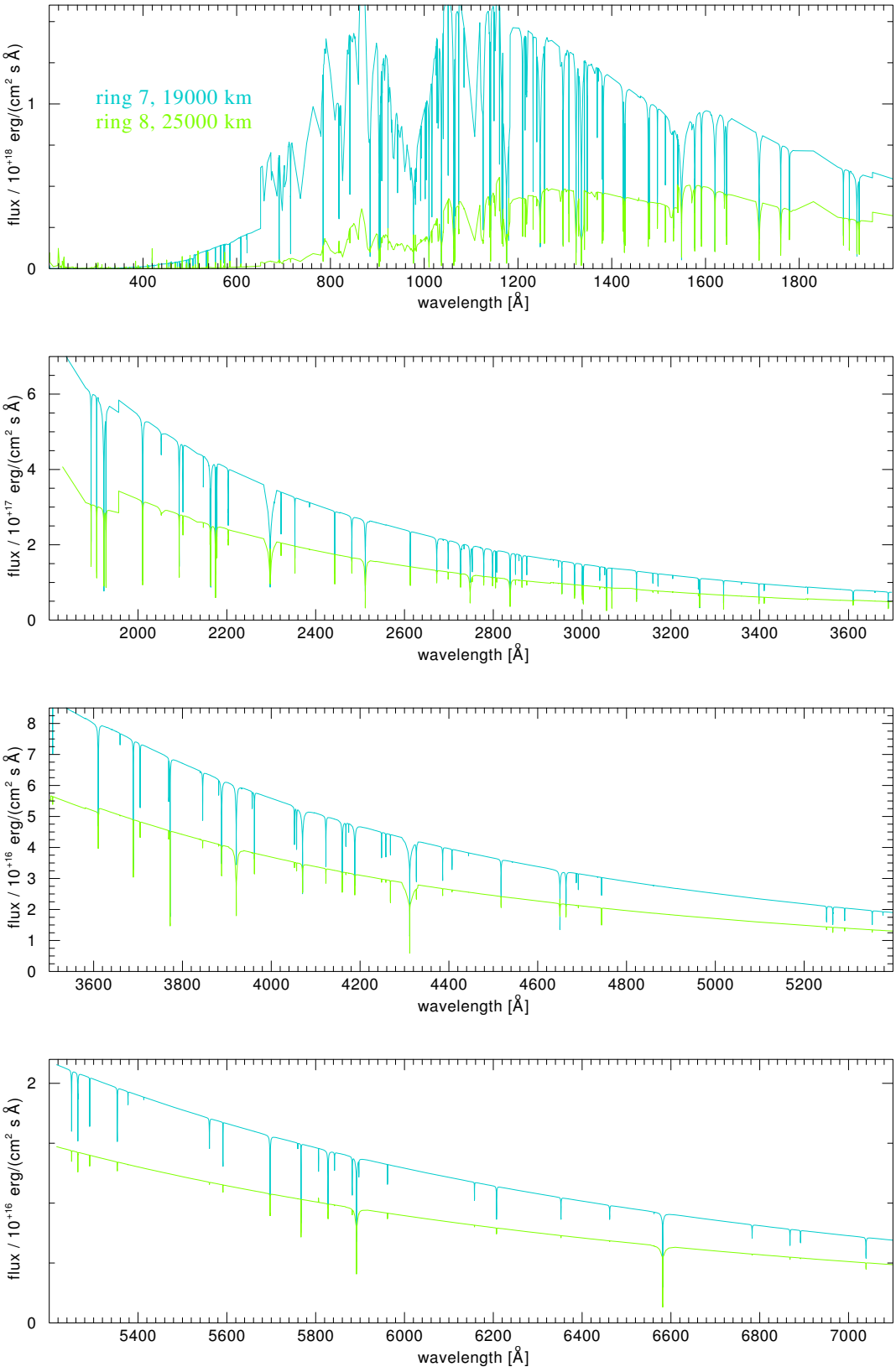

Figure D.8: Spectrum of irradiated non-LTE models for the rings 7 and 8

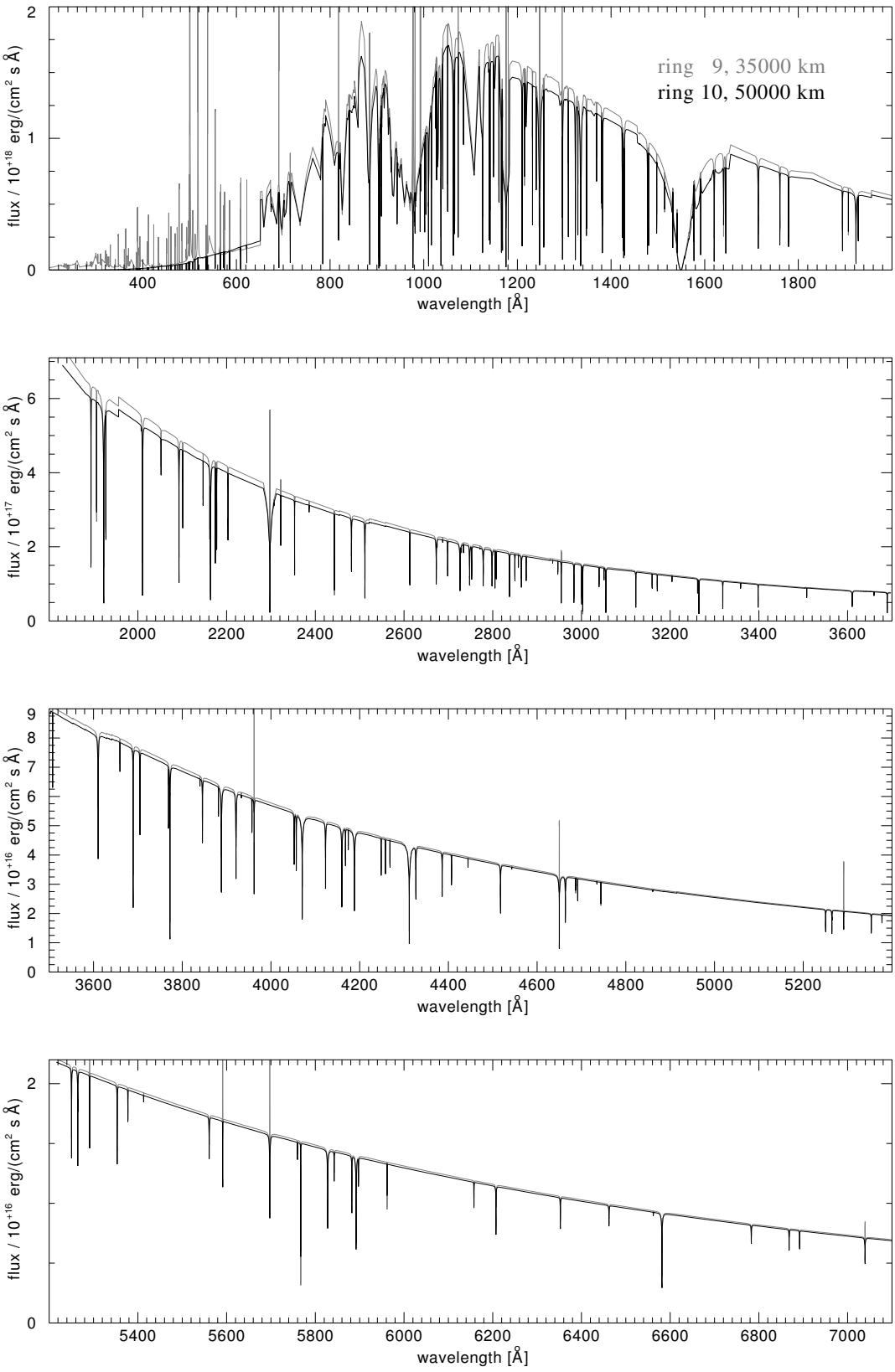

Figure D.9: Spectrum of irradiated non-LTE models for the rings 9 and 10

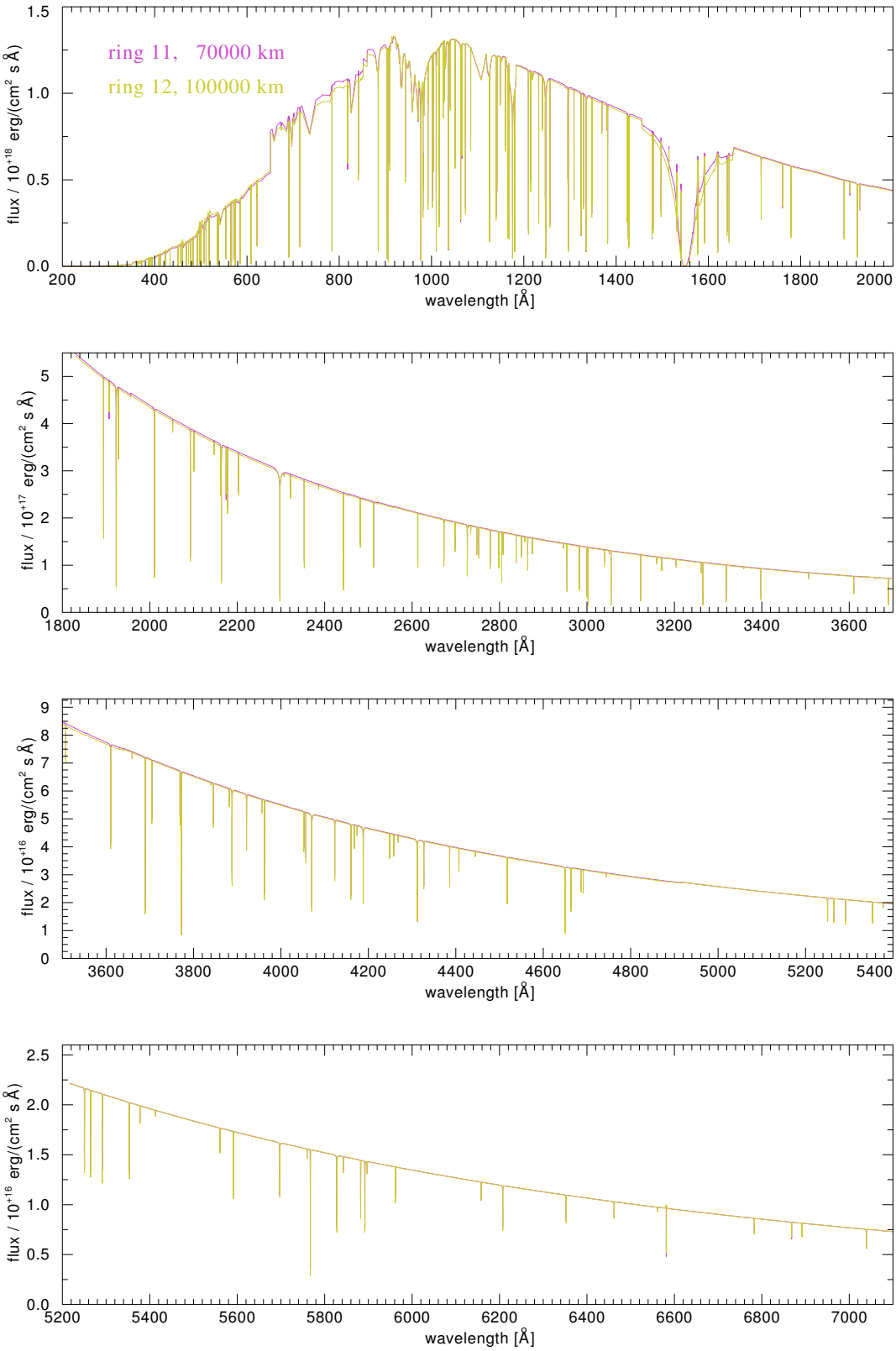

Figure D.10: Spectrum of irradiated non-LTE models for the rings 11 and 12

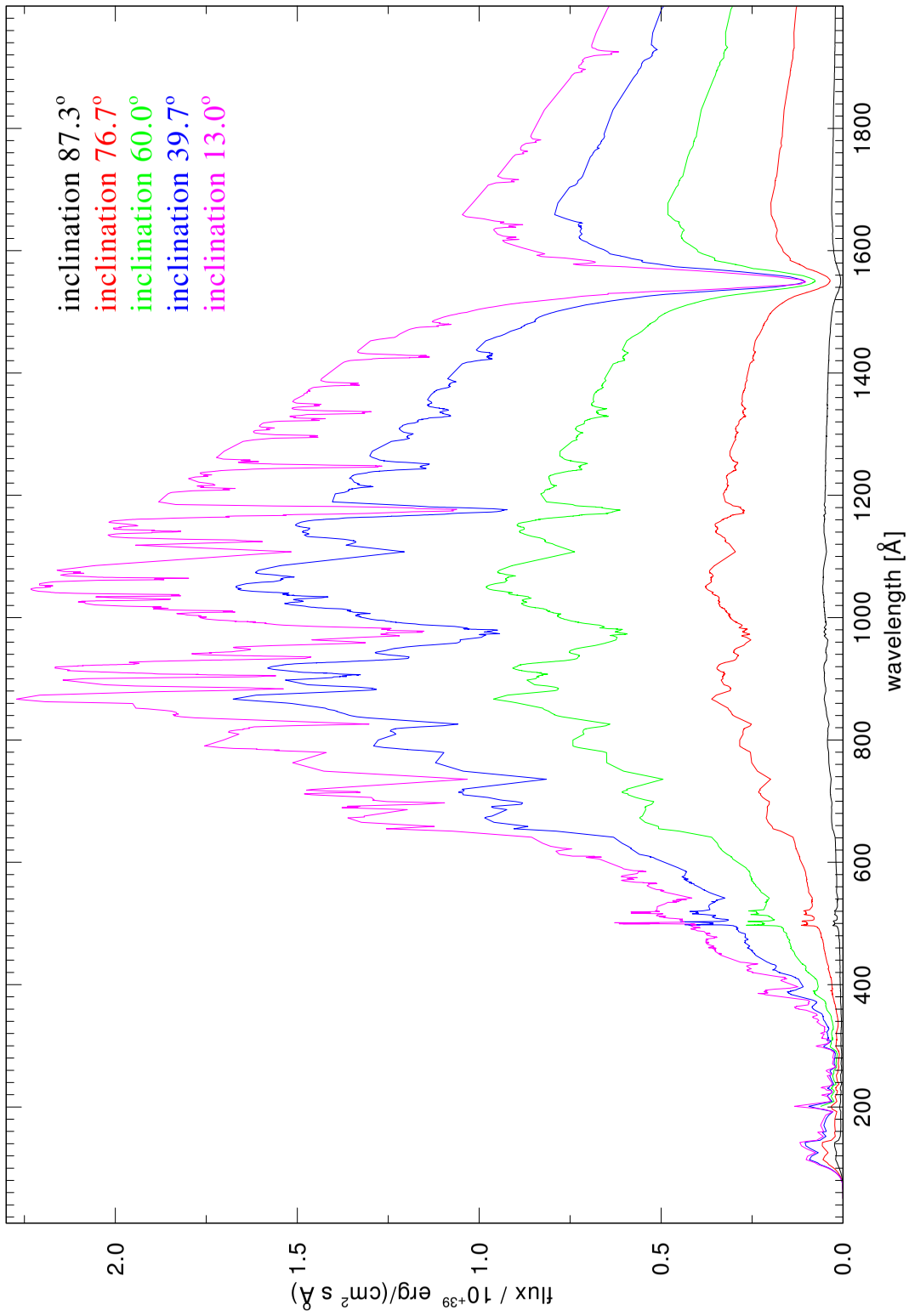

Figure D.11: Spectrum of an irradiated non-LTE accretion disc model, part 1

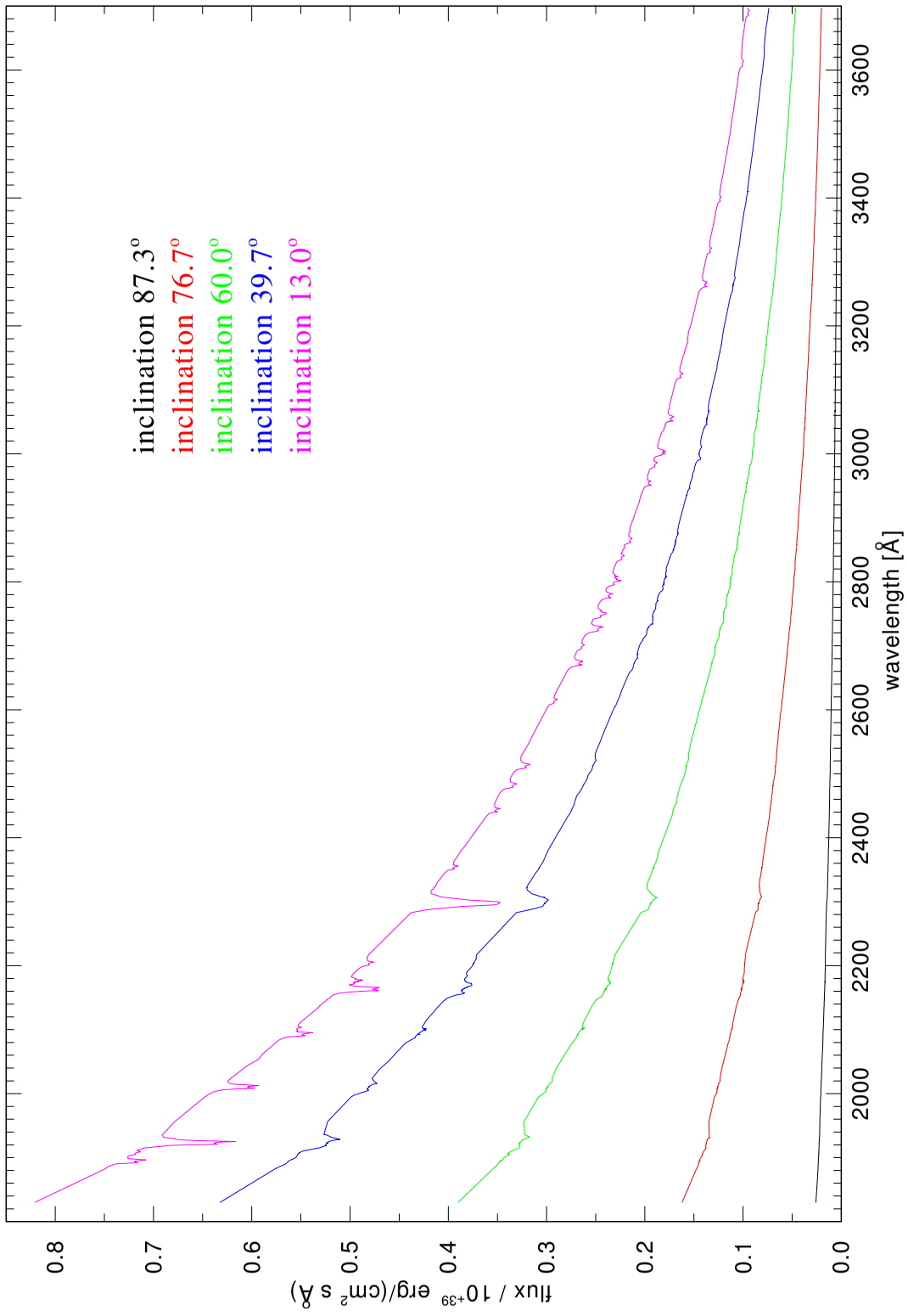

Figure D.12: Spectrum of an irradiated non-LTE accretion disc model, part 2

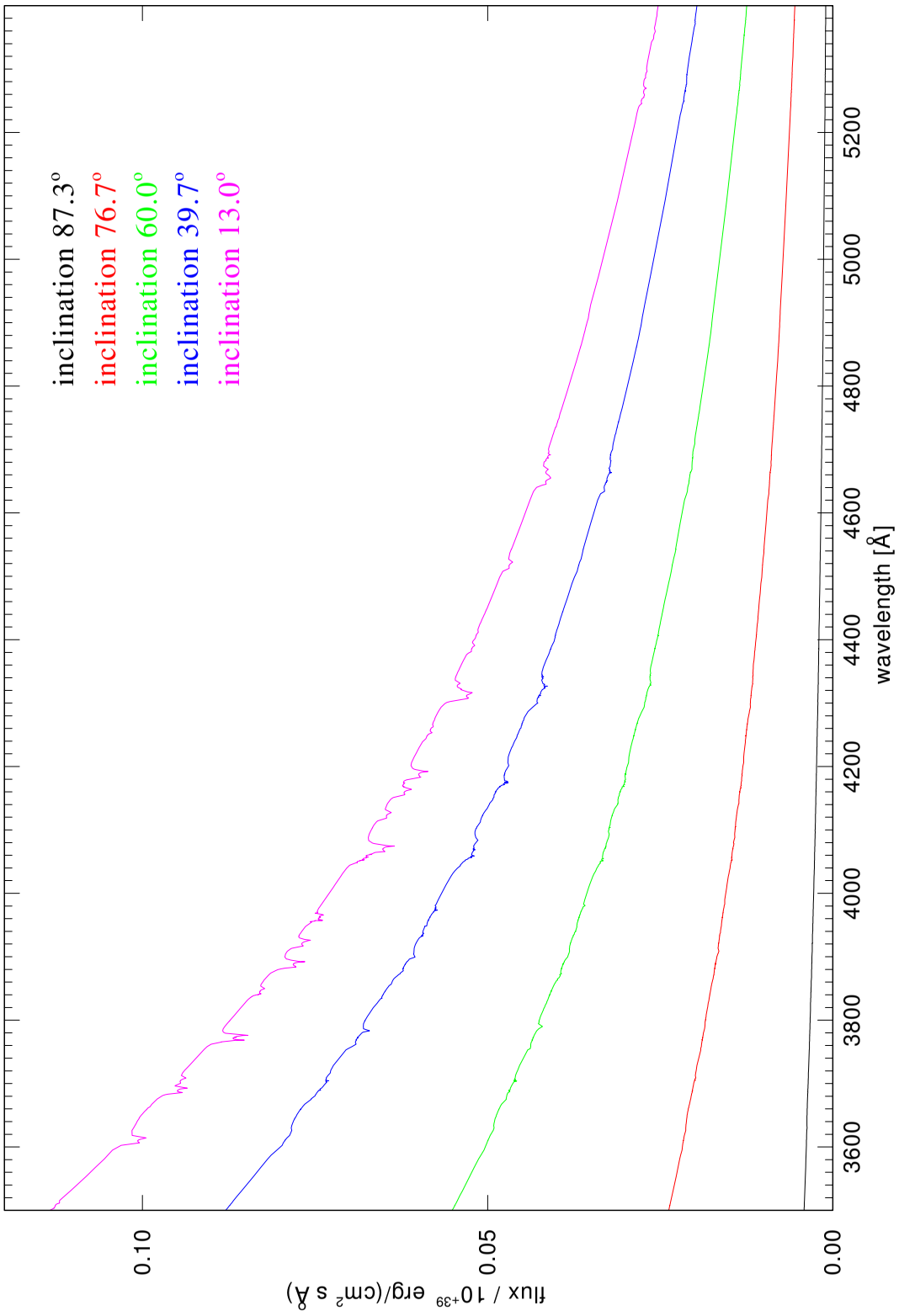

Figure D.13: Spectrum of an irradiated non-LTE accretion disc model, part 3

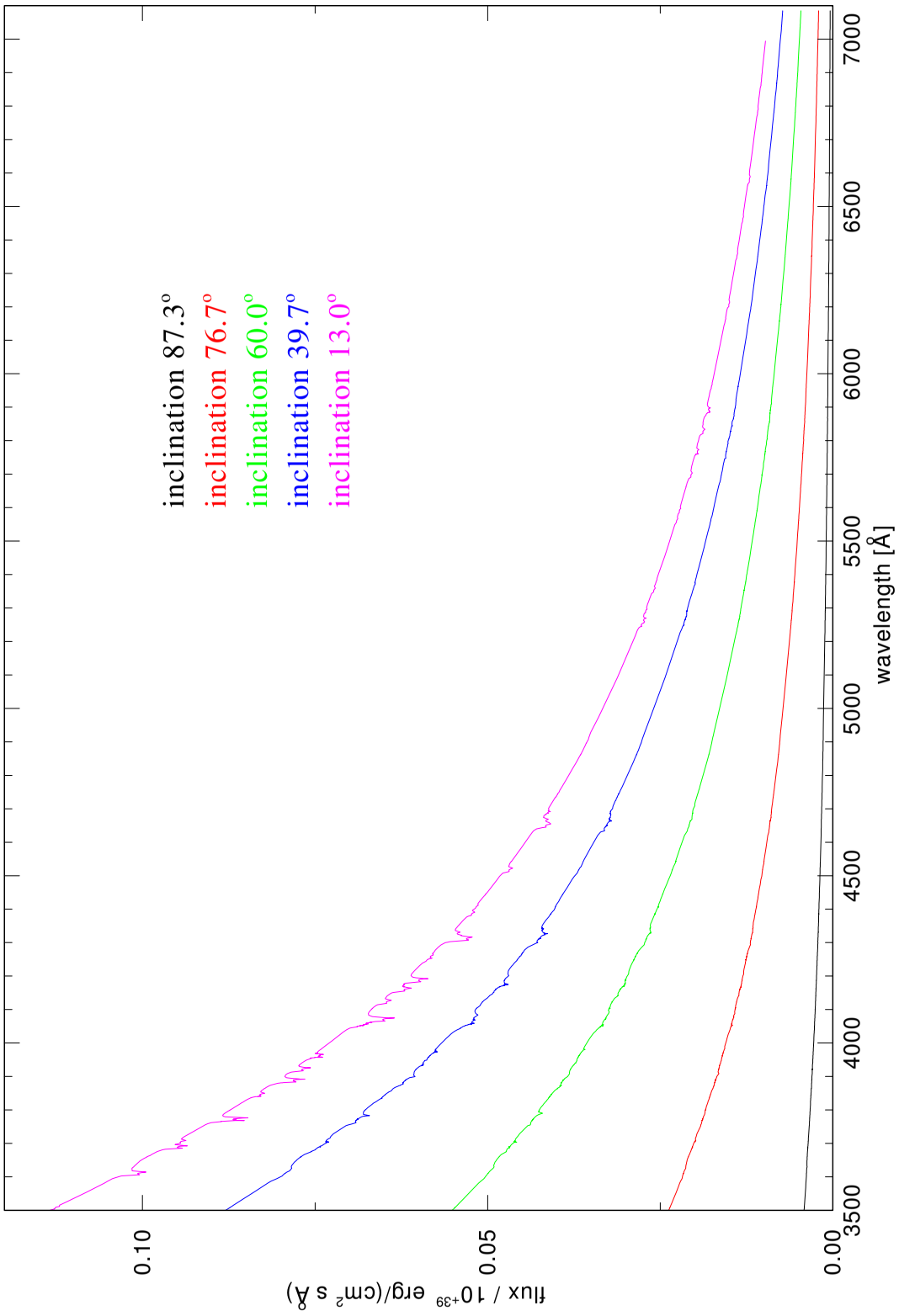

Figure D.14: Spectrum of an irradiated non-LTE accretion disc model, part 4

Acknowledgement

First I like to thank Prof. Dr. Klaus Werner, that he believed in my potentials, and has given me this complex topic to work on. He is and was a brilliant taskmaster and I feel honoured that he had cultivated me the last few years.

Then I like to thank Prof. Dr. Stefan Dreizler for all his endurance he invested in my education. He has taught me really a lot of useful and interesting things.

I like to thank Dr. Thorsten Nagel, for introducing me in to the world of AcDc and accretion disc modelling. We had, for my part, a very well corporation and lots of hours of very good and inspiring discussions.

I like to thank Dr. Thomas Rauch, the master of atomic data, for helping me with a lot of problems on that topic.

I like to thank Dr. habil. Jörn Wilms and Dr. Ingo Kreykenbohm for teaching me a lot about computer and LINUX. Special thanks to Jörn for providing this diploma thesis LaTeXstyle.

Iris Traulsen and Agnes Hoffmann, I would like to thank in particular for sharing the time as student research assistants at the AIT with me for more than three years.

And I like to thank Dr. Jochen Deetjen and Sonja Schuh for helping me with so many problems. Thanks to Daniel Kusterer for correcting the language of this thesis. I also have to thank the other members or former members of the working group for a lot of good discussions and a very good working atmosphere. These are J. Deetjen, S. Dreizler, A.I.D. Hoffmann, S. Jordan, T. Kellermann, D.J. Kusterer, T. Nagel, T. Rauch, E.S. Reiff, S. Schuh, I. Traulsen, and K. Werner.

I also like to thank the Institute's members of the IAAT for giving me a very interesting, joyful and wonderful time.

At last I like to thank my wonderful parents for escorting me through my path of life and providing me help for every situation.

Bibliography

Anderson, E., Bai, Z., Bischof, C., et al., 1991, LAPACK User Guide, SIAM Publishing

Anderson, L.S., 1985, ApJ, 298, 848

Brandt, S., Castro-Tirado, A.J., Lund, N., et al., 1992, 262, L15+

Bronstein, I.N., Semandjajew, K.A., Musiol, G., Mühlig, H., 1999, Taschenbuch der Mathematik, Frankfurt am Main: Verlag Harri Deutsch, fourth edition

Cannon, A.J., Pickering, E.C., 1918, The Henry Draper catalogue, Cambridge, Mass., The Observatory, 1918-24.

Chakrabarty, D., 1998, ApJ, 492, 342

Deetjen, J.L., 2002, Atmosphären und synthetische Spektren von Neutronensternen, Ph.D. thesis, Eberhard-Karls-Universität Tübingen

Frank, J., King, A., Raine, D.J., 2002, Accretion Power in Astrophysics: Third Edition, Accretion Power in Astrophysics: Third Edition, by Juhan Frank, Andrew King, and Derek J. Raine. Cambridge University Press, 2002, 398 pp.

Fraunhofer, J., 1823, Astronomische Nachrichten, 1, 295

Haken, H., Wolf, H., 1996, Atom- und Quantenphysik, Berlin Heidelberg New York: Springer, sixth edition

Hellier, C., 2001, Cataclysmic Variable Stars, Berlin Heidelberg New York: Springer

Hertzsprung, E., 1911, Publikationen des Astrophysikalischen Observatoriums zu Potsdam, 63

Hjellming, R.M., Johnston, K.J., 1988, ApJ, 328, 600

Hubeny, I., 1990, ApJ, 351, 632

Hubeny, I., Hubeny, V., 1997, ApJL, 484, L37+

Hubeny, I., Hubeny, V., 1998, ApJ, 505, 558

Juett, A.M., Psaltis, D., Chakrabarty, D., 2001, ApJL, 560, L59

Kant, I., 1781, Kritik der reinen Vernunft

Koesterke, L., Hamann, W.R., Kosmol, P., 1992, 255, 490

Kopka, H., 2000, LATEX Band1: Einführung, Addison-Wesley

Kube, J., 2002, Indirect Imaging of Cataclysmic Variable Stars, Ph.D. thesis, Georg-August-Universität zu Göttingen

Kurucz, R.L., 1979, ApJS, 40, 1

Lawson, C.L., Hanson, R.J., Kincaid, D.R., Krogh, F.T., 1979, ACM Transactions on Mathematical Software, 5, 308

Lewin, W.H.G., van Paradijs, J., van den Heuvel, E.P.J., 1995, X-ray binaries, Cambridge Astrophysics Series, Cambridge, MA: Cambridge University Press, ©1995, edited by Lewin, Walter H.G.; Van Paradijs, Jan; Van den Heuvel, Edward P.J.

Lotz, W., 1968, Zeitschrift für Physik, 216, 241

Massey, H.S.W., Burhop, E.H.S., Gilbody, H.B., 1974, Electronic and ionic impact phenomena, The International Series of Monographs on Physics, Oxford: Clarendon Press, 1969-1974, second edition

Middleditch, J., Mason, K.O., Nelson, J.E., White, N.E., 1981, ApJ, 244, 1001

Mihalas, D., 1978, Stellar Atmospheres, New York: W. H. Freeman and Company, second edition

Nagel, T., 2003, Synthetische Spektren und Vertikalschichtungen von Akkretionscheiben, Ph.D. thesis, Eberhard-Karls-Universität Tübingen

Nahar, S.N., 2003, in ASP Conf. Ser. 288: Stellar Atmosphere Modeling, 651

Orlandini, M., Fiume, D.D., Frontera, F., et al., 1998, ApJL, 500, 163

Paczynski, B., Sienkiewicz, R., 1981, ApJL, 248, L27

Piraino, S., Santangelo, A., Ford, E.C., Kaaret, P., 1999, 349, L77

Russell, H.N., 1913, The Observatory, 36, 324

Salpeter, E.E., 1964, ApJ, 140, 796

Schulz, N.S., Chakrabarty, D., Marshall, H.L., et al., 2001, ApJ, 563, 941

Seaton, M., 1987, Journal of Physics B Atomic Molecular Physics, 20, 6363

Seaton, M.J., 1962, in D. Bates (ed.), Atomic and Molecular Processes, Vol. 79, Proc. Phys. Soc 1105, New York: Academic, 374

Seaton, M.J., Yan, Y., Mihalas, D., Pradhan, A.K., 1994, MNRAS, 266, 805

Shakura, N.I., Sunyaev, R.A., 1973, A&A, 24, 337

Shklovsky, I.S., 1967, ApJL, 148, L1+

Swank, J.H., Boldt, E.A., Holt, S.S., et al., 1978, MNRAS, 182, 349

Trümper, J., Pietsch, W., Reppin, C., et al., 1978, ApJL, 219, L105

Unsöld, A., 1930, Zeitschrift für Astrophysik, 1, 1

Unsöld, A., 1934, Zeitschrift für Astrophysik, 8, 225

Unsöld, A., Baschek, B., 1999, Der neue Kosmos, Berlin Heidelberg New York: Springer, sixth edition

van Regemorter, H., 1962, ApJ, 136, 906

Vogel, H., 1997, Gerthsen Physik, Berlin Heidelberg New York: Springer, nineteenth edition

Werner, K., 1986, A&A, 161, 177

Werner, K., Dreizler, S., 1999, J. Comp. Applied. Math., 109, 65

Yungelson, L.R., Nelemans, G., van den Heuvel, E.P.J., 2002, A&A, 388, 546

Zimmermann, H., Weigert, A., 1999, Lexikon der Astronomie, Berlin Heidelberg New York: Spektrum Akademischer Verlag, eighth edition

Online References

Astrophysics Data System (ADS), National Aeronautics and Space Administration (NASA):
http://adswww.harvard.edu/index.html

Dhillon, V., 2001, *The Lives of Binary Stars*, University of Sheffield:
http://www.shef.ac.uk/physics/people/vdhillon/seminars/sas/masstrans.html

Rutten, R.J., 2000, *Radiativ Transfer in Stellar Atmospheres*, lecture notes, Utrecht Unversity, 7th edition:
http://www.astro.uu.nl/~rutten/node19.html

Werner et al., 2004, *User's Guide to the Tübingen NLTE Model Atmosphere Package*
http://astro.uni-tuebingen.de/groups/stellar/tmap/bib/TMAPUserGuide.ps.gz